SprinklerModel: A field-scale solid set sprinkler irrigation system hydraulic model, program documentation

By

D. Zerihun and C.A. Sanchez

University of Arizona
Maricopa Agricultural Center
37860 West Smith-Enke Road
Maricopa, Arizona 85238

A report submitted to the USBR

Contents

List of Figures

Chapter 1. Introduction

This report presents a field-scale solid set sprinkler system hydraulic model. The model has functionalities for hydraulic characterization, simulation, and design of sprinkler systems. In addition, the model can compute test-plot scale and field-scale irrigation uniformity estimates based on data sets collected through standard field uniformity tests.

Two types of field-scale solid set sprinkler system layout configurations, commonly used in the Yuma Valley Irrigation Districts, can be simulated with the hydraulic model presented here. The typical system layout in the Yuma Valley consists of a mainline running across the head end of the field supplying irrigation water to a line of laterals installed on one side of the main. Such systems are described here as having a single-line laterals field layout configuration (Figure 1a). Another widely used field layout configuration consists of a mainline installed in between two adjacent irrigated fields, or somewhere within an irrigated field, and supplies irrigation water to two sets of laterals, each installed on either side of the main (Figure 1b). Such a system is described here as one having double-line laterals layout configuration. With this layout each set of laterals irrigate either some fraction of the field or each of the adjacent fields.

The water source for a field-sprinkler system could be surface or subsurface. However, in the Yuma Valley Irrigation Districts, typically, lined field supply canals are the source of irrigation water, with pumps (often centrifugal pumps) providing the energy input. Laterals can be installed at any desired angle to the mainline and the lengths of the laterals can be the same or can be varied following the geometry of the irrigated field. Slopes, diameters, and hydraulic roughness characteristics can vary along a lateral, between laterals, and along the mainline. In addition, sprinkler characteristics can vary along a lateral or between laterals and the model can compute energy losses due to various types of pipe appurtenances along laterals and the mainline.

The model can be run in four computational modes: sprinkler system hydraulic characterization, design, simulation, and field evaluation. Given the hydraulic, geometric, and topographic characteristics of a sprinkler system, the system characterization mode

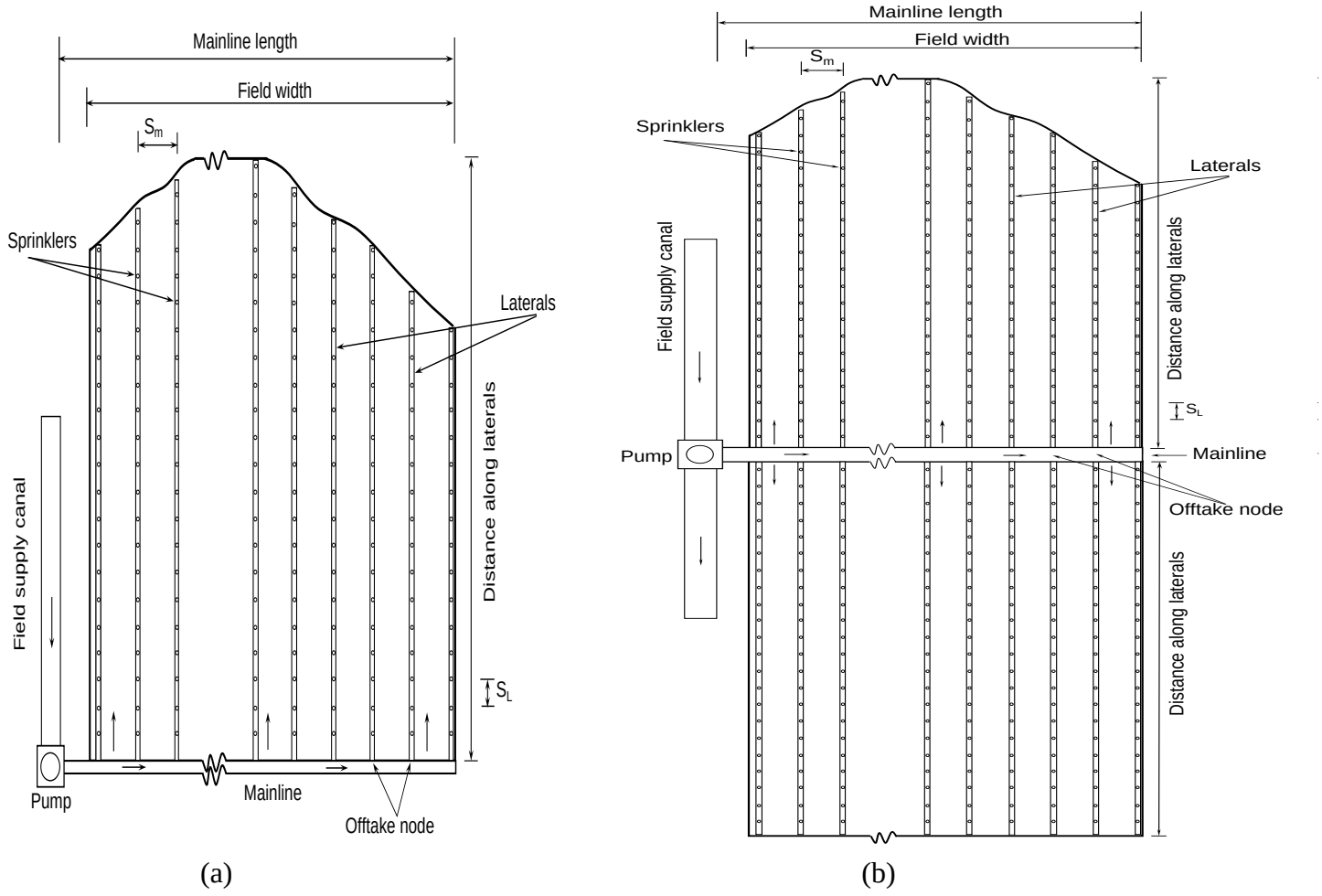

Figure 1 Field-scale solid set sprinkler system layout configurations (a) single-line laterals (b) double-line laterals (S_L = sprinkler spacing along laterals and S_m = lateral spacing)

provides the functionality for computing the system hydraulic characteristic curves at preset computational nodes in the system. Outputs of the hydraulic characterization computation are useful in pump selection or evaluation. However, the main significance of the system characterization computations is in defining the hydraulic characteristics of the mainline outlets, which is essential for executing subsequent hydraulic design and simulation computations.

The hydraulic design mode computation typically produces a feasible yet suboptimal field-scale sprinkler system design that meets a specified requirement on the minimum acceptable sprinkler pressure head. However, repeated simulations and sensitivity analysis with alternative scenarios (considering different combinations of sprinkler layouts, pipe diameters, sprinkler characteristics, and pipe appurtenances) can be used to develop acceptable designs.

With the simulation mode, the model generates the spatial distribution of field-scale sprinkler discharges and pressure heads given the total dynamic head at the sprinkler system inlet. Because the spatial distribution of sprinkler pressure heads and discharges are good indicators of field-scale irrigation uniformity, the hydraulic simulation functionality of the model described here can be considered as a useful tool in evaluating the potential irrigation uniformity of an existing system.

The field evaluation functionality of the model can be used to estimate irrigation uniformity (in terms of Christiansen's uniformity index and the low-quarter distribution uniformity) at the scale of a uniformity evaluation-plot or an irrigated field.

The system characterization, design, and simulation computations are all based on the basic principles of manifold hydraulics (Larock et al., 2000; Miller, 2009), which couples the energy equation for each pipe segment along with the continuity equation at a node and solves the resulting expression iteratively. The basic numerical algorithms used here for modeling the hydraulics of a field-scale solid set sprinkler system with single-line laterals layout configuration were developed as part of an earlier study (Zerihun and

Sanchez, 2011). Further development and enhancement of the hydraulic model has been performed within the framework of the study reported here: (1) The formulation and numerical solution of the hydraulic equations for a sprinkler system with double-line laterals layout configuration; (2) An interpolation scheme, based on cubic splines, was developed and incorporated into the current version of the model as an interface for coupling the numerical solutions of the lateral and mainline hydraulic equations; (3) A one-dimensional optimization algorithm is developed and incorporated into the hydraulic simulation and design functionalities of the model; (4) Enhancements were made to earlier version of the model in order to accommodate field layouts with irregular boundaries (variable lateral lengths); and (5) A new functionality for computing test-plot scale and field-scale sprinkler irrigation uniformity from field data is developed.

Model evaluation is conducted by comparing the output of the model with field measured hydraulic (discharge and pressure head) data. Results of model evaluation and application of the model in field evaluation, system hydraulic characterization, simulation, and design is presented in a companion document (Zerihun and Sanchez, 2012). In addition, component of the model designed for hydraulic analysis of single-line laterals layout configuration was evaluated through comparison with field data as part of a previous study cited above.

This report is organized into five chapters. Chapter 1 is the introduction section of the report. Chapter 2 presents a formulation of the basic hydraulic equations governing flow in a field-scale solid set sprinkler system and their numerical solutions. Chapter 3 describes the computational capabilities of the model (hydraulic characterization, design, simulation, and field evaluation). It also presents the formulation and numerical solution, of the sprinkler system hydraulic design and simulation problems, as a one-dimensional optimization problem. Chapter 4 discusses the program components, model functionality, input/output data files and directory structure, and procedures for the installation and running of the program. In Chapter 5 limitations of the current version of model is discussed.

Chapter 2. Hydraulic model

2.1 Introduction

The hydraulics of a field-scale agricultural sprinkler system is a physical description of water flow through an open pipeline network, consisting of a main and laterals (Figure 1). A sprinkler lateral or main is a special type of manifold, a pipe consisting of multiple outlets with constant or variable spacing, hydraulic characteristics, and discharge. Typically, for solid set sprinkler systems spacing between outlets along a lateral or a mainline are constant and discharges are variable. Considering the entire length of a lateral or a mainline, flow velocity is spatially variable, however, in between outlets (assuming a constant pipe size) flow is uniform. At the scale of an irrigated field transient flow occurs over short durations following valve opening or closure (e.g., when a pump is turned on or off). Hence, during normal operations flow in such systems can be hydraulically described as steady without loss of generality. This implies that simpler forms of the energy conservation and mass continuity equations (applicable to steady incompressible flow) can be used to describe the hydraulics of such systems (Granger, 1995; Larock et al., 2000; Miller, 2009). A brief review of the basic hydraulic principles/concepts and associated equations for computing friction and local head losses and the distribution of the components of the specific energy along the length of a flow-through pipe (a pipe without outlets) is presented in a companion document (Zerihun and Sanchez, 2012). In this chapter, these concepts are used to formulate the governing equations of flow in a field-scale solid set sprinkler system. In addition, the chapter develops numerical solutions to the hydraulic equations.

2.2 Sprinkler lateral hydraulics: assumptions, equations, and numerical solution

Assumptions

The following set of assumptions apply to the equations presented subsequently: (1) Flow is steady, (2) A lateral is comprised of multiple pipe sections and nodes; (3) For computational purposes a lateral pipe section is considered to be composed of a segment spanning two consecutive nodes with constant diameter, slope, and hydraulic resistance

coefficient; (4) A computational node along a lateral could be an off-take node (consisting of a sprinkler riser pipe) or a none off-take node consisting of a pipe fitting or appurtenance or simply a change in pipe diameter that induces a drop in energy but no change in the through-flow discharge; (5) It then follows from assumptions 2 to 4 above that flow in a pipe section is uniform; (6) Sprinkler riser pipes are vertical, and (7) Leakage losses in pipe fittings and elsewhere in the field-sprinkler system is negligible.

Equations and numerical solution for the distal segment of the lateral

Figure 2 depicts the *jth* segment of a lateral obtaining its supply from the *kth* mainline off-take node. Following convention in manifold hydraulics, the computational nodes along the lateral (and sprinklers) are numbered sequentially starting from the distal node (where $j = 1$ and $Q_{j-1}^{k} = 0$) and moving upstream in ascending order.

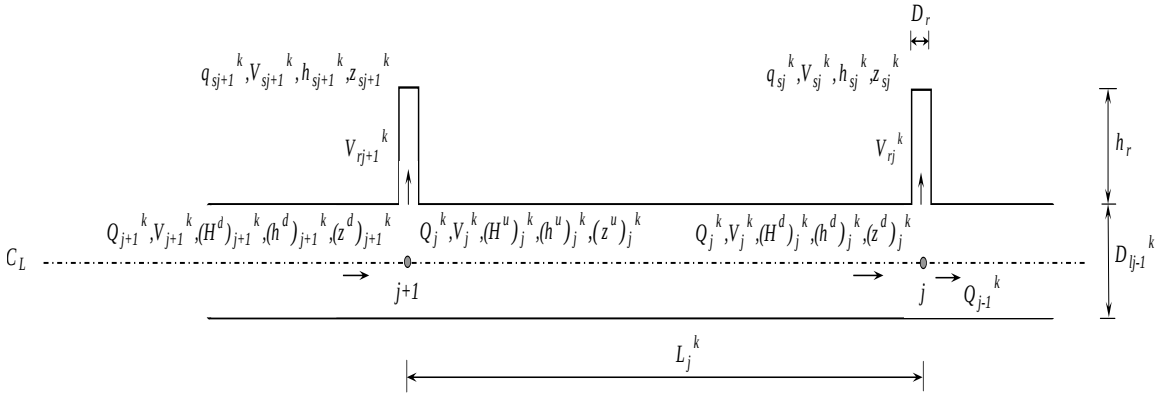

Figure 2 Schematics of the *jth* segment of the lateral obtaining its supply from the *kth* off-take node of the mainline

where C_L = centre line of pipe, Q = lateral discharge *(L/s)*; V = average cross-sectional velocity *(m/s)*; H = total head at a computational node *(m)*; h = pressure head *(m)*, z = nodal elevation, referenced from a datum *(m)*; D = pipe diameter *(mm)*; q_s = sprinkler discharge *(L/s)*; the subscripts *l*, *r*, and *s* define hydraulic, geometric, and topographic variables associated with lateral, riser pipe, or sprinkler nozzle, respectively; the subscripts *u* and *d* define flow conditions at the downstream and upstream ends of a

lateral section, respectively; and L_j^k = distance between the *jth* and *(j+1)th* computational nodes of the lateral obtaining its supply from the *kth* off-take node of the mainline (when both of these computational nodes consist of sprinklers, then $L_j^k = S_L$). Noting that flow in a lateral segment is uniform (sections 2.2), it then follows that cross-sectional velocity, *V*, and discharge, *Q*, are constant over a lateral segment; hence in Figure 2 they are not appended with the superscripts *u* and *d*.

Numerical computation along a lateral begins at the distal end sprinkler of the lateral and proceeds upstream. Referring to Figure 2, application of the energy conservation principle between a point just upstream of the inlet to the distal sprinkler riser pipe (where *j=1*) and the distal sprinkler nozzle is given as

$$\frac{\left(V_1^k\right)^2}{2g} + \left(h^d\right)_1^k + \left(z^d\right)_1^k = \frac{\left(V_{s1}^k\right)^2}{2g} + z_{s1}^k + h_{fr} + k_L \frac{\left(V_1^k\right)^2}{2g} \qquad (1)$$

In Eq. 1, *g* = acceleration due to gravity ($9.81 m/s^2$), h_{fr} = friction head loss in the sprinkler riser pipe (*m*), and k_L = the local head loss coefficient at the inlet to the distal sprinkler riser pipe *(-)*. Note that the energy equation, Eq. 1, assumes that at a short distance within the sprinkler riser pipe, following the contraction at the entrance to the pipe, the flow becomes fully developed.

Friction head loss in a pipe segment can be computed with the Darcy-Weisbach equation

$$h_f = k_{dw} f \frac{Q^2}{D^5} L \qquad (2)$$

Or with the Hazen-Williams equation

$$h_f = \frac{k_{hw}}{D^{4.87}} \left(\frac{Q}{C}\right)^{1.852} L \qquad (3)$$

In Eqs. 2 and 3, k_{dw} = a dimensional constant equal to $10^{7.917}\, mm^5 (s/L)^2$, k_{hw} = a dimensional constant equivalent to $1.22 \times 10^{10} mm^{4.87} (s/L)^{1.852}$, *f* = Darcy-Weisbach friction factor, and *C* = Hazen-Williams friction coefficient, *L* = pipe section length (when applied to the sprinkler riser pipe, $L = h_r$, $Q = q_s$, and $D = D_r$).

Noting that the velocity head at the sprinkler nozzle, V_{s1}^k, can be given as

$$\frac{(V_{s1}^k)^2}{2g} + hn = \frac{(V_{r1}^k)^2}{2g} + h_{s1}^k \qquad (4)$$

where h_n is energy loss in the nozzle and is assumed here negligible. Eq. 1 can be expressed as:

$$\left(E^d\right)_1^k = \frac{\left(V_{r1}^k\right)^2}{2g} + h_{s1}^k + (h_r + \frac{D_{l1}^k}{2}) + h_{fr} + k_L \frac{\left(V_1^k\right)^2}{2g} \qquad (5)$$

where

$$\left(E^d\right)_1^k = \left(h^d\right)_1^k + \frac{\left(V_1^k\right)^2}{2g} \qquad (6)$$

Using the Darcy-Weisbach equation to compute friction head loss in the sprinkle riser pipe, Eq. 5 can be given as:

$$\left(E^d\right)_1^k = h_{s1}^k + k_{vh} \frac{\left(q_{s1}^k\right)^2}{D_r^4} + k_L k_{vh} \frac{\left(q_{s1}^k\right)^2}{\left(D_{l1}^k\right)^4} + \left(k_{dw} f \frac{\left(q_{s1}^k\right)^2}{D_r^5} + 1 \right) h_r + \frac{D_{l1}^k}{2} \qquad (7)$$

In Eqs. 7, k_{vh} = a dimensional constant of the velocity head term, equivalent to $10^{4.917}$ $(mm)^4 m(s/L)^2$. Note that a similar equation can be derived if Eq. 3 is used to compute friction head loss. In Eq. 7, there are three unknowns $(E^d)_1^k$, h_{s1}^k, and q_{s1}^k. However, h_{s1}^k and q_{s1}^k are related by the pressure head-discharge relationship of the sprinkler, a data provided by the sprinkler manufacturer:

$$q_{s1}^k = \alpha_1 (h_{s1}^k)^{\alpha_2} \qquad (8)$$

In Eq. 8, α_1 $(L/s/m^{\alpha 2})$ and α_2 $(-)$ = empirical curve fitting parameters. Although the velocity head at the sprinkler nozzle is closely approximated by the sum of the velocity head and pressure head in the riser pipe just upstream of the nozzle (Eq. 4), it is a common practice to assume the velocity head upstream of the nozzle as negligible compared to the pressure head there and use a simpler approximation given by Eq. 8 to relate nozzle discharge directly to the pressure head. As will be described in subsequent

sections, the pressure head at the distal sprinkler of the lateral obtaining its supply from the *kth* mainline outlet, h_{s1}^k, is known (sections 3.1-3.3). Given h_{s1}^k, the following procedure can be used to solve Eqs. 7 and 8 for the unknowns, $(E^d)_1^k$ and q_{s1}^k:

1. Specify the desired sprinkler pressure head, h_{s1}^k;
2. Substitute h_{s1}^k in Eq. 8 and compute the corresponding q_{s1}^k;
3. Substitute h_{s1}^k and q_{s1}^k values (steps 1 and 2, above) into Eq. 7 and calculate $(E^d)_1^k$;
4. Calculate V_1^k as a function of Q_1^k and $(D_{l1})^k$ with Eq. 9 and $(h^d)_1^k$ with Eq. 6.

$$V_1^k = k_v \frac{Q_1^k}{\left(D_{l1}^k\right)^2} \qquad (9)$$

In Eq. 9, k_v = a dimensional constant in the equation for computing average cross-sectional velocity, equal to $10^{3.105}(mm)^2m/L$. Note that when Eq. 2 is used to compute friction head loss, a procedure for computing the friction factor, *f*, as a function of *e/D* and *Re* (Zerihun and Sanchez, 2012) is imbedded within the above algorithm (which is iterative for conditions in which $4000<Re$). Although the friction factor varies from lateral to lateral and along a lateral, for notational simplicity *f* is used to represent the friction factor for the entire sprinkler system.

The pressure head at a point just downstream of the second node, $(h^u)_1^k$ (Figure 2), can then be computed with the energy equation written for the distal segment of the lateral obtaining its supply from the *kth* mainline outlet (i.e., the lateral segment between the 1st and 2nd computational nodes):

$$\left(h^u\right)_1^k = \Delta z_1^k + \left(h^d\right)_1^k + k_{dw} f \frac{\left(Q_1^k\right)^2}{\left(D_{l1}^k\right)^5} L_1^k \qquad (10)$$

In Eq. 10, $\Delta z_1^k = (z^d)_1^k - (z^u)_1^k$; (i.e., the elevation difference over the distal lateral segment).

Equations and numerical solution for all segments upstream of the distal segment of a lateral

For all lateral segments upstream of the distal segment computation proceeds as follows: if the computational node at the upstream end of the *jth* lateral segment *(*node *j+1)* is not a sprinkler riser pipe, then the incoming discharge to the computational node, Q_{j+1}^k, is the same as the through-flow discharge, Q_j^k, computed in the preceding step. Hence, the local head loss and associated changes in velocity and pressure head, if any, across the *(j+1)th* node can be computed directly. However, if the *(j+1)th* node consists of a sprinkler riser pipe, then both the incoming discharge to the computational node, Q_{j+1}^k, and the *(j+1)th* sprinkler discharge are unknowns. Two equations derived based on the application of the energy conservation principle across the *(j+1)th* node (along the lateral for the through-flow and along the sprinkler riser pipe), coupled with the sprinkler head-discharge function and the continuity equation (Eq. 2) applied to node *j+1*, can be used to compute the *(j+1)th* sprinkler discharge, q_{sj+1}^k, and pressure head, h_{sj+1}^k. Accordingly, the energy equation for the through flow across the *(j+1)th* node of the lateral is

$$\left(E^d\right)_{j+1}^k = \left(h^u\right)_j^k + k_{vh}\frac{\left(Q_j^k\right)^2}{\left(D_{lj}^k\right)^4} + k_L k_{vh}\frac{Q_{j+1}^2}{\left(D_{lj+1}^k\right)^4} \qquad (11)$$

where k_L = is the local head loss coefficient for the through-flow at the *(j+1)th* node. From continuity at a node we have $Q_{j+1}^k = Q_j^k + q_{sj+1}^k$, hence Eq. 11 is a function of two unknowns: $(E^d)_{j+1}^k$ and q_{sj+1}^k. Noting that the sprinkler discharge, q_{sj+1}^k, is related to the pressure head, h_{sj+1}^k with:

$$q_{sj+1}^k = \alpha_1 (h_{sj+1}^k)^{\alpha_2} \qquad (12)$$

then q_{sj+1}^k and $(E^d)_{j+1}^k$ can be computed iteratively with Eqs. 11 and 12. However, the values of q_{sj+1}^k and $(E^d)_{j+1}^k$ computed as such needs to satisfy the energy equation written between node *j+1* and the *(j+1)th* sprinkler nozzle, Figure 2, given as

$$\left(E^d\right)_{j+1}^k = h_{sj+1}^k + k_{vh}\frac{\left(q_{sj+1}^k\right)^2}{D_r^4} + k_L k_{vh}\frac{\left(Q_{j+1}^k\right)^2}{\left(D_{lj+1}^k\right)^4} + \left(k_{dw} f \frac{\left(q_{sj+1}^k\right)^2}{D_r^5} + 1\right)h_r + \frac{D_{lj+1}^k}{2} \qquad (13)$$

It then follows that Eqs. 11-13 can be solved iteratively for q_{sj+1}^k, h_{sj+1}^k, and $(E^d)_{j+1}^k$ as follows:

1. Initialize q_{sj+1}^{k}: set the iteration index $i = 1$ and let the initial value of q_{sj+1}^{k} be $(q_{sj+1}^{k})^{i}$, a good choice is setting $(q_{sj+1}^{k})^{i} = q_{sj}^{k}$;
2. Noting that $Q_{j+1}^{k} = Q_{j}^{k} + q_{sj+1}^{k}$, substitute $(q_{sj+1}^{k})^{i}$ for q_{sj+1}^{k} and compute $(E^{d})_{j+1}^{k}$ with Eq. 11;
3. Substitute estimates of q_{sj+1}^{k} and $(E^{d})_{j+1}^{k}$ (steps 1 and 2 above) into Eq. 13 and compute an estimate of h_{sj+1}^{k};
4. Substitute estimate of h_{sj+1}^{k} from step 3 above into Eq. 12 and calculate a revised estimate of q_{sj+1}^{k}, $(q_{sj+1}^{k})^{i+1}$;
5. Compute relative error, $\Delta\varepsilon_q$, given as

$$\Delta\varepsilon_q = \frac{\left|\left(q_{sj+1}^{k}\right)^{i+1} - \left(q_{sj+1}^{k}\right)^{i}\right|}{\left(q_{sj+1}^{k}\right)^{i}} \qquad (14)$$

6. If $\Delta\varepsilon_q \leq 10^{-5}$, then the numerical solution has converged and the solution is $(q_{sj+1}^{k})^{i+1}$, computed in step 4 above. On the other hand, if $10^{-5} < \Delta\varepsilon_q$, then set $i = i+1$ and proceed through steps 2 to 6.

The distribution of sprinkler discharge and pressure head as well as the components of total head along a lateral is determined through repeated application of the algorithm presented above to each section of the lateral, sequentially starting from the distal end and proceeding upstream to the inlet end. However, for field-wide simulation or design applications, individual laterals cannot be considered in isolation. In stead, these algorithm need to be coupled with those developed for the mainline.

2.3 Sprinkler mainline hydraulics: introduction and assumptions

As described above, the sprinkler mainline can be considered as a hydraulic manifold consisting of multiple outlets spanning its length (Figure 1). The set of assumptions introduced in the description of lateral hydraulics also apply to mainline hydraulics, presented subsequently. The exception being that instead of sprinkler riser pipes that need to be set vertical (which is the case with laterals), here there are mainline outlet sections with the same longitudinal slopes as the corresponding laterals (Figures 3 and 4). A mainline off-take node can have one or two outlets, each supplying irrigation

water to a lateral with known hydraulic characteristics: discharge and total head, *Q(H)*, function. When a field-scale sprinkler system has a mainline supplying water to a line of laterals installed on one side of the main only, it is described here as a system with single-line laterals layout configuration. If, on the other hand, a sprinkler main has two sets of laterals installed on either side of the main, then it is referred to as a system with double-line laterals layout configuration.

As will be discussed in some detail later, the hydraulic characteristic of each lateral is defined, at a preselected computational node close to its inlet, during the system hydraulic characterization computations (section 3.1). The point at which the hydraulic characteristics of a lateral is defined (hence forth referred to as node of lateral hydraulic characterization, or node ℓ) is set at a distance of $\ell = S_L/2$ from the lateral inlet (Figures 3 and 4), where S_L is the spacing between sprinklers along the lateral. Although node ℓ along a lateral does not represent a physical outlet, for computational purposes it is treated as a mainline outlet and is referred to as such in subsequent discussion. Considering a sprinkler system with a sing-line laterals layout configuration for instance, it can be noted that for a lateral obtaining its supply from the *kth* off-take node of the mainline, the discharge at node ℓ of the lateral, Q_ℓ^k, is equal to the discharge at the lateral inlet, Q_k, but the total head at node ℓ, H_ℓ^k, would be less than that at the lateral inlet, H_k. Because the total head at the inlet to a lateral, H_k, can be determined only as part of the hydraulic computation along the mainline and not as part of the lateral hydraulic characterization phase, the lateral inlet itself cannot be used as the point of lateral hydraulic characterization.

Although the basic principles of manifold hydraulics as applied to a mainline with a single-line or double-line laterals layout configuration remain the same, the number of equations and the numerical solution techniques used are different. Hence, the formulation of the mainline hydraulic problem and associated numerical solution for sprinkler systems with single-line and double-line laterals are described in separate sections.

2.3.1 Sprinkler mainline hydraulics for single-line laterals layout configuration: equations and numerical solutions

The schematics of the distal segment of a sprinkler mainline that supplies irrigation water to a single-line of laterals is shown in Figure 3.

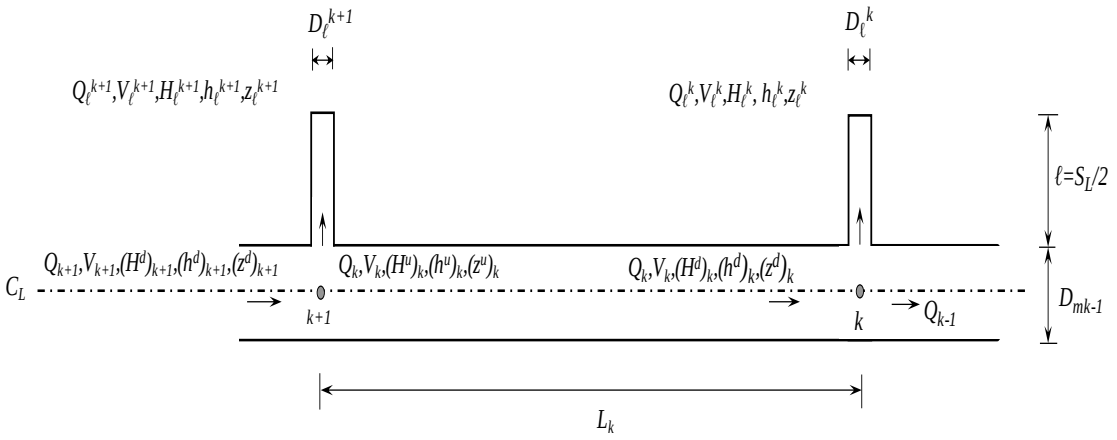

Figure 3 Schematics of the *kth* segment of sprinkler mainline with a single-line of laterals (Definition of the variables *Q*, *V*, *H*, *h*, and *z* is the same as in Figure 2, ℓ = lateral hydraulic characterization node, a point along a lateral at which the hydraulic characteristics of the lateral is defined; the subscripts ℓ and *m* define flow conditions and variables at the hydraulic characterization node of a lateral, respectively. When both the *kth* and *(k+1)th* computational nodes are off-take nodes, hence L_k is equal to lateral spacing, S_m)

Equations and numerical solution for the distal segment of the mainline

Computation starts at the distal end of the main (where $k=1$ and $Q_{k-1} = 0$) and proceeds upstream. When the Darcy-Weisbach equation is used to compute friction head loss, the energy equation between a point just upstream of the distal computational node along the mainline *(k=1)* and the hydraulic characterization node, ℓ, of the distal lateral (which also represents the distal mainline outlet) is given as:

$$\left(E^d\right)_1 = H_\ell^1 - \left(z^d\right)_1 + k_{dw} f \frac{\left(Q_\ell^1\right)^2}{D_{\ell k}^5}\ell + k_L k_{vh} \frac{\left(Q_\ell^1\right)}{D_{m1}^4} \qquad (15)$$

where

$$\left(E^d\right)_1 = \left(h^d\right)_1 + k_{vh} \frac{Q_1^{\,2}}{D_{m1}^4} \qquad (16)$$

and k_L = local head loss coefficient at the inlet to the distal lateral *(-)*. In addition, the lateral discharge at node ℓ (Figure 3), Q_ℓ^l, is related to, H_ℓ^l, as follows

$$Q_\ell^1 = f(H_\ell^1) \qquad (17)$$

Equation 17 represents the hydraulic characteristic curve (a table of values of Q_ℓ^1-H_ℓ^1) for the distal mainline outlet and is generated as part of the hydraulic characterization computation (section 3.1). During mainline hydraulic computations the outlet discharge is interpolated from the lateral hydraulic characteristic table (Q_ℓ^k-H_ℓ^k, for the lateral obtaining its supply from the *kth* mainline off-take node) as a function of H_ℓ^k. For a mainline with single-line of laterals linear interpolation can provide satisfactory accuracy, if used along with a lateral hydraulic characteristics table with sufficiently fine subinterval size. However, as will be discussed subsequently such an approach cannot be used for a mainline with double-line of laterals, because the iterative solution requires evaluation of both the $Q(H_\ell^k)$ function and its derivative. The cubic spline interpolation scheme can interpolate the function value, $Q(H_\ell^k)$ from the lateral hydraulic characteristics table, and also provide approximations of the derivatives, $Q'(H_\ell^k)$, hence it is applied in the model described here. A description of the cubic spline interpolation scheme as applied to the problem of interpolating mainline outlet discharges from the respective lateral hydraulic characteristic tables is presented in section 2.4.

Following the same procedure as that described for laterals; the discharge at the distal mainline outlet (or the inlet discharge for the lateral obtaining its supply from the distal off-take node) Q_ℓ^l, can be computed as follows:

1. Specify H_ℓ^l. As will be discussed subsequently (section 3.1-3.3) for both the system design and simulation options, the total head at the distal mainline outlet, H_ℓ^l, is known from prior computations.
2. Compute Q_ℓ^l, through interpolation, as a function of the corresponding H_ℓ^l (Eq. 17).
3 Substitute H_ℓ^1 and Q_ℓ^1 values obtained in steps 1 and 2 above into Eq. 15 and compute $(E^d)_1$;
4 Calculate V_1 as a function of Q_1 and D_{1l} and then $(h^d)_1$ with Eq. 16;

The energy equation written for the distal mainline segment (i.e., between the 1st and the 2nd computational nodes of the sprinkler main) can be solved for the unknown pressure head at a point just downstream of the 2nd node, $(h^u)_1$ (Figure 3):

$$\left(h^u\right)_1 = \Delta z_1 + \left(h^d\right)_1 + k_{dw} f \frac{Q_1^2}{D_{m1}^5} L_1 \qquad (18)$$

In Eq. 18, $\Delta z_1 = (z^d)_1 - (z^u)_1$ (i.e., elevation difference across the distal mainline segment).

Equations and numerical solution for all segments upstream of the distal segment of a mainline

For all computational nodes upstream of the distal segment the numerical computation proceeds as follows: If the computational node at the upstream end of the *kth* mainline segment (node *k+1*) is not a lateral inlet, then the incoming discharge to the computational node, Q_{k+1}, is the same as the through flow discharge, Q_k, computed in the preceding step. Hence, the local head loss and associated changes in velocity and pressure head, if any, across the *(k+1)th* node can be computed directly. However, if the *(k+1)th* node consists of a lateral inlet, then both the incoming flow to the computational node, Q_{k+1}, and the *(k+1)th* lateral inlet discharge, $Q_\ell{}^{k+1}$, are unknowns. Two equations derived through the application of the energy equation across the *(k+1)th* node (along the mainline and along the inlet segment of the lateral), coupled with the lateral hydraulic characteristics function, $Q(H_\ell^{k+1})$, and the continuity equation applied to the *(k+1)th* node can solved iteratively for the unknowns.

Accordingly, the energy equation for the through-flow across the *(j+1)th* node of the main is

$$\left(E^d\right)_{k+1} = \left(h^u\right)_k + k_{vh} \frac{Q_k^2}{D_{mk}^4} + k_L k_{vh} \frac{Q_{k+1}^2}{D_{mk+1}^4} \qquad (19)$$

In Eq. 19, k_L = the local loss coefficient at the *(k+1)th* node associated with the through flow *(-)*. From continuity at a node we have $Q_{k+1} = Q_k + Q_\ell{}^{k+1}$, hence in Eq. 19 there are two unknowns: $(E^d)_{k+1}$ and Q_ℓ^{k+1}. Noting that the lateral discharge at node ℓ (Figure 3), Q_ℓ^{k+1}, is related to, H_ℓ^{k+1}, with

$$Q_\ell^{k+1} = f(H_\ell^{k+1}) \qquad (20)$$

then Eqs. 19 and 20 can be solved iteratively for the unknowns: H_ℓ^{k+1} and $(E^d)_{k+1}$. However, the values of $(E^d)_{k+1}$ and H_ℓ^{k+1} computed as such need to satisfy the energy equation between a point just upstream of the $(k+1)th$ node and the system characterization node along the $(k+1)th$ lateral.

$$\left(E^d\right)_{k+1} = H_\ell^{k+1} - (z^d)_{k+1} + k_{dw} f \frac{\left(Q_\ell^{k+1}\right)^2}{\left(D_\ell^{k+1}\right)^5} \ell + k_L k_{vh} \frac{Q_{k+1}^2}{D_{mk+1}^4} \qquad (21)$$

Although the model can simulate a sprinkler system in which the distance between the mainline off-take node and the corresponding outlet, ℓ, is variable from lateral to lateral; for reasons of notational simplicity, in Eq. 15, the notation ℓ is used for the entire system. Note that in Eq. 21, the friction factor as well is variable.

It then follows that Eqs. 19-21 can be solved iteratively for Q_ℓ^{k+1}, H_ℓ^{k+1}, and $(E^d)_{k+1}$ as follows:

1. Initialize Q_ℓ^{k+1}, set the iteration index $i = 1$ and let the initial estimate of Q_ℓ^{k+1} be $(Q_\ell^{k+1})^i$. A good choice for $(Q_\ell^{k+1})^i$ is Q_ℓ^k.
2. Noting that $Q_{k+1} = Q_k + Q_\ell^{k+1}$, substitute $(Q_\ell^{k+1})^i$ for Q_ℓ^{k+1} in Eq. 19 and compute $(E^d)_{k+1}$.
3. Substitute estimates of Q_ℓ^{k+1} and $(E^d)_{k+1}$ obtained in steps 1 and 2 above into Eq. 21 and calculate H_ℓ^{k+1}.
4. Substitute estimates of H_ℓ^{k+1} into Eq. 20 and calculate a revised estimate of Q_ℓ^{k+1}, $(Q_\ell^{k+1})^{i+1}$;
5. Compute relative error, $\Delta\varepsilon_Q$, with

$$\Delta\varepsilon_{Q_\ell} = \frac{\left|\left(Q_\ell^{k+1}\right)^{i+1} - \left(Q_\ell^{k+1}\right)^i\right|}{\left(Q_\ell^{k+1}\right)^i} \qquad (22)$$

6. If $\Delta\varepsilon_{Q\ell} \le 10^{-5}$, then the numerical solution has converged and the solution is $(Q_\ell^{k+1})^{i+1}$. On the other hand, if $10^{-5} < \Delta\varepsilon_{Q\ell}$, then set $i = i+1$ and proceed through steps 2-6.

Repeated applications of the numerical algorithms described above at each of the mainline computational nodes are used to determine, the distribution of total head and its

components and lateral inlet discharges along the mainline, for a sprinkler system with single-line laterals layout configuration. Description of the procedures used to couple the numerical solutions of the lateral and mainline hydraulic equations is presented in sections 2.4 and 3.1. As indicated above, for systems with double-line laterals layout configuration the number of equations and applicable numerical solutions are different and will be developed in subsequent sections.

2.3.2 Sprinkler mainline hydraulics for double-line laterals layout configuration: equations and numerical solution

A schematics of a typical segment (the *kth* pipe section) of a sprinkler main with double-line laterals is depicted in Figure 4. Variables with the subscript *k* represent flow conditions and geometric variables at the *kth* computational node of the main, numbered sequentially in ascending order starting from the distal end, where $k = 1$ and $Q_{k-1} = 0$ (Figure 4). As can be noted from Figure 4, a sprinkler main with a double-line of laterals has two sets of outlets, each installed on either side of the mainline. Note that the lateral configuration considered here assumes that each mainline off-take node supplies irrigation water to a pair of outlets. As described in section 2.3.1, each mainline outlet represents a lateral with a known hydraulic characteristic curve: discharge and total head

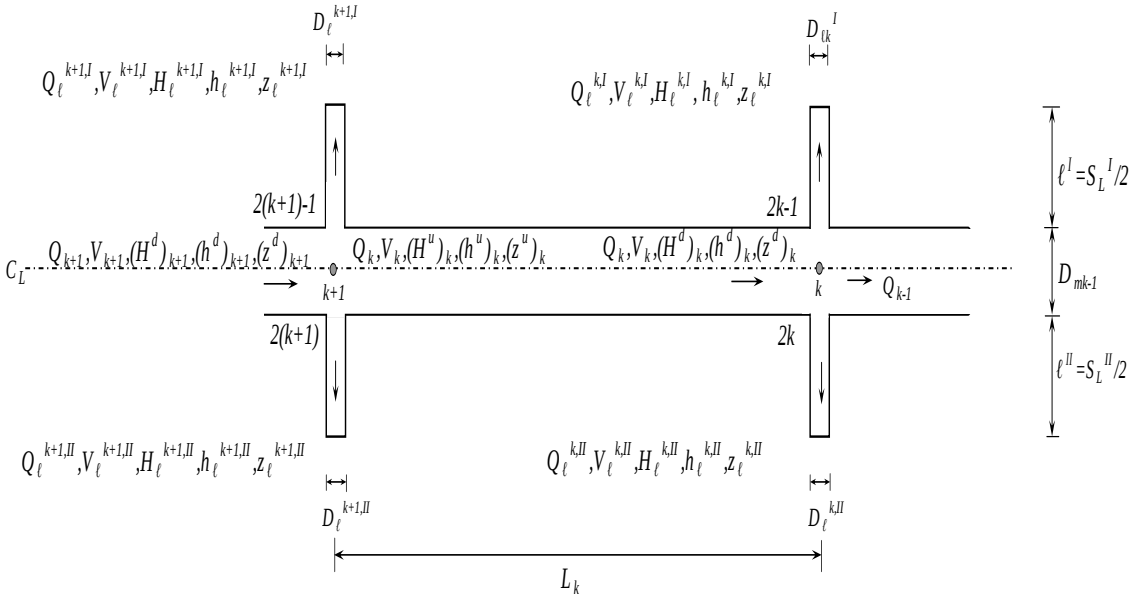

Figure 4 Schematics of the *kth* segment and the *kth* and the *(k+1)th* off-take nodes of a sprinkler mainline for a system with double-line laterals layout configuration

(Q_ℓ -H_ℓ) function. The numbering of laterals here is such that each pair obtaining its supply from the same mainline off-take node is numbered sequentially starting from the distal end (Figure 4). This results in an arrangement in which laterals installed on one side of the main are odd-numbered and those installed on the other as even-numbered. Hence, as can be noted from Figure 4, variables defining flow conditions at any given mainline outlet are superscripted with the nodal index, *k* (which identifies the corresponding mainline off-take node) and the notations *I* or *II*, identifying whether the outlet represents an odd-numbered or even-numbered lateral, respectively.

Equations and numerical solution for the distal segment of the mainline

Numerical computation along the mainline starts at the distal node, in which case the mainline off-take node index, *k = 1*, and the residual outflow $Q_{k-1} = 0$ (Figure 4). Based on the principles of energy conservation two equations can be written between a point just upstream of the distal off-take node along the mainline and the corresponding outlets. Following the approach described for single-line laterals (section 2.3.1) and using the Darcy-Weisbach equation to compute friction head loss (noting that a similar set of equations can be derived if the Hazen-Williams equation is used instead), the energy equation between a point just upstream of the distal off-take node of the mainline (*k = 1*) and the odd-numbered outlet obtaining its supply from the same node is given as

$$\left(E^d\right)_k = H_\ell^{1,I} - \left(z^d\right)_k + k_{dw} f^I \frac{\left(Q_\ell^{1,I}\right)^2}{\left(D_\ell^{1,I}\right)^5} \ell^I + k_L^I k_{vh} \frac{Q_1^2}{D_{m1}^4} \qquad (23)$$

and along the path between the distal off-take node of the mainline and the even-numbered outlet at the same computational node is given as

$$\left(E^d\right)_1 = H_\ell^{1,II} - \left(z^d\right)_1 + k_{dw} f^{II} \frac{\left(Q_\ell^{1,II}\right)^2}{\left(D_\ell^{1,II}\right)^5} \ell^{II} + k_L^{II} k_{vh} \frac{Q_1^2}{D_{m1}^4} \qquad (24)$$

In Eqs. 23 and 24, k_L^I *(-)* and k_L^{II} *(-)* = local head loss coefficients for the flow into the odd-numbered and the even-numbered outlets, respectively, and f^I *(-)* and f^{II} *(-)* = the friction factor for the odd-numbered and even-numbered mainline outlet pipe sections, respectively. Equations 23 and 24 consist of six unknowns: the sum of pressure head and

velocity head at a point just upstream of the distal computational node of the mainline, $(E^d)_1$; the total head at the mainline outlets obtaining their supply from the distal off-take node, $H_\ell^{1,I}$ and $H_\ell^{1,II}$, and the corresponding discharges, $Q_\ell^{1,I}$ and $Q_\ell^{1,II}$; and the mainline discharge in the distal segment, Q_1. Applying the principle of continuity at the distal off-take node results in

$$Q_k = Q_\ell^{1,I} + Q_\ell^{1,II} \qquad (25)$$

The functional relationship between the mainline outlet discharge and the corresponding total head can be expressed as:

$$Q_\ell^{1,I} = f(H_\ell^{1,I}) \qquad (26)$$

for the odd-numbered outlet and

$$Q_\ell^{1,II} = f(H_\ell^{1,II}) \qquad (27)$$

for the even-numbered outlet. As described in the section 2.3.1 above, Eqs. 26 and 27 represent a table of values generated during the system hydraulic characterization computation (section 3.1). Hence, in the course of a numerical solution of the mainline hydraulic equations, outlet discharges ($Q_\ell^{k,I}$ or $Q_\ell^{k,II}$) are to be interpolated from the corresponding outlet hydraulic characteristics curves ($Q_\ell^{k,I}$-$H_\ell^{k,I}$ or $Q_\ell^{k,II}$-$H_\ell^{k,II}$) with the cubic-spline interpolation scheme (section 2.4). Substituting Eqs. 25-27 in Eqs. 23 and 24 results in two equations in three unknowns, which can be combined into a nonlinear equation in two unknowns, $H_\ell^{1,I}$ and $H_\ell^{1,II}$:

$$H_\ell^{1,I} - H_\ell^{1,II} + \alpha_1 \left[Q\left(H_\ell^{1,I}\right)\right]^2 + \alpha_2 \left[Q\left(H_\ell^{1,II}\right)\right]^2 + \alpha_3 Q_\ell^{1,I} Q_\ell^{1,II} = 0 \qquad (28)$$

In Eq. 28

$$\alpha_1 = \frac{\alpha_3}{2} + \frac{k_{dw} f^I \ell^I}{\left(D_\ell^{1,I}\right)^5}, \quad \alpha_2 = \frac{\alpha_3}{2} - \frac{k_{dw} f^{II} \ell^{II}}{\left(D_\ell^{1,II}\right)^5}, \quad \text{and} \quad \alpha_3 = \frac{2k_{vh}\left[k_L^I - k_L^{II}\right]}{D_{m1}^4} \qquad (29)$$

Note that in Eq. 29, the variables f^I and f^{II} represent the Darcy-Weisbach friction factor for the odd- and even-numbered mainline outlet pip sections, respectively, and they are a

function of pipe absolute roughness, diameter, and Reynolds number, *Re*. On the other hand, if the Hazen-Williams equation is used, instead, to compute friction head loss the friction coefficient is considered constant for a given pipe material. Given the total head at one of the mainline outlets, Eq. 28 can be solved iteratively for the other unknown. Following the approach presented for a system with single-line laterals layout configuration, and considering (for computational purposes) the odd-numbered outlet at the distal off-take node (Figure 4) as the distal outlet of the mainline; the total head at the distal outlet is given as $H_\ell^{1,I}$ and can be considered known (section 3.1-3.3). In which case, the only unknown in Eq. 28 is $H_\ell^{1,II}$. Using the Newton-Raphson method, the following recursive formula is used to compute $H_\ell^{1,II}$ iteratively:

$$\left[H_\ell^{1,II}\right]^{i+1} = \left[H_\ell^{1,II}\right]^{i} - \frac{F\left(\left[H_\ell^{1,II}\right]^{i}\right)}{F'\left(\left[H_\ell^{1,II}\right]^{i}\right)} \qquad (30)$$

In Eq. 30, $F\left(\left[H_\ell^{1,II}\right]^{i}\right)$ is an approximation of Eq. 28 based on the value of $H_\ell^{1,I}$ at the *ith* iteration, $\left[H_\ell^{1,II}\right]^{i}$:

$$F\left(\left[H_\ell^{1,II}\right]^{i}\right) = \alpha_2\left(Q\left(\left[H_\ell^{1,II}\right]^{i}\right)\right)^2 + \alpha_4 Q\left(\left[H_\ell^{1,II}\right]^{i}\right) - \left[H_\ell^{1,II}\right]^{i} + \alpha_5 \qquad (31)$$

and $F'\left(\left[H_\ell^{1,II}\right]^{i}\right)$ is the derivative of Eq. 28 evaluated based on the value of $H_\ell^{1,II}$ at the *ith* iteration, $\left[H_\ell^{1,II}\right]^{i}$:

$$F'\left(\left[H_\ell^{1,II}\right]^{i}\right) = \left.\frac{dF}{dH_\ell^{1,II}}\right|_{\left[H_\ell^{1,II}\right]^{i}} = 2\alpha_2\left(Q\left(H_\ell^{1,II}\right)^{i}\right)Q'\left(\left[H_\ell^{1,II}\right]^{i}\right) + \alpha_4 Q'\left(\left[H_\ell^{1,II}\right]^{i}\right) + \alpha_6\left(Q\left(\left[H_\ell^{1,II}\right]^{i}\right)\right)^2 f^{II\,\prime}\left(\left[H_\ell^{1,II}\right]^{i}\right) - 1.0 \qquad (32)$$

where

$$\alpha_4 = \alpha_3 Q\left(H_\ell^{1,I}\right), \quad \alpha_5 = \alpha_1 Q\left(H_\ell^{1,I}\right)^2 + H_\ell^{1,I}, \text{ and } \quad \alpha_6 = -\frac{k_{dw}\ell^{II}}{\left(D_\ell^{1,II}\right)^5},$$

$$Q'\left(\left[H_\ell^{1,II}\right]^{i}\right) = \left.\frac{dQ}{dH_\ell^{1,II}}\right|_{\left[H_\ell^{1,II}\right]^{i}} \qquad (33)$$

$$\left.\begin{aligned} f^{II\prime}\left(\left[H_\ell^{1,II}\right]^i\right) &= \frac{-81.472}{\nu D_\ell^{1,II}\left(\boldsymbol{Re}\left(\left[H_\ell^{1,II}\right]^i\right)\right)^2} Q'\left(\left[H_\ell^{1,II}\right]^i\right) \quad for \quad \boldsymbol{Re} \le 4000, and \\ f^{II\prime}\left(\left[H_\ell^{1,II}\right]^i\right) &= -18.7\frac{\boldsymbol{Re}\left(\left[H_\ell^{1,II}\right]^i\right) f^{II\prime}\left(\left[H_\ell^{1,II}\right]^i\right) + \left(\frac{2.546}{\nu D_\ell^{1,II}}\right) Q'\left(\left[H_\ell^{1,II}\right]^i\right) f^{II}\left(\left[H_\ell^{1,II}\right]^i\right)}{\left(\frac{e}{D_\ell^{1,II}} + \frac{9.35}{\boldsymbol{Re}\left(\left[H_\ell^{1,II}\right]^i\right)\sqrt{f^{II}\left(\left[H_\ell^{1,II}\right]^i\right)}}\right)\left(\boldsymbol{Re}\left(\left[H_\ell^{1,II}\right]^i\right)\right)^2} \quad for \quad 4000 < \boldsymbol{Re} \end{aligned}\right\} \quad (34)$$

In Eq. 34, $f^{II\prime}([H_\ell^{1,II}]^i)$ = is the derivative of the Darcy-Weisbach friction factor for the even-numbered outlet pipe section obtaining its supply from the distal mainline off-take node, ν = the kinematic viscosity of water (m^2/s), $D_\ell^{1,II}$ = the diameter of the even-numbered outlet pipe section obtaining its supply from the distal mainline off-take node (mm), e = pipe absolute roughness (mm), and Re = Reynolds number (-). The mainline outlet discharge, $Q_\ell^{1,I}$ and $Q_\ell^{1,II}$, is interpolated as a function of the total head, $H_\ell^{1,I}$ and $H_\ell^{1,II}$, from the lateral hydraulic characteristics table with a cubic polynomial of the form (section 2.4):

$$Q_\ell^{1,II} = \beta_{n,1}^{1,II} + \beta_{n,2}^{1,II}\left(H_\ell^{1,II} - \left[H_\ell^{1,II}\right]_n\right) + \beta_{n,3}^{1,II}\left(H_\ell^{1,II} - \left[H_\ell^{1,II}\right]_n\right)^2 + \beta_{n,4}^{1,II}\left(H_\ell^{1,II} - \left[H_\ell^{1,II}\right]_n\right)^3 \quad (35)$$

It then follows

$$\left.\frac{dQ}{dH_\ell^{1,II}}\right|_{\left[H_\ell^{1,II}\right]^i} = \beta_{n,2}^{1,II} + 2\beta_{n,3}^{1,II}\left(\left[H_\ell^{1,II}\right]^i - \left[H_\ell^{1,II}\right]_n\right) + 3\beta_{n,4}^{1,II}\left(\left[H_\ell^{1,II}\right]^i - \left[H_\ell^{1,II}\right]_n\right)^2 \quad (36)$$

In Eqs. 35 and 36, $\beta_{n,1}^{1,II}$, $\beta_{n,2}^{1,II}$, $\beta_{n,3}^{1,II}$, and $\beta_{n,4}^{1,II}$ = parameters of the interpolating polynomial for the *nth* subinterval of the hydraulic characteristics table of the even-numbered outlet at the distal off-take node, n = the index of the subinterval in which $[H_\ell^{1,II}]_n \le [H_\ell^{1,II}]^i \le [H_\ell^{1,II}]_{n+1}$, and $[H_\ell^{1,II}]_n$ and $[H_\ell^{1,II}]_{n+1}$ = the total head corresponding to the lower and upper limits, respectively, of the *nth* subinterval of the outlet hydraulic characteristic curve. The iterative solution of Eq. 28 proceeds as follows:

1. Set the iteration index, $i = 1$, and $\left[H_{\ell}^{1,II}\right]^{i} = H_{\ell}^{1,I}$;

2. Evaluate Eq. 31 as a function of $\left[H_{\ell}^{1,II}\right]^{i}$;

3. If $F\left(\left[H_{\ell}^{1,II}\right]^{i}\right) \leq 10^{-5}$, the numerical solution has converged and end computation. If, on the other hand, $10^{-5} < F\left(\left[H_{\ell}^{1,II}\right]^{i}\right)$ proceed to the next step;

4. Compute $\left[H_{\ell}^{1,II}\right]^{i+1}$ as a function of $\left[H_{\ell}^{1,II}\right]^{i}$ (Eq. 30);

5. Set $i = i+1$, Evaluate Eq. 31 as a function of $\left[H_{\ell}^{1,II}\right]^{i}$;

6. If $F\left(\left[H_{\ell}^{1,II}\right]^{i}\right) \leq 10^{-5}$ the numerical solution has converged and end computation. If, on the other hand, $10^{-5} < F\left(\left[H_{\ell}^{1,II}\right]^{i}\right)$ repeat steps 4 through 6.

Once the total head at each of the distal outlets ($H_{\ell}^{1,I}$ and $H_{\ell}^{1,II}$) is computed the corresponding discharges ($Q_{\ell}^{1,I}$ and $Q_{\ell}^{1,II}$) as well emerge from the solution. The discharge through the distal segment of the mainline, Q_1, can then be computed with Eq. 25. The velocity head at a point just upstream of the distal off-take node of the mainline can be computed as a function of Q_1 and D_{m1}. The sum of the pressure head and velocity head at a point just upstream of the distal off-take node, $(E^d)_1$, can then be computed with Eqs. 23 or 24 and the corresponding pressure head, $(h^d)_1$, follows from Eq. 16. The pressure head at a point just downstream of the *(k+1)th* node, $(h^u)_1$ (Figure 4), can then be computed with the energy equation written for the distal segment of the mainline (i.e., between the 1st and 2nd nodes of the sprinkler main), with Eq. 18.

Equations and numerical solution for all segments upstream of the distal segment of the mainline

For all mainline segments upstream of the distal segment, say the *kth* mainline segment (Figure 4), computation proceeds as follows: If the computational node at the upstream end of the *kth* mainline segment (node *k+1*) is not a lateral inlet, then the incoming discharge to the computational node, Q_{k+1}, is the same as the through flow discharge, Q_k, computed in the preceding step. Hence, the local head loss and associated changes in velocity and pressure head, if any, across the *(k+1)th* node can be computed

directly. However, if the *(k+1)th* node consists of a lateral inlet, then both the incoming flow to the computational node, Q_{k+1}, and the *(k+1)th* lateral inlet discharge, Q_ℓ^{k+1}, are unknowns. Three equations derived through the application of the energy equation across the *(k+1)th* node (along the mainline and along the inlet segments of the laterals), coupled with the lateral hydraulic characteristics functions, $Q(H_\ell^{k+1,I})$ and $Q(H_\ell^{k+,I1})$, and the continuity equation applied to the *(k+1)th* node can solved iteratively for the unknowns.

Following the approach described for systems with single-line laterals layout configuration, the energy equation for the through flow across the *(k+1)th* node can be obtained by adapting Eq. 19 for the *(k+1)th* node. In addition, two equations with the same form as those of Eqs. 23 and 24 can be derived between a point just upstream of the *(k+1)th* off-take node of the mainline and each of the outlets obtaining their supply from the *(k+1)th* node. The energy equation between the *(k+1)th* off-take node and the corresponding odd-numbered lateral is

$$\left(E^d\right)_{\boldsymbol{k+1}} = H_\ell^{\boldsymbol{k+1,I}} - \left(z^d\right)_{k+1} + k_{dw} f^{\,I} \frac{\left(Q_\ell^{k+1,I}\right)^2}{\left(D_\ell^{\boldsymbol{k+1,I}}\right)^5} \ell^{\,I} + k_L^I k_{vh} \frac{Q_{k+1}^2}{D_{mk+1}^4} \qquad (37)$$

and along the path between the (*k+1)th* off-take node of the mainline and the even-numbered outlet at the same computational node is given as

$$\left(E^d\right)_{\boldsymbol{k}+1} = H_\ell^{k+1,II} - \left(z^d\right)_{\boldsymbol{k+1}} + k_{dw} f^{\,II} \frac{\left(Q_\ell^{\boldsymbol{k+1},II}\right)^2}{\left(D_\ell^{\boldsymbol{k+1},II}\right)^5} \ell^{\,II} + k_L^{II} k_{vh} \frac{Q_{k+1}^2}{D_{mk+1}^4} \qquad (38)$$

Eqs. 19, 37, and 38 are functions of six variables: $(E^d)_{k+1}$, $H_\ell^{\,k+1,I}$, $H_\ell^{\,k+1,II}$, $Q_\ell^{\,k+1,I}$, $Q_\ell^{\,k+1,II}$, and Q_{k+1}. Application of the principle of continuity at the *(k+1)th* mainline off-take node yields

$$Q_{k+1} = Q_k + Q_\ell^{\boldsymbol{k+1,I}} + Q_\ell^{\boldsymbol{k+1,II}} \qquad (39)$$

Considering the hydraulic characteristics functions of the corresponding odd-numbered and even-numbered outlets, two additional equations of the form given in Eqs. 26 and 27 can be obtained. Substituting Eq. 39 and applicable hydraulic characteristics functions in Eqs. 19, 37, and 38 and rearranging results in:

$$\left(E^d\right)_{k+1} + \phi_1\left[Q_\ell^{k+1,I}\right]^2 + \phi_1\left[Q_\ell^{k+1,II}\right]^2 + 2\phi_1 Q_\ell^{k+1,I} Q_\ell^{k+1,II} + 2\phi_1 Q_k Q_\ell^{k+1,I} + 2\phi_1 Q_k Q_\ell^{k+1,II} + \lambda_1 = 0 \quad (40)$$

$$\left(E^d\right)_{k+1} + \phi_2\left[Q_\ell^{k+1,I}\right]^2 + \phi_3\left[Q_\ell^{k+1,II}\right]^2 + 2\phi_3 Q_\ell^{k+1,I} Q_\ell^{k+1,II} + 2\phi_3 Q_k Q_\ell^{k+1,I} + 2\phi_3 Q_k Q_\ell^{k+1,II} - H_\ell^{k+1,I} + \lambda_2 = 0 \quad (41)$$

$$\left(E^d\right)_{k+1} + \phi_4\left[Q_\ell^{k+1,I}\right]^2 + \phi_5\left[Q_\ell^{k+1,II}\right]^2 + 2\phi_4 Q_\ell^{k+1,I} Q_\ell^{k+1,II} + 2\phi_4 Q_k Q_\ell^{k+1,I} + 2\phi_4 Q_k Q_\ell^{k+1,II} - H_\ell^{k+1,II} + \lambda_3 = 0 \quad (42)$$

where ϕ_1, ϕ_2, ϕ_3, ϕ_4, and ϕ_5 are coefficients and λ_1, λ_2, and λ_3 are constants in Eqs. 40-42, given as:

$$\left.\begin{aligned}
&\phi_1 = -\frac{k_{vh} k_L}{D_{mk+1}^4}, \quad \lambda_1 = -\left(h^u\right)_k - \left(\frac{k_{vh}}{D_{mk}^4} - \phi_1\right) Q_k^2, \qquad \phi_2 = \phi_3 - \frac{k_{dw} f^I \ell^I}{\left(D_\ell^{k+1,I}\right)^5}, \\
&\phi_3 = -\frac{k_{vh} k_L^I}{D_{mk+1}^4}, \quad \lambda_2 = \left(z^d\right)_{k+1} + \phi_3 Q_k^2, \quad \phi_4 = -\frac{k_{vh} k_L^{II}}{D_{mk+1}^4}, \\
&\phi_5 = \phi_4 - \frac{k_{dw} f^{II} \ell^{II}}{\left(D_\ell^{k+1,II}\right)^5}, \quad \lambda_3 = \left(z^d\right)_{k+1} + \phi_4 Q_k^2,
\end{aligned}\right\} \quad (43)$$

Because the mainline outlet discharges, $Q_\ell{}^{k+1,I}$ and $Q_\ell{}^{k+1,II}$, are functions of, $H_\ell{}^{k+1,I}$ and $H_\ell{}^{k+1,II}$ (i.e., functions of the from given by Eqs. 26 and 27, applicable to the *(k+1)th* node), it can be noted that Eqs. 40-42 represent a system of nonlinear equations with three unknowns ($(E^d)_{k+1}$, $H_\ell{}^{k+1,I}$, and $H_\ell{}^{k+1,II}$) that can be solved iteratively. With the Newton-Raphson method, a system of linear equations of the form given in Eq. 44 is solved during each iterative step:

$$\boldsymbol{J}^i \delta \boldsymbol{x}^{i+1} = -\boldsymbol{F}^i \quad (44)$$

In Eq. 44, following convention the bold faced variables represent a matrix or vectors; $\boldsymbol{J}^i$ = the Jacobian matrix, for Eqs. 40-42, evaluated based on the values of the variables at the *ith* iteration, $\delta \boldsymbol{x}^{i+1}$ = vector of the incremental change in the variables during the *(i+1)th* iteration, and $\boldsymbol{F}^i$ = the function vector evaluated based on the values of the variables at the *ith* iteration:

$$\boldsymbol{J}^i=\begin{pmatrix}\nabla\boldsymbol{F}_1^i\\ \nabla\boldsymbol{F}_2^i\\ \nabla\boldsymbol{F}_3^i\end{pmatrix},\ \delta\boldsymbol{x}^{i+1}=\begin{pmatrix}\left[\left(E^d\right)_{k+1}\right]^{i+1}-\left[\left(E^d\right)_{k+1}\right]^i\\ \left[H_\ell^{k+1,I}\right]^{i+1}-\left[H_\ell^{k+1,I}\right]^i\\ \left[H_\ell^{k+1,II}\right]^{i+1}-\left[H_\ell^{k+1,II}\right]^i\end{pmatrix},\ and\ \boldsymbol{F}^i=\begin{pmatrix}F_1\left(\left[\left(E^d\right)_{k+1}\right]^i,\left[H_\ell^{k+1,I}\right]^i,\left[H_\ell^{k+1,II}\right]^i\right)\\ F_2\left(\left[\left(E^d\right)_{k+1}\right]^i,\left[H_\ell^{k+1,I}\right]^i,\left[H_\ell^{k+1,II}\right]^i\right)\\ F_3\left(\left[\left(E^d\right)_{k+1}\right]^i,\left[H_\ell^{k+1,I}\right]^i,\left[H_\ell^{k+1,II}\right]^i\right)\end{pmatrix}\quad(45)$$

In Eq. 45, $F_1{}^i$, $F_2{}^i$, and $F_3{}^i$ are the functions given in Eqs. 40-42, respectively, evaluated based on the values of the variables at the *ith* iteration and $\nabla\boldsymbol{F}$ is the transpose of the gradient vector of the function, $\boldsymbol{F}$. The elements of the Jacobian matrix evaluated based on the values of the variables at the *ith* iteration are

$$\left.\frac{\partial F_1}{\partial\left(E^d\right)_{k+1}}\right|_{\left[\left(E^d\right)_{k+1}\right]^i}=1.0,\ \left.\frac{\partial F_1}{\partial H_\ell^{k+1,I}}\right|_{\left[H_\ell^{k+1,I}\right]^i}=2\phi_1\xi_1^iQ'\left(\left[H_\ell^{k+1,I}\right]^i\right),\quad and$$

$$\left.\frac{\partial F_1}{\partial H_\ell^{k+1,II}}\right|_{\left[H_\ell^{k+1,II}\right]^i}=2\phi_1\xi_1^iQ'\left(\left[H_\ell^{k+1,II}\right]^i\right)\qquad(46)$$

$$\left.\frac{\partial F_2}{\partial\left(E^d\right)_{k+1}}\right|_{\left[\left(E^d\right)_{k+1}\right]^i}=1.0,\ \left.\frac{\partial F_2}{\partial H_\ell^{k+1,I}}\right|_{\left[H_\ell^{k+1,I}\right]^i}=2\xi_2^iQ'\left(\left[H_\ell^{k+1,I}\right]^i\right)$$

$$+\phi_6\left(Q\left(\left[H_\ell^{k+1,I}\right]^i\right)\right)^2f^{I\prime}\left(\left[H_\ell^{k+1,I}\right]^i\right)-1.0,\ and\ \left.\frac{\partial F_2}{\partial H_\ell^{k+1,II}}\right|_{\left[H_\ell^{k+1,II}\right]^i}=2\phi_3\xi_1^iQ'\left(\left[H_\ell^{k+1,II}\right]^i\right)\quad(47)$$

$$\left.\frac{\partial F_3}{\partial\left(E^d\right)_{k+1}}\right|_{\left[\left(E^d\right)_{k+1}\right]^i}=1.0,\left.\frac{\partial F_3}{\partial H_\ell^{k+1,I}}\right|_{\left[H_\ell^{k+1,I}\right]^i}=2\phi_4\xi_1^iQ'\left(\left[H_\ell^{k+1,I}\right]^i\right),\ and$$

$$\left.\frac{\partial F_3}{\partial H_\ell^{k+1,II}}\right|_{\left[H_\ell^{k+1,II}\right]^i}=2\xi_3^iQ'\left(\left[H_\ell^{k+1,II}\right]^i\right)+\phi_7\left(Q\left(\left[H_\ell^{k+1,II}\right]^i\right)\right)^2f^{II\prime}\left(\left[H_\ell^{k+1,I}\right]^i\right)-1.0\qquad(48)$$

Where

$$\left.\begin{aligned}&Q'\left(\left[H_\ell^{k+1,I}\right]^i\right)=\left.\frac{\partial Q(H_\ell^{k+1,I})}{\partial H_\ell^{k+1,I}}\right|_{\left[H_\ell^{k+1,I}\right]^i},\quad Q'\left(\left[H_\ell^{k+1,II}\right]^i\right)=\left.\frac{\partial Q(H_\ell^{k+1,II})}{\partial H_\ell^{k+1,II}}\right|_{\left[H_\ell^{k+1,II}\right]^i},\\ &\xi_1^i=Q\left(\left[H_\ell^{k+1,I}\right]^i\right)+Q\left(\left[H_\ell^{k+1,II}\right]^i\right)+Q_k\ ,\ \ \xi_2^i=\phi_2Q\left(\left[H_\ell^{k+1,I}\right]^i\right)+\phi_3\left\{Q\left(\left[H_\ell^{k+1,II}\right]^i\right)+Q_k\right\},\\ &\xi_3^i=\phi_4\left\{Q\left(\left[H_\ell^{k+1,I}\right]^i\right)+Q_k\right\}+\phi_5Q\left(\left[H_\ell^{k+1,II}\right]^i\right),\ \phi_6=-\frac{k_{dw}\ell^I}{\left(D_\ell^{k+1,I}\right)^5},\ \phi_7=-\frac{k_{dw}\ell^{II}}{\left(D_\ell^{k+1,II}\right)^5},\end{aligned}\right\}\qquad(49)$$

$$\left.\begin{aligned} f'\left(\left[H_\ell\right]^i\right) &= \frac{-81.472}{vD_\ell\left(Re\left(\left[H_\ell\right]^i\right)\right)^2} Q'\left(\left[H_\ell\right]^i\right) \quad for \quad Re \le 4000, \text{ and} \\ f'\left(\left[H_\ell\right]^i\right) &= -18.7\frac{Re\left(\left[H_\ell\right]^i\right) f'\left(\left[H_\ell\right]^i\right) + \left(\frac{2.546}{vD_\ell}\right) Q'\left(\left[H_\ell\right]^i\right) f\left(\left[H_\ell\right]^i\right)}{\left(\frac{e}{D_\ell} + \frac{9.35}{Re\left(\left[H_\ell\right]^i\right)\sqrt{f\left(\left[H_\ell\right]^i\right)}}\right)\left(Re\left(\left[H_\ell\right]^i\right)\right)^2} \quad for \quad 4000 < Re \end{aligned}\right\} \quad (50)$$

In Eq. 50, $f'([H_\ell]^i)$ = the derivative of the Darcy-Weisbach friction factor for a mainline outlet pipe section, which could be odd- or even-numbered. Note that H_ℓ and D_ℓ need to be superscripted with appropriate indices depending on the mainline off-take node and outlet combination.

The iterative solution of the nonlinear system of equations (Eqs. 40-42) proceeds as follows:

1. Set iteration index $i = 1$ and initialize variables: $\left[H_\ell^{k+1,I}\right]^i = H_\ell^{k,I}$ and $\left[H_\ell^{k+1,II}\right]^i = H_\ell^{k,II}$ and compute $\left[\left(E^d\right)_{k+1}\right]^i$ with Eq. 40;
2. Substitute $\left[\left(E^d\right)_{k+1}\right]^i$, $\left[H_\ell^{k+1,I}\right]^i$, and $\left[H_\ell^{k+1,II}\right]^i$ in Eqs. 41 and 42 and compute $F_2{}^i$ and $F_3{}^i$;
3. If both $F_2{}^i$ and $F_3{}^i$ are less than 10^{-5}, solution has converged and end computation. If, on the other hand, either of the function values ($F_2{}^i$ or $F_3{}^i$) exceed 10^{-5}, then proceed to the next step;
4. Compute the elements of the Jacobian matrix, $\boldsymbol{J}^i$, based on the values of the variables at the *ith* iteration (Eqs. 46-48);
5. Solve Eq. 44 for $\delta\boldsymbol{x}^{i+1}$ with Cramer's rule:

   5a. Compute the determinant of the Jacobian matrix, $\Delta\boldsymbol{J}^i$, based on the values of the variables at the *ith* iteration;

   5b. Compute $\delta\boldsymbol{x}^{i+1}$ with Eq. 51:

$$\left[\delta\left(E^d\right)_{k+1}\right]^{i+1} = \frac{\Delta\left(\left(E^d\right)_{k+1}\right)^i}{\Delta\boldsymbol{J}^i}, \left[\delta H_\ell^{k+1,I}\right]^{i+1} = \frac{\Delta\left(H_\ell^{k+1,I}\right)^i}{\Delta\boldsymbol{J}^i}, \text{ and } \left[\delta H_\ell^{k+1,II}\right]^{i+1} = \frac{\Delta\left(H_\ell^{k+1,II}\right)^i}{\Delta\boldsymbol{J}^i} \quad (51)$$

In Eq. 51, Δ(.) = the determinant of matrix (.). The matrices corresponding to the numerators of Eq. 51; $\left(\left(E^d\right)_{k+1}\right)^i$, $\left(H_\ell^{k+1,I}\right)^i$, and $\left(H_\ell^{k+1,II}\right)^i$; are obtained by modifying the Jacobian matrix at the *ith* iteration, $\boldsymbol{J}^i$, through substitution of the function vector, $\boldsymbol{F}^i$, at an appropriate column corresponding to each variable;

5c. Update the variables: $\left[\left(E^d\right)_{k+1}\right]^{i+1} = \left[\left(E^d\right)_{k+1}\right]^i + \left[\delta\left(E^d\right)_{k+1}\right]^{i+1}$,

$\left[H_\ell^{k+1,I}\right]^{i+1} = \left[H_\ell^{k+1,I}\right]^i + \left[\delta H_\ell^{k+1,I}\right]^{i+1}$, and $\left[H_\ell^{k+1,II}\right]^{i+1} = \left[H_\ell^{k+1,II}\right]^i + \left[\delta H_\ell^{k+1,II}\right]^{i+1}$;

6. Set $i = i+1$ and evaluate the function vector (compute $\boldsymbol{F}^i$), Eq. 45, based on the values of the variables computed in step 5c above;
7. If $\boldsymbol{F}^i \leq 10^{-5}$ the solution has converged and end computation. If not, repeat steps 4 though 7 above.

The algorithms described above represent the basic building blocks of the hydraulic computational procedure implemented in the field-scale sprinkler irrigation system design and simulation model (*SprinklerModel*) developed as part of the current study. The specifics of the implementation of these algorithms vary depending on the computational mode and this is discussed in Chapter 3. In the following section, however, the interpolation scheme, used to compute mainline outlet discharges as a function of the total head from a table of values generated during the system characterization phase (section 3.1), is described.

2.4 Cubic spline interpolation

For a given mainline water off-take node (say the *kth* node), the function relating the discharge from an outlet obtaining its supply from the *kth* off-take node with total head, $Q(H_\ell^k)$, is defined in the form of tables of values, generated during the system characterization computation phase. Hence, in system design and simulation computations (sections 3.2 and 3.3), mainline outlet discharges are interpolated from the respective *Q-H* tables. As described for sprinkler systems with single-line laterals layout configuration, linear interpolation can be used with satisfactory accuracy, provided the step size used to discretize the *Q-H* table is sufficiently fine. However, for systems with double-line laterals, the applicable numerical solution requires the specification of

derivatives, *Q'(H*), and function values, *Q(H)*. With piecewise linear fit the derivatives at the data points are not continuous, hence application of the linear interpolation approach to systems with double-line laterals layout configuration may not lead to accurate results. On the other hand, given a function defined over a closed interval (e.g., a *Q-H* table), its cubic spline interpolant has not only continuous first and second derivatives at the data points but it also exhibits the least oscillatory behavior among higher order interpolating polynomials (Mathews and Fink, 2004), hence it can be considered the most accurate. In the model described here, the cubic spline interpolation scheme is used to interpolate the mainline outlet discharge function, *Q(H)*, and approximate its derivative, *Q'(H*), from the corresponding lateral hydraulic characteristics curve. To simplify subsequent discussion, within this section, a system with single-line laterals layout configuration is assumed; with the implication that appropriate notational modifications can be applied to adapt the resulting procedure and equations for systems with double-line laterals configuration.

2.4.1 Description, properties, and equations for cubic spline parameters

The cubic spline interpolation scheme involves piecewise cubic approximation of a function (defined over a closed interval and quantified at a finite number of data points within the interval), such that the cubic polynomials (interpolants) exactly match the function at the data points. Furthermore, cubic spline interpolation requires that the interpolants for consecutive subintervals have the same first and second derivatives at a common data point. In the current application, the function to be approximated is the discharge at a mainline outlet (or lateral inlet) obtaining its supply from the *kth* off-take node, Q_ℓ^k, expressed in terms of the corresponding total head, H_ℓ^k. Considering a closed interval $[H_\ell^{k,min}, H_\ell^{k,max}]$, over which the function Q_ℓ^k is defined, with *N* subintervals and *N+1* data points and a cubic polynomial, $S(H_\ell^k)$, as the interpolant for Q_ℓ^k over a subinterval, $[(H_\ell^k)_n, (H_\ell^k)_{n+1}]$, where *n* is an integer such that $n \in [0,N-1]$; it follows from the preceding description that $S(H_\ell^k)$ can be described as cubic spline, if there exist *N* polynomials of the form (e.g., Mathews and Fink, 2004):

$$S_n(H_\ell^k) = \beta_{n,1} + \beta_{n,2}\left(H_\ell^k - \left(H_\ell^k\right)_n\right) + \beta_{n,3}\left(H_\ell^k - \left(H_\ell^k\right)_n\right)^2 + \beta_{n,4}\left(H_\ell^k - \left(H_\ell^k\right)_n\right)^3 \quad (52)$$

with the following properties

$$(a)\ S\left(\left(H_\ell^k\right)_n\right) = Q\left(\left(H_\ell^k\right)_n\right) \quad for \quad n = 0,1,2,\ldots N \qquad (53)$$

$$(b)\ S_n\left(\left(H_\ell^k\right)_{n+1}\right) = S_{n+1}\left(\left(H_\ell^k\right)_{n+1}\right) \quad for \quad n = 0,1,2,\ldots N-2 \qquad (54)$$

$$(c)\ S_n^{'}\left(\left(H_\ell^k\right)_{n+1}\right) = S_{n+1}^{'}\left(\left(H_\ell^k\right)_{n+1}\right) \quad for \quad n = 0,1,2,\ldots N-2 \qquad (55)$$

$$(d)\ S_n^{''}\left(\left(H_\ell^k\right)_{n+1}\right) = S_{n+1}^{''}\left(\left(H_\ell^k\right)_{n+1}\right) \quad for \quad n = 0,1,2,\ldots N-2 \qquad (56)$$

where S_n is the cubic interpolant for the *nth* subinterval, $[(H_\ell^k)_n, (H_\ell^k)_{n+1}]$; $(H_\ell^k)_n$ = the lower limit of the *nth* subinterval; $(H_\ell^k)_{n+1}$ = the upper limit of the *nth* subinterval; $\beta_{n,1}$ $\beta_{n,2}$, $\beta_{n,3}$, and $\beta_{n,4}$ = are parameters of the interpolating polynomial of the *nth* subinterval; $S_n^{'}$ = the first derivative of the cubic interpolant for the *nth* subinterval; and $S_n^{''}$ = the second derivative of the cubic interpolant for the *nth* subinterval. Note that given known conditions at the interval bounds over which the $Q(H_\ell^k)$ function is defined, it can be shown that there exists a unique cubic spline interpolant, to the function, with the properties listed in Eqs. 53-56 (Mathews and Fink, 2004; Burden et al., 1981).

In order to simplify the notations in subsequent discussion within the current section, the total head at the hydraulic characterization node of the lateral obtaining its supply from the *kth* mainline off-take node, H_ℓ^k, is referred to as H and the discharge will be defined as Q instead of Q_ℓ^k. On the other hand, the notations H_n and Q_n, or $Q(H_n)$, are used to refer to the *nth* data point in the Q_ℓ^k-H_ℓ^k table generated during the lateral hydraulic characterization computation.

Considering a mainline outlet, the use of cubic polynomials (of the form given in Eq. 52) to interpolate its $Q(H)$ function over the interval $[H^{min}, H^{max}]$ requires that the parameters of the cubic polynomial for each subinterval be defined. It can be shown that for each subinterval (say the *nth* subinterval, $[H_n, H_{n+1}]$), the parameters of the associated cubic interpolant $[\beta_{n,1}, \beta_{n,2}, \beta_{n,3}, \beta_{n,4}]$ can be expressed in terms of the function values (Q_n, Q_{n+1}), second derivatives of the interpolant at the lower and upper limits of the subinterval ($S_n^{''}, S_{n+1}^{''}$), and the subinterval size, $\delta H_n = H_{n+1} - H_n$, as follows:

Constant of the cubic spline function (Eq. 52) , $\beta_{n,1}$: Considering the cubic interpolant for the *nth* subinterval, S_n; an expression for the constant, $\beta_{n,1}$, can be derived by evaluating S_n at the lower limit of the subinterval *($H = H_n$)* and noting property (*a)* of a cubic spline, resulting in

$$\beta_{n,1} = Q_n \qquad (57)$$

Coefficient of the linear term of the cubic spline (Eq. 52), $\beta_{n,2}$: Evaluate the cubic polynomial for the *nth* and *(n+1)th* subintervals, S_n and S_{n+1}, at $H = H_{n+1}$. Equating the resulting expressions (note property *(b)* of a cubic spline, Eq. 54) and rearranging yields an expression for the coefficient of the linear term of S_n, $\beta_{n,2}$, as a function of $\beta_{n+1,1;}$ $\beta_{n,1;}$ $\beta_{n,3}$; $\beta_{n,4}$; and δH_n. Substituting the expressions for $\beta_{n,1}$; $\beta_{n,3}$; and $\beta_{n,4}$ (Eqs. 57, 59, and 60) in the resulting equation yields

$$\beta_{n,2} = \frac{Q_{n+1} - Q_n}{\delta H_n} - \frac{\delta H_n}{6}\left(S''_{n+1} + 2S''_n\right) \qquad (58)$$

Coefficient of the quadratic term of the cubic interpolant, $\beta_{n,3}$: Differentiating the cubic function for the *nth* subinterval, S_n (Eq. 52), twice and evaluating the resulting expression at the lower limit of the subinterval *($H = H_n$)*, yields:

$$\beta_{n,3} = \frac{S''_n}{2} \qquad (59)$$

Coefficient of the cubic term of the interpolant, $\beta_{n,4}$: Differentiate Eq. 52 twice to obtain the second derivatives of the cubic spline for the *nth* and the *(n+1)th* subintervals and evaluate each of the resulting expressions at $H = H_{n+1}$. Equating the resulting expressions (noting property *(d)* of a cubic spline, Eq. 56) and rearranging yields an equation for the coefficient of the cubic term in Eq. 54, $\beta_{n,4}$:

$$\beta_{n,4} = \frac{S''_{n+1} - S''_n}{6\delta H_n} \qquad (60)$$

Note that in Eqs. 58-60, the cubic spline parameters are expressed in terms of the second derivatives of the interpolant, which are unknown. However, based on the properties of a cubic spline listed above (Eqs. 53-56), for each mainline outlet a system of linear equations can be formulated with the second derivatives of the cubic interpolant as the unknowns. After having been coupled with known boundary conditions, this system of equations can be solved simultaneously for the unknowns. The solution can then be substituted in Eqs. 58-60 to obtain estimates of the cubic spline parameters for each subinterval. There are two alternative approaches for deriving the system of linear equations (Matthews and Fink, 1999; Burden et a, 1981), both approaches leading to the same equations. In subsequent discussion the approach described by Matthews and Fink (1999) is followed.

2.4.2 Formulation of a system of linear equations with the second derivatives of the cubic spline interpolants as variables

Noting that the piecewise interpolation function, S_n, for the subinterval $[H_n,H_{n+1}]$ is a cubic polynomial, it follows that the second derivative of S_n is a linear function of H over the same interval. Hence, the interpolation formula for the second derivative of the cubic interpolant of the *nth* subinterval, $S_n''(H)$, can be expressed as:

$$S_n''(H) = S_n'' \frac{H_{n+1} - H}{\delta H_n} + S_{n+1}'' \frac{H - H_n}{\delta H_n} \qquad (61)$$

where $S_n'' = S''(H_n)$, $\delta H_n = H_{n+1} - H_n$, and n is an integer such that $n \in [0,N-1]$. Integrating Eq. 61 twice results in the cubic function, $S_n(H)$, with two integration constants. Expressions can be derived for the integration constants in terms of the function values, the second derivatives of the interpolant, and the subinterval size by evaluating the cubic function at the limits of the subinterval ($H = H_n$ and $H = H_{n+1}$) and taking into consideration property *(a)* of a cubic spline (Eq. 52). Back substituting these expressions in the cubic function, $S_n(H)$, and rearranging results in:\

$$S_n(H) = \frac{S_n''}{6\delta H_n}(H_{n+1} - H)^3 + \frac{S_{n+1}''}{6\delta H_n}(H - H_n)^3 + \left(\frac{Q_n}{\delta H_n} - \frac{S_n''}{6}\delta H_n\right)(H_{n+1} - H) + \left(\frac{Q_{n+1}}{\delta H_n} - \frac{S_{n+1}''}{6}\delta H_n\right)(H - H_n) \qquad (62)$$

Although Eq. 62 is cubic in *H*, it is a linear function of the second derivatives (the unknowns). Based on property *(c)* of a cubic spline (Eq. 54), Eq. 62 can be written in a form that can readily be solved for the unknowns (the second derivatives). Accordingly, differentiating Eq. 62 once with respect to *H* and evaluating the resulting expression at the lower limit of the *nth* subinterval, $H = H_n$, and rearranging yields the expression for $S_n'(H_n)$:

$$S_n'(H_n) = -\frac{S_n''}{3}\delta H_n - \frac{S_{n+1}''}{6}\delta H_n + \frac{Q_{n+1} - Q_n}{\delta H_n} \qquad (63)$$

Similarly, the $S'(H)$ equation for the *(n-1)th* subinterval can be obtained and evaluated at $H = H_n$ resulting in an expression for $S_{n-1}'(H_n)$. Noting property *(c)* of cubic spline and equating the expression for $S_n'(H_n)$ given in Eq. 63 with $S_{n-1}'(H_n)$ and rearranging yields:

$$\delta H_{n-1}S_{n-1}'' + 2(\delta H_{n-1} + \delta H_n)S_n'' + \delta H_n S_{n+1}'' = 6\left[\frac{Q_{n+1} - Q_n}{\delta H_n} - \frac{Q_n - Q_{n-1}}{\delta H_{n-1}}\right] \qquad (64)$$

Equation 64 is a linear equation relating the function values, *Q(H)*, at three consecutive data points (*n-1*, *n*, and *n+1*) straddling the subintervals $[H_{n-1}, H_{n+1}]$ with the corresponding second derivatives. Considering *N+1* data points and *N* subintervals (covering the interval $[H^{min}, H^{max}]$ over which a mainline outlet *Q(H)* function is defined), a system of *N-1* linear equations with *N+1* unknowns of the form given in Eq. 66 can be formulated:

$$2(\delta H_{n-1} + \delta H_n)S_n'' + \delta H_n S_{n+1}'' = \gamma_n - \delta H_{n-1}S_{n-1}'' \quad for \quad n = 1 \qquad (65)$$

$$\delta H_{n-1}S_{n-1}'' + 2(\delta H_{n-1} + \delta H_n)S_n'' + \delta H_n S_{n+1}'' = \gamma_n \quad for \quad n \in [2, N-2] \qquad (66)$$

$$\delta H_{n-1}S_{n-1}'' + 2(\delta H_{n-1} + \delta H_n)S_n'' = \gamma_n - \delta H_n S_{n+1}'' \quad for \quad n = N-1 \qquad (67)$$

In Eqs. 65-67, γ_n is

$$\gamma_n = 6\left[\frac{Q_{n+1}-Q_n}{\delta H_n} - \frac{Q_n - Q_{n-1}}{\delta H_{n-1}}\right] \qquad (68)$$

When coupled with known boundary conditions at the upper and lower limits of the interval, $[H^{min},H^{max}]$; the linear system of equations reduces to a form (with *2(N-1)* equations in *2(N-1)* unknowns) that can be solved simultaneously. A list of alternative standard boundary conditions applicable to the solution of the linear system (Eqs. 65-67) is described by Mathews and Fink (2004). They involve specification of actual values of the second derivatives at the interval boundaries, some approximations of the second derivatives based on simplifying assumptions, or expressions that can be used to compute the second derivatives at the boundaries as a function of the corresponding first derivatives. A widely used and relatively simple approach, referred to as the natural boundary condition, involves setting the second derivatives at the interval limits to zero. This approach is often used for fitting experimental data and is also used in the current application. With the natural boundary condition, the expression $\delta H_{n-1} S''_{n-1}$ and $\delta H_n S''_{n+1}$ in Eqs. 65 and 67, respectively, becomes zero. The resulting system of linear equations can then be expressed in vector form as

$$\boldsymbol{\delta H S''} = \boldsymbol{\gamma} \qquad (69)$$

Following convention, in Eq. 69 the bold faced notations are used to represent matrices and vectors, where:

$$\boldsymbol{\delta H} = \begin{bmatrix} b_1 & c_1 & 0 & & & & \\ a_2 & b_2 & c_2 & 0 & & & \\ 0 & a_3 & b_3 & c_3 & 0 & & \\ & & . & . & . & & \\ & & & . & . & . & \\ & & & & 0 & a_{N-2} & b_{N-2} & c_{N-2} \\ & & & & & 0 & a_{N-1} & b_{N-1} \end{bmatrix}, \quad \boldsymbol{S''} = \begin{bmatrix} S''_1 \\ S''_2 \\ S''_3 \\ . \\ . \\ S''_{N-2} \\ S''_{N-1} \end{bmatrix}, \quad \boldsymbol{\gamma} = \begin{pmatrix} \gamma_1 \\ \gamma_2 \\ \gamma_3 \\ . \\ . \\ \gamma_{N-2} \\ \gamma_{N-1} \end{pmatrix} \qquad (70)$$

It then follows from Eqs. 65-67 that in Eq. 70 the elements of the coefficient matrix, $\boldsymbol{\delta H}$ (a tridiagonal matrix), can be computed with the following recursive relationships:

$$a_n = \delta H_{n-1} \quad for \quad n \in [2, N-1] \qquad (71)$$

$$b_n = 2(\delta H_{n-1} + \delta H_n) \quad for \quad n \in [1, N-1] \qquad (72)$$

$$c_n = \delta H_n \quad for \quad n \in [1, N-2] \qquad (73)$$

2.4.3 Solution of the linear system of equations with the second derivatives of the cubic splines as variables

The system of equations given in Eq. 69 can be solved efficiently with an *LU* factorization algorithm (Burden et al., 1981; Harris and Stocker, 1998; Press et al., 2000). The procedure is summarized in the following steps: (1) *Factorization of the tridiagonal matrix,* $\boldsymbol{\delta H}$ (Eq. 70): write $\boldsymbol{\delta H}$ as the product of a lower and an upper triangular matrix, $\boldsymbol{L_H}$ and $\boldsymbol{U_H}$, respectively:

$$\boldsymbol{\delta H S''} = \boldsymbol{L_H U_H S''} = \boldsymbol{\gamma} \qquad (74)$$

Equation 74 can be given as

$$\boldsymbol{L_H \zeta} = \gamma \qquad (75)$$

where $\boldsymbol{\zeta}$ is a vector of the form

$$\boldsymbol{U_H S''} = \boldsymbol{\zeta} \qquad (76)$$

Using the method of Crout's (Burden et al., 1981; Harris and Stoker, 1998), the following is a summary of the steps used to factorize the $\boldsymbol{\delta H}$ matrix into the corresponding $\boldsymbol{L_H}$ and $\boldsymbol{U_H}$ matrices:

$$\boldsymbol{L_H} = \begin{bmatrix} l_{11} & 0 & & & & & \\ l_{21} & l_{22} & 0 & & & & \\ 0 & l_{32} & l_{33} & 0 & & & \\ & \ddots & \ddots & \ddots & & & \\ & & \ddots & \ddots & \ddots & & \\ & & & 0 & l_{N-2,N-3} & l_{N-2,N-2} & 0 \\ & & & & 0 & l_{N-1,N-2} & l_{N-1,N-1} \end{bmatrix}$$

and

$$\boldsymbol{U_H} = \begin{bmatrix} 1 & u_{12} & 0 & & & & \\ 0 & 1 & u_{23} & 0 & & & \\ & 0 & 1 & u_{34} & 0 & & \\ & & \ddots & \ddots & \ddots & & \\ & & & \ddots & \ddots & \ddots & \\ & & & & 0 & 1 & u_{N-2,N-1} \\ & & & & & 0 & 1 \end{bmatrix} \qquad (77)$$

where l and u = elements of the $\boldsymbol{L_H}$ and $\boldsymbol{U_H}$ matrices, respectively; and the subscripts of l or u represent the row and column of the matrix an element belongs to. Elements of the $\boldsymbol{L_H}$ and $\boldsymbol{U_H}$ matrices are computed as a function of the coefficient matrix of the linear system of equations, $\boldsymbol{\delta H}$ (Eq. 69), with the following equations:

$$l_{n1} = b_1 \quad and \quad u_{n2} = \frac{c_1}{l_{n1}} \quad for \quad n = 1 \qquad (78)$$

$$l_{n,n-1} = a_n, \quad l_{nn} = b_n - l_{n,n-1}u_{n-1,n}, \quad for \quad n \in [2, N-1]$$

$$and \quad u_{n,n+1} = \frac{c_n}{l_{nn}} \quad for \quad n \in [2, N-2] \qquad (79)$$

(2) Solve Eq. 75 for the unknown vector, $\boldsymbol{\zeta}$: Noting that the $\boldsymbol{L_H}$ matrix is a special case of a lower triangular matrix (with nonzero elements only along its main diagonal and the sub-diagonal elements immediately below the main diagonal, Eq. 77); Eq. 75 can then be solved for $\boldsymbol{\zeta}$ through forward substitution by using equations of the form:

$$\zeta_n = \frac{\gamma_n}{l_{nn}} \quad for\ n = 1 \ and \quad \zeta_n = \frac{\gamma_n - l_{n,n-1}\zeta_{n-1}}{l_{nn}} \quad for\ n \in [2, N-1] \qquad (80)$$

where ζ_n = the *nth* element of the $\boldsymbol{\zeta}$ vector (Eq. 75).

(3) Solve Eq. 76 for the variable vector, $\boldsymbol{S}''$: Equation 76 can be solved for the second derivatives of the cubic splines through backward substitution with:

$$S_n'' = \zeta_n \quad for\ n = N-1\ and\ S_n'' = \zeta_n - u_{n,n+1}S_{n+1}'' \quad for\ n \in [1, N-2] \qquad (81)$$

The algorithm described above has a unique solution provided the tridiagonal coefficient matrix, $\boldsymbol{\delta H}$, is diagonally dominant (Press et al., 2000). A tridiagonal matrix is considered diagonally dominant, if for each row of the matrix the absolute value of the diagonal element exceeds the sum of the absolute values of the elements on the sub-diagonals immediately above or below the main diagonal. It can be noted from Eqs. 71-73 that the corresponding coefficient matrix, Eq. 69, is always diagonally dominant, if the subinterval size is constant. In the current application the subinterval size is constant, hence the resulting matrix has the desired property of diagonal dominance and application of the algorithm described above will result in a unique solution to the system of linear equations expressed in Eq. 69. Once the vector of the second derivatives of the cubic spline is computed, then the parameter estimates for each cubic spline interpolant can be calculated with Eqs. 57-60.

The basic hydraulic equations governing steady flow in a field-scale solid set sprinkler system, the numerical solution algorithms, and the interpolation scheme used for coupling lateral and mainline hydraulics (as implemented in the *SprinklerModel* developed in this study) are presented in this chapter. The numerical procedures described here constitute the basic building blocks of the hydraulic model. However, the specifics of their implementation vary depending on the computational modes in which the model is run and this is discussed in the next chapter.

Chapter 3. Computational modes

The sprinkler model presented here (*SprinklerModel*) can be run in any one of the following four computational modes (Figure 5): *(i)* sprinkler system hydraulic characterization, *(ii)* Sprinkler system hydraulic design, *(iii)* Sprinkler system hydraulic simulation, and *(iv)* Sprinkler system field evaluation.

Given the layout of a field-scale solid set sprinkler system, the diameter(s) of the pipes, nodal elevations, the friction factor, the locations, and types of pipe fittings/appurtenances along with their associated local head loss coefficients; the hydraulic characterization mode provides the functionality for computing the system hydraulic characteristics curve defined at the mainline inlet and also the *Q*-*H* relationship for each lateral defined at its hydraulic characterization node (Figure 4). With the hydraulic design mode, the minimum acceptable sprinkler pressure head in the system is specified at the input. The model then computes the field-scale distribution of sprinkler pressure head and discharge and the corresponding total dynamic head such that the design requirement with respect to the minimum acceptable sprinkler pressure head is satisfied (Figure 4). On the other hand, the system simulation functionality provides a capability to compute the distribution of pressure and discharge over the sprinkler network, given a design scenario or a certain total head at the mainline inlet. The sprinkler system field evaluation functionality provides a capability for computing evaluation-plot scale and field-scale irrigation uniformity based on data collected through standard field tests or for a hypothetical irrigation scenario (Figure 5).

During system design and simulation computations, the tables of Q_ℓ^k-H_ℓ^k values (generated for each lateral during the system characterization phase) are used as the head-discharge characteristics of the respective mainline outlets. Hence, system characterization computation is always conducted prior to system design and simulation computations. In addition, system design computation is followed by system simulation.

A description of these model functionalities with respect to input data requirements, computational procedure, and output data types is presented subsequently. Although subsequent descriptions of the system hydraulic characterization, design, and simulation computations apply to systems with single-line or double-line laterals layout configurations, to simplify the discussion the notations used are those of single-line laterals. Appropriate notional modifications can be applied to adapt the procedures developed here for sprinkler systems with double-line laterals layout configuration.

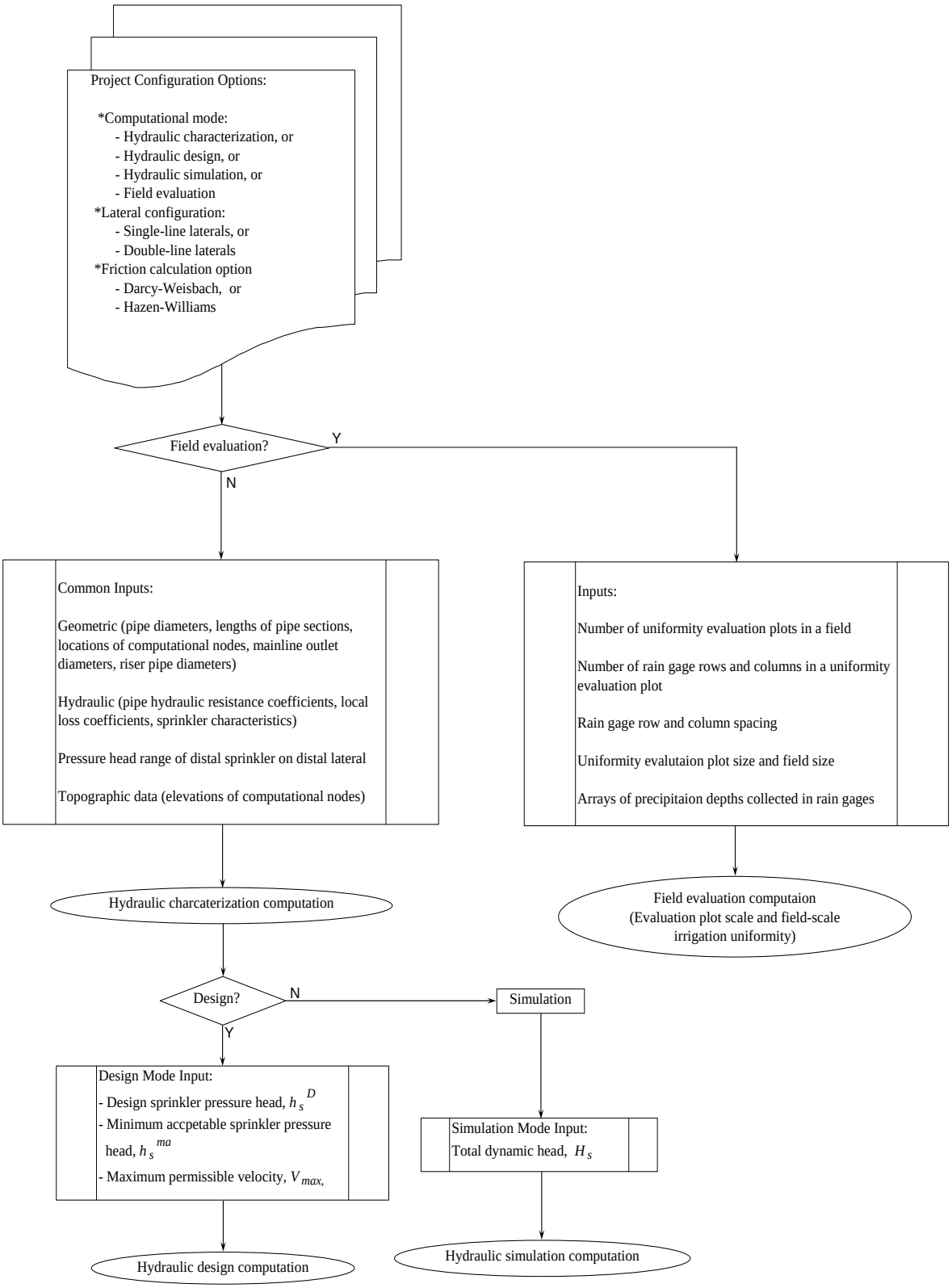

Figure 5. Flow diagram showing computational modes and input data

3.1 Sprinkler system hydraulic characterization mode

The goal of a hydraulic characterization computation is to generate an array of data relating the total head, H, with discharge, Q, at the hydraulic characterization node, ℓ, of each lateral and at the mainline inlet (Figure 6). Although the hydraulic characterization node along a lateral does not represent a physical outlet of the mainline, for computational purposes it is considered as such (section 2.3, mainline hydraulics). Hence the hydraulic characteristic curve generated for each lateral $(Q_\ell^k\text{-}H_\ell^k)$ also defines the hydraulic characteristics of the corresponding mainline outlet. The mainline outlet hydraulic characteristics curves along with the interpolation procedure described above provide the interface for coupling numerical solutions, of the lateral and the mainline hydraulic equations, described in the preceding sections.

As can be noted form Figure 6, the hydraulic characterization computation is performed in two consecutive steps: (1) Determination of the hydraulic characteristics of the mainline outlets (Q_ℓ^k -H_ℓ^k tables) along with the parameters of the respective interpolating polynomials (section 2.4) and (2) Determination of the system hydraulic characteristics curve, $Q(H_s)$, through iterative computations along the mainline.

Hydraulic characterization of mainline outlets

Computation: Referring to the discussion on lateral hydraulics, it can be shown that for a lateral (say the lateral that obtains its supply from the *kth* off-take node) with a given set of geometric, topographic, and hydraulic attributes, if the pressure head at the distal sprinkler, h_{s1}^k, is set; then a unique value of Q_ℓ^k and H_ℓ^k can be computed at the hydraulic characterization node of the lateral (Figures 4 and 6). Systematic variation of h_{s1}^k within a predefined range, $[h_{s1}^{k,min}, h_{s1}^{k,max}]$, results in an array of pressure head values for the distal sprinkler of the lateral (Figures 6 and 7). For each h_{s1}^k value, within the predefined range, hydraulic computations along the lateral (section 2.2) results in the hydraulic characteristic curve of the lateral (or of the corresponding mainline outlet), $Q(H_\ell^k)$, Figures 6 and 7. The pressure head range at the distal sprinkler of the distal lateral, $[h_{s1}^{1,min}, h_{s1}^{1,max}]$, is specified at the input. Given the range of h_{s1}^1, the hydraulic characterization computation of the distal lateral proceeds as follows (Figures 6 and 7):

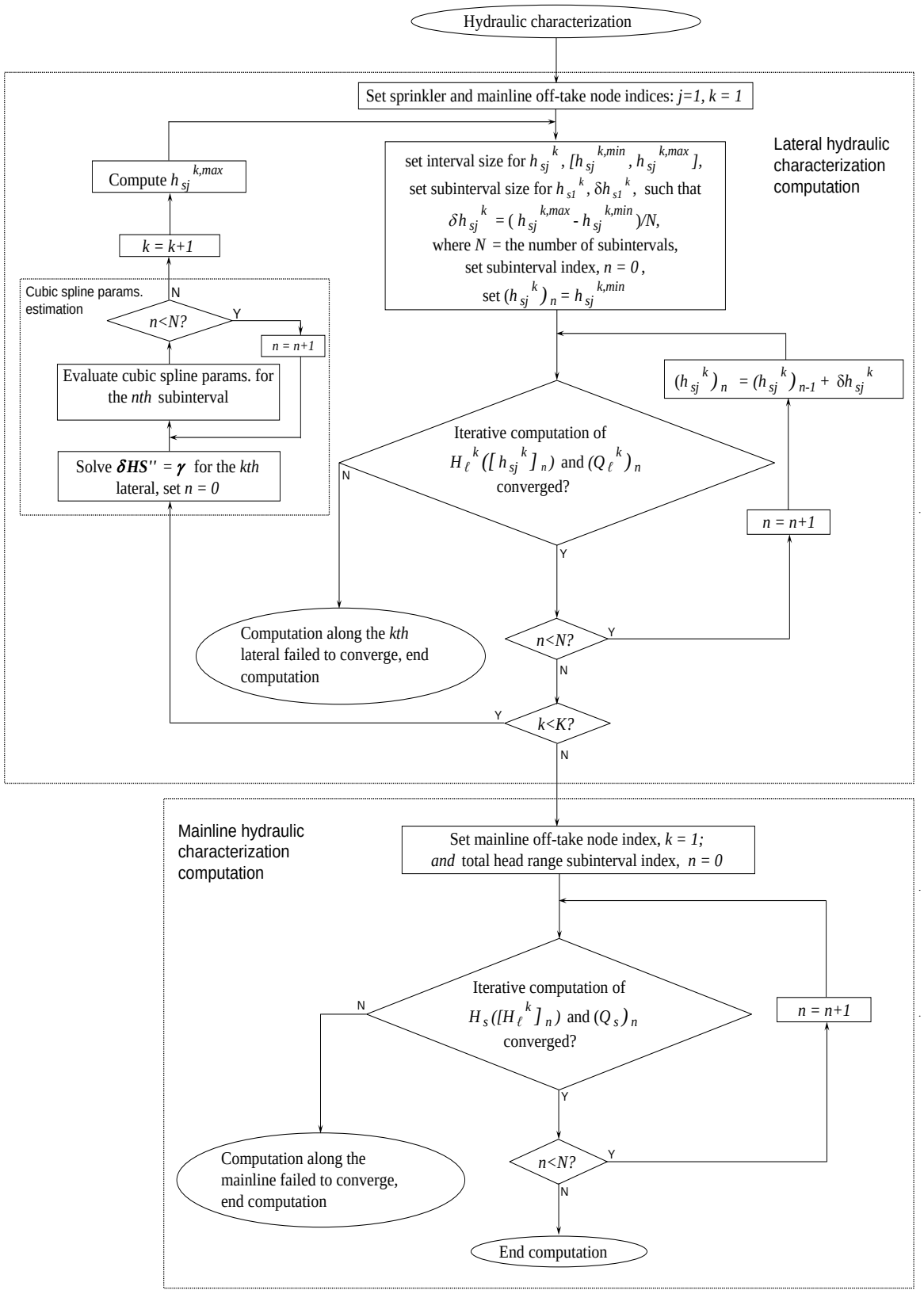

Figure 6 Flow diagram depicting hydraulic characterization computation

(1) The specified pressure head range is discretized into N subinterval and $N+1$ data points (or pressure head values, $(h_{s1}^{1})_n$, where n is a data point index such that $n \in [0,N]$) and (2) Using the numerical procedure described for laterals, for each $(h_{s1}^{1})_n$ value (within the specified range) compute the corresponding $(Q_\ell^1)_n$-$(H_\ell^1)_n$ value.

The computation to define the hydraulic characteristics of all the laterals upstream of the distal lateral follows the same basic steps described above. However, the fact that the total head along the mainline decreases in the direction of flow (due to energy loss) implies that the range of the Q_ℓ^k-H_ℓ^k table for each lateral should be increased as the system characterization computation proceeds upstream along the main. Hence, in Figure 7 the following relationships must hold for successive laterals: $h_{s1}^{1,\,max} < h_{s1}^{2,max} < \ldots < h_{s1}^{K,max}$. Noting that the total head at the hydraulic characterization node of the lateral that obtains its supply from the *kth* mainline off-take node, H_ℓ^k, is an increasing function of the corresponding h_{s1}^k, the following relationship should also hold for successive laterals: $H_\ell^{1,max} < H_\ell^{2,max} < \ldots < H_\ell^{K,max}$. In the model described here this requirement is met by a progressive increase in the maximum pressure head at the distal end sprinkler of the laterals as the computation proceeds upstream, while keeping the minimum pressure head at the same level as that specified for the distal end sprinkler of the distal lateral. A power function of the form given in Eq. 82 is used to compute the maximum pressure head for the distal sprinkler of a lateral, $h_{s1}^{k,max}$, as a function of the maximum pressure head specified at the input for the distal end sprinkler of the distal lateral, $h_{s1}^{1,max}$:

$$h_{s1}^{k,\boldsymbol{max}} = \left(\theta_1 k^{\theta_2} + \theta_3\right) h_{s1}^{1,\boldsymbol{max}} \qquad (82)$$

In Eq. 82, θ_1 *(-),* θ_2 *(-),* and θ_3 *(-)* are parameters, the values of which can be specified at the input and k = mainline off-take node index ($k=1$ for the distal end lateral and is incremented by one for each subsequent lateral upstream). Note that the lateral number index is the same as the mainline off-take node index for a system with single-line lateral layout. However, for systems with double-line laterals layout, the lateral number index can be different from the off-take node index (Figure 4). The parameters in Eq. 82 can be varied depending on the largest required range of the Q_ℓ^k-H_ℓ^k table and the desired rate of

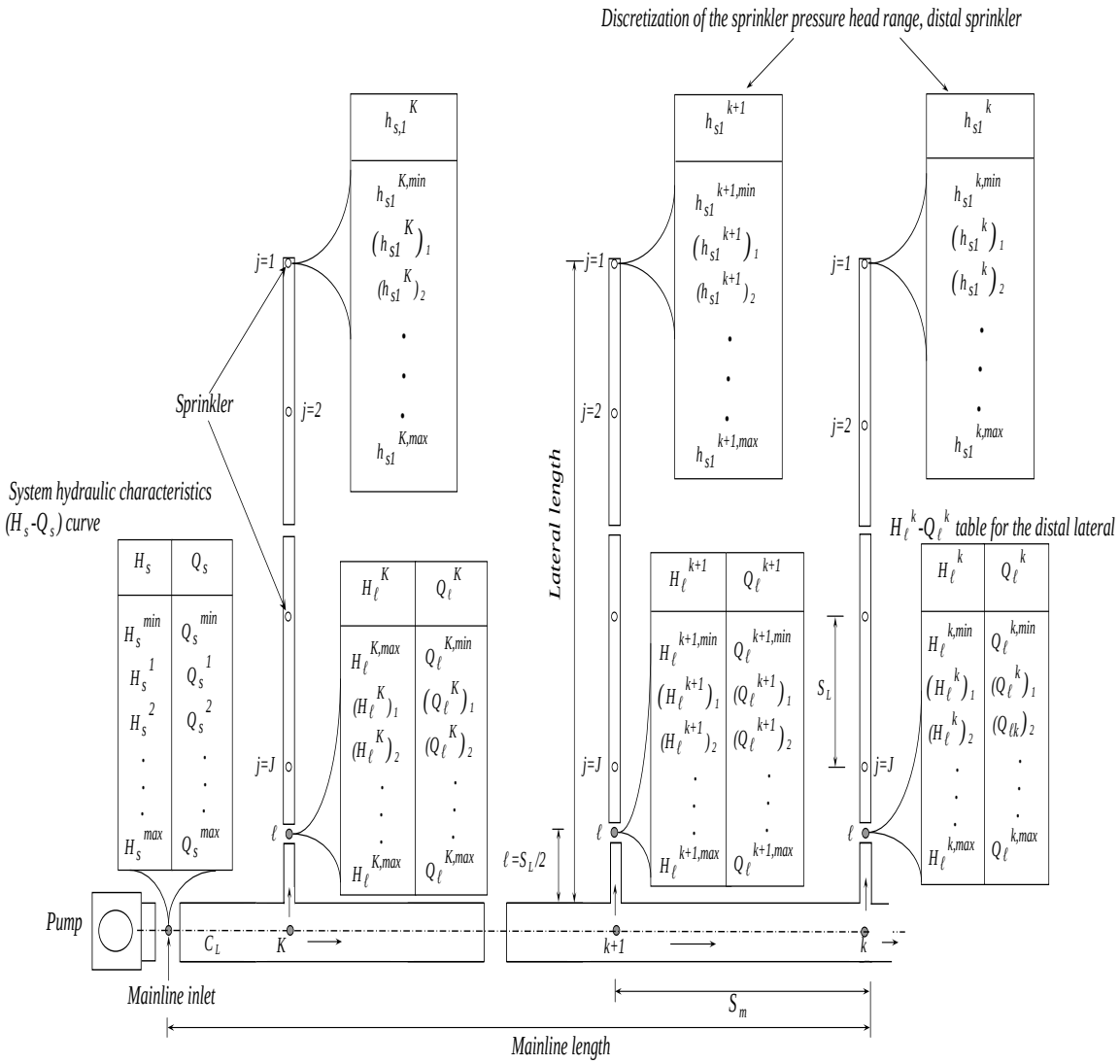

Figure 7 Schematization of a field-scale solid set sprinkler system depicting system hydraulic characterization computation

increase as the computation proceeds upstream. In order for the maximum pressure head at the distal sprinkler of the distal lateral computed with Eq. 82 to be equal to the user specified value, the sum of θ_1 and θ_3 should be equal to 1.0. In addition, θ_2 should be greater than zero so that the resulting maximum distal end sprinkler pressure head increases with each lateral as the computation proceeds upstream starting from the distal end lateral. Based on numerical experiments, in the current program setting, default values of $\theta_1 = 0.15$, $\theta_2 = 1.45$, and $\theta_3 = 0.85$ are used, but these values can be changed if necessary. For systems with double-line of laterals two sets of parameters are used: $\theta_1 =$

0.15, θ_2 = 1.45, and θ_3 = 0.85 for odd-numbered laterals and θ_1 = 0.2, θ_2 = 1.45, and θ_3 = 0.8 for even-numbered laterals. This allows for flexibility in hydraulic characterization of the two sets of laterals and improves model robustness.

Considerations in setting the pressure head range for the distal sprinkler of the distal lateral: The upper limit of the user specified pressure head range of the distal end sprinkler of the distal lateral should be sufficiently large so that the pressure head ranges computed for the upstream laterals have adequate spread. The lower limit of the pressure head range specified at the input should be large enough to maintain positive pressure in the lateral. This is particularly important when the lateral has a steep negative slope and/or a relatively large diameter. In general both the lower and upper limit of the pressure head range specified for the distal sprinkler of the distal lateral should take into account the pressure head range of the sprinkler specified in the manufacturer's catalogue. Once the maximum pressure head at the distal end sprinkler of a lateral is computed with Eq. 82, the pressure head range for the distal end sprinkler of the lateral is defined. The specified pressure head range for the distal sprinkler of the lateral can then be discretized and the hydraulic characteristics curve for the lateral can be generated by applying the steps outlined above for the distal end lateral.

Typically sprinkler pressure head ranges that are larger than those specified in the manufacturer's catalogue should be used so that the head-discharge characteristic curves of the mainline outlets have sufficient spread, which contributes to model robustness. However, if the sprinkler pressure heads computed during the hydraulic design or simulation phases fall outside the pressure head ranges specified in the manufacturer's catalogue by a significant margin, then the program prints cautionary note that the results may not be accurate. Based on which the design can be revised by selecting pipe sizes that are compatible with design limitations of the sprinklers or by selecting sprinklers with different characteristics and modifying the spacing accordingly or some combination thereof. For simulation problems, on the other hand, such a result shows under current irrigation practices the sprinklers are being operated at pressure heads that are outside the design ranges, hence their performance could be suboptimal. In general the number and size of the subintervals into which the distal end sprinkler pressure head range is

discretized is the same for all laterals in a given problem, but it can be varied by the user from one problem to another. A finer discretization (large number of subintervals), within the limits of rounding-off errors, implies that the head-discharge characteristics of the associated mainline outlet can be interpolated more accurately from the resulting Q_ℓ-H_ℓ table, but it also means a heavier computational burden. Hence, the selection of the number of subintervals, into which the distal end sprinkler pressure head ranges are to be discretized, needs to balance the computational requirements with considerations of accuracy. Based on numerical experiments, for most practical applications discretization of the sprinkler pressure head range into four hundred subintervals, with four hundred and one pressure head values has been deemed satisfactory.

Hydraulic characterization mainline inlet

Following hydraulic characterization of the mainline outlets and the determination of the parameters of the cubic spline interpolants for each outlet (Figure 6); computations can be conducted along the main to define the hydraulic characteristics of the field-scale sprinkler system (Figures 6 and 7). As described above during lateral hydraulic characterization computation a table of Q_ℓ^k-H_ℓ^k values with $N+1$ data points is generated for each mainline outlet, including the distal outlet. Based on which, system hydraulic characterization computation along the mainline can proceed as follows (Figures 6 and 7): (1) Set the total head at the distal mainline outlet H_ℓ^1 to $H_\ell^{1,min}$ and conduct a hydraulic computation along the mainline (section 2.3) to determine the corresponding total head and discharge at the system inlet (H_s^{min},Q_s^{min}) and (2) Repeat step 1 above for each $(H_\ell^1)_n$ in the range $[H_\ell^{1,min},H_\ell^{1,max}]$, where n is a data point index such that $n \in [0,N]$ and $(H_\ell^1)_0 = H_\ell^{1,min}$ and $(H_\ell^1)_N = H_\ell^{1,max}$. In addition, for each $(H_\ell^1)_n$ value at the distal mainline outlet the preceding computation generates the distribution of specific energy, its components, and the corresponding outlet discharges along the mainline.

The system hydraulic characterization computational mode produces output that can directly be used in pump selection and/or evaluation. However, the main significance of the system hydraulic characterization computation is in generating the data sets (Q_ℓ^k-H_ℓ^k tables for each mainline outlet) required for executing subsequent computations: hydraulic deign or simulation, described next.

3.2 Sprinkler system hydraulic design mode

When the model is run in the system design mode, the design sprinkler pressure head, h_s^D, the minimum acceptable sprinkler pressure head, h_s^{ma}, along with the hydraulic, geometric, and topographic characteristics of the sprinkler system are specified at the input (Figure 8). The model then computes the field-wide distribution of sprinkler pressure head and discharge and the corresponding total dynamic head such that the pressure head at the critical sprinkler (the sprinkler with the minimum pressure head in the irrigated field, h_s^{min}) is sufficiently close to the acceptable minimum. As can be noted from Figure 8, system design computation is performed in four distinct steps:

1. Conduct system hydraulic characterization computation: this step defines the hydraulic characteristic curve (Q_ℓ^k-H_ℓ^k table) for each mainline outlet and computes the parameter estimates of the corresponding cubic interpolant (Figure 6);
2. Along each lateral determine the critical sprinkler, associated pressure head, and the total head required at the lateral inlet for the (computed) minimum sprinkler pressure head along the lateral, $h_s^{k,min}$, to be sufficiently close to h_s^{ma}. For the lateral obtaining its supply from the *kth* off-take node of the mainline (referred here as the *kth* lateral), the computation proceeds as follows:

   (2a) Set the pressure head at the distal end sprinkler of the *kth* lateral, h_{s1}^k, to h_s^{ma} to initiate the iterative computation. Note that this step assumes that the minimum sprinkler pressure head, $h_s^{k,min}$, occurs at the distal end of the lateral;

   (2b) Compute pressure head and discharge distribution along the *kth* lateral following the procedure described in section 2.2 (lateral hydraulics):

   - If the lateral is installed on a level surface or on a surface with a positive slope or with a small negative slope (such that the energy loss, due to friction and local losses, exceeds the total drop in elevation over the entire length of the lateral); then the assumption made in the preceding step regarding the location of h_s^{min} is correct and it is the distal end of the lateral.
   - If the slope of the lateral is sufficiently steep that the gain in pressure head due to the decrease in elevation exceeds the energy loss along the lateral, then the minimum sprinkler pressure head occurs somewhere along the lateral upstream

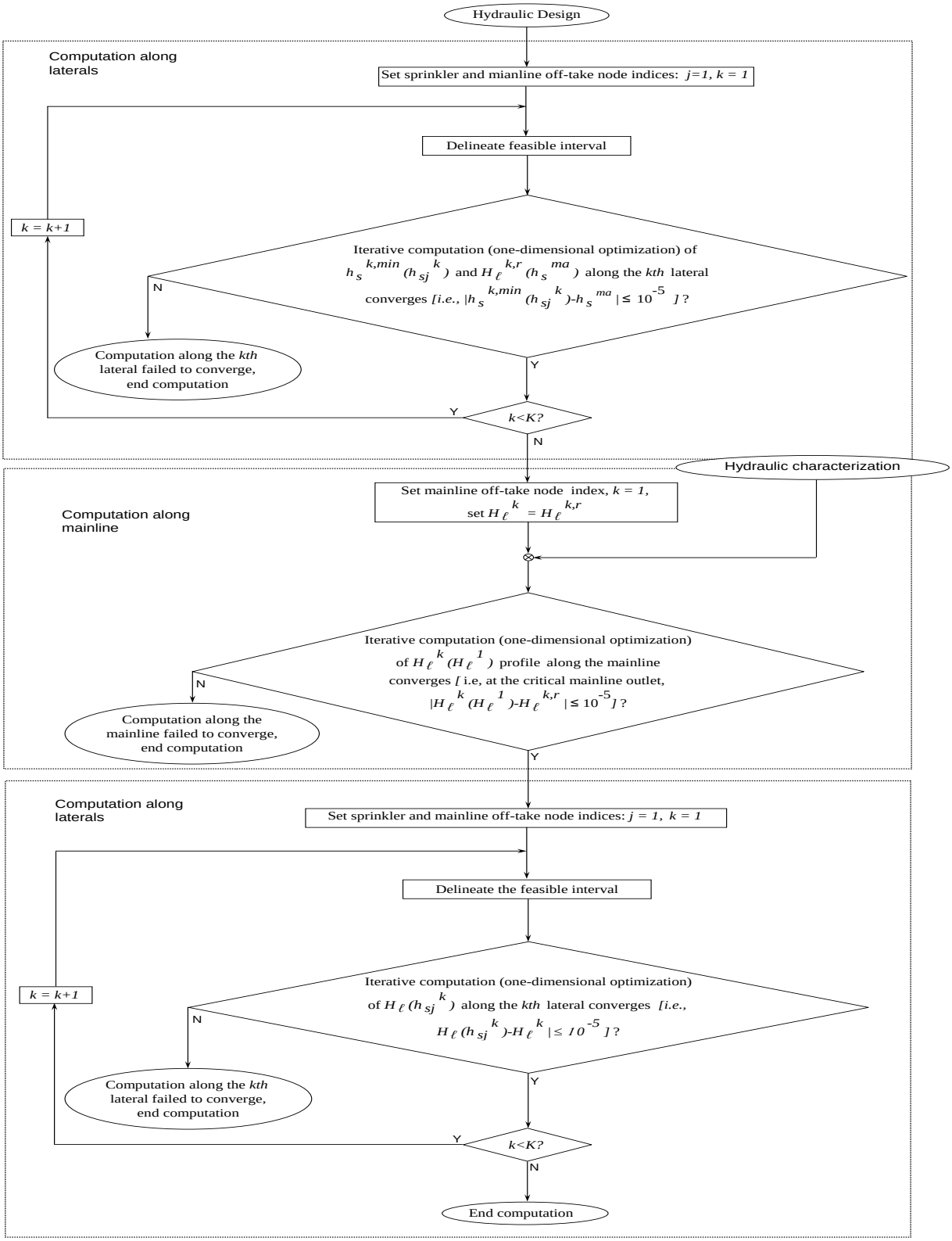

Figure 8. Flow diagram showing the design computational mode

of the distal sprinkler. In such a scenario, setting $h_{s1}^{k} = h_s^{ma}$ will lead to a pressure head profile along the lateral with an $h_s^{k,min}$ value that is less than h_s^{ma}. If the absolute difference between the $h_s^{k,min}$ and h_s^{ma} exceeds a specified error margin, then the solution is considered infeasible and an iterative computation is initiated to determine the value of h_{s1}^{k} that results in a pressure head profile that meets the design requirement with respect to h_s^{ma}. Pertinent numerical procedure is presented in section 3.5.

In order to illustrate this point a numerical example of sprinkler pressure head profiles, along a lateral, obtained through an iterative computation of the distal sprinkler pressure head, h_{s1}^{k}, is summarized in Figure 9a. The lateral is installed on a relatively steep uniform slope of -0.3% and it has constant diameter of 76.2mm and an absolute roughness of 0.127mm. It has 41 sprinklers installed at a regular spacing of 9.14m. The sprinkler pressure head profile computed in the initial iteration (i.e., for $h_{s1}^{k} = h_s^{ma}$ = 31.5m) has a minimum sprinkler pressure head, $h_s^{k,min}$, of 31.1m (occurring at 25th sprinkler referenced from the distal end), a value less than the specified h_s^{ma} of 31.5m (Figure 9a). Considering an error margin of 10^{-5}, this solution is deemed infeasible. Hence, an iterative computation is initiated to determine the h_{s1}^{k} value that meets the design requirement. As can be noted from Figure 9a, a pressure head profile along the lateral with an $h_s^{k,min}$ value of 31.5m is obtained for h_{s1}^{k} = 31.9m.

3. Repeat step 2 above for all the laterals and determine the critical sprinkler for each lateral, the required total head at the corresponding mainline outlets, $H_\ell^{k,r}$, and the critical sprinkler for the irrigated field.
4. Set the total head at the distal mainline outlet, H_ℓ^{1}, to the required total head at the distal outlet, $H_\ell^{1,r}$, and conduct hydraulic computation along the mainline to determine the longitudinal distribution of the specific energy (its components) and discharge following the procedure described in section 2.2 (mainline hydraulics). The following scenarios can be discerned:

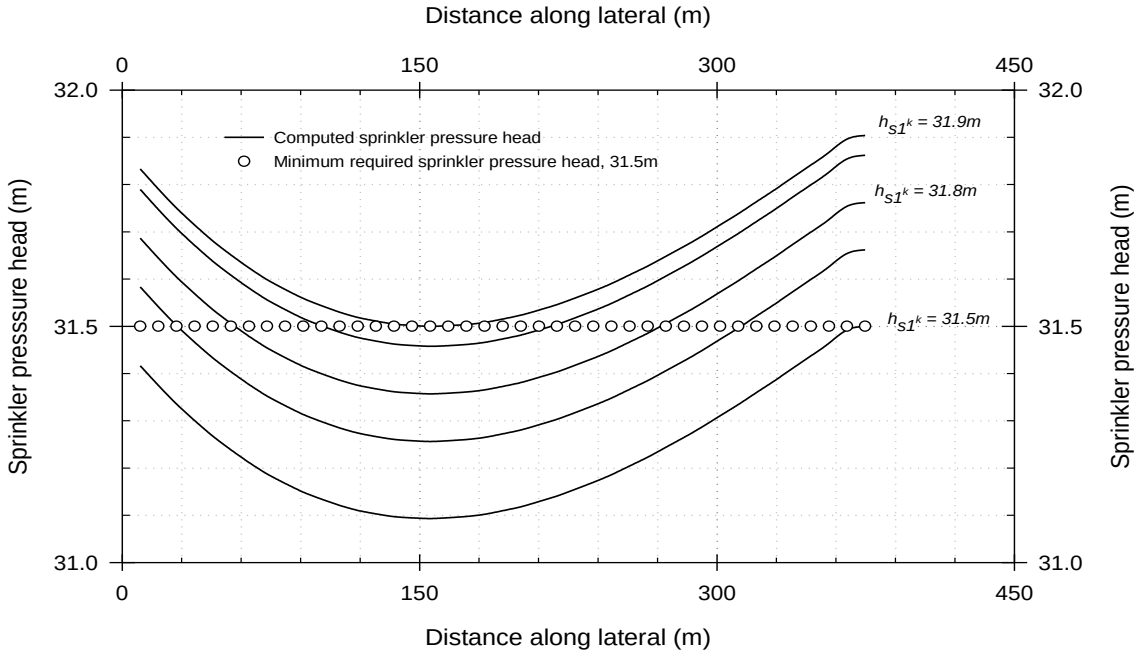

(a)

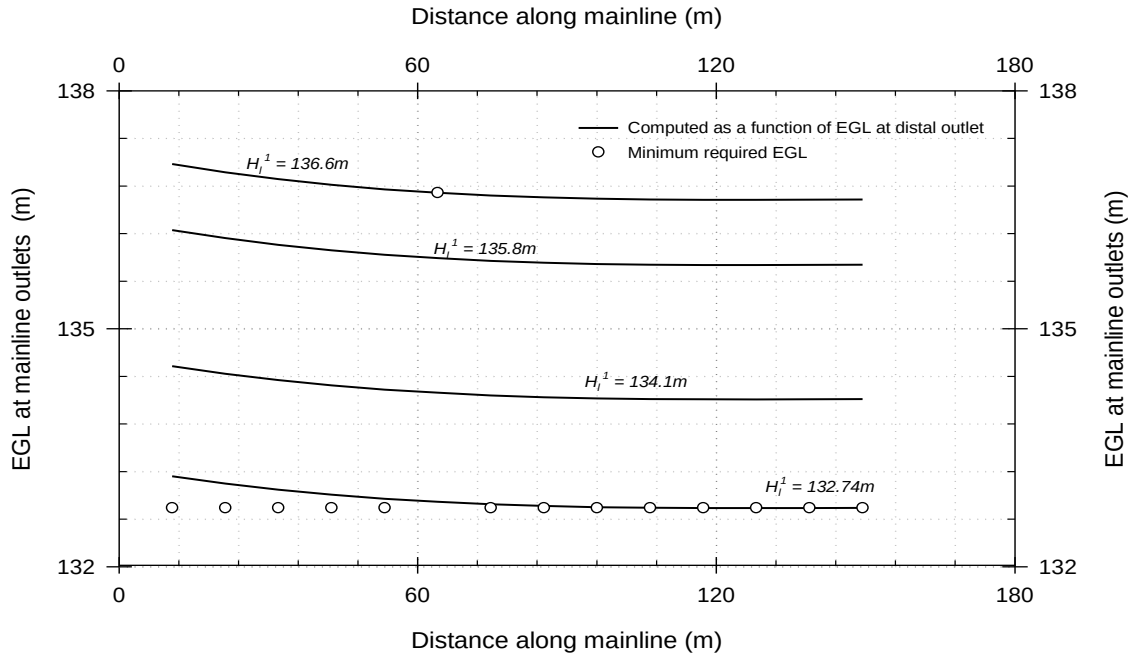

(b)

Figure 9: (a) The longitudinal sprinkler pressure head profile (along a lateral with a negative slope) computed as a function of the distal sprinkler pressure head and the minimum required sprinkler pressure head and (b) Energy line (EGL) along a mainline computed as a function of total head at the distal outlet and the minimum required total head at the mainline outlets

(4a) For each mainline outlet the required total head, $H_\ell^{k,r}$ (computed in step 3 above), is at least equal to the total head computed at the outlet as a function of the required total head at the distal outlet, $H_\ell^k(H_\ell^{1,r})$: $H_\ell^{k,r} \leq H_\ell^k(H_\ell^{1,r})$. In which case, a single sweep along the mainline (following the procedure described on mainline hydraulics) establishes the distribution of specific energy and its components; or

(4b) At one or more of the mainline outlets upstream of the distal outlet the following holds: $H_\ell^k(H_\ell^{1,r}) < H_\ell^{k,r}$, which could be attributed to the hydraulic, topographic, and geometric characteristics of the corresponding lateral(s). If the maximum difference between $H_\ell^k(H_\ell^{1,r})$ and $H_\ell^{k,r}$ exceeds a preset error margin, then the solution is considered infeasible. In which case, the total head at the distal mainline outlet, H_ℓ^1, needs to be computed iteratively such that at the critical mainline outlet the absolute difference between $H_\ell^{k,r}$ and $H_\ell^k(H_\ell^1)$ is reduced to a level within a specified error margin. The critical mainline outlet is the outlet with the maximum difference between $H_\ell^k(H_\ell^{1,r})$ and $H_\ell^{k,r}$ computed in step 2 above. Pertinent numerical algorithm is presented in section 3.5.

In order to illustrate the point described above, a numerical example is presented in Figure 9b depicting the distribution of total head along a mainline for a sprinkler system with single-line laterals configuration. The mainline consists of pipe section of 203.2mm diameter and all the laterals have the same diameter (76.2mm), the same absolute roughness (0.127mm), and the same number and type of pipe appurtenances. In addition, all the laterals except the lateral obtaining its supply from the ninth mainline off-take node (referenced from the distal node) are installed on a relatively flat negative slope of -0.05%, but the lateral obtaining its supply from the ninth mainline off-take node is installed on a relatively steep upward slope of 0.1%. As can be seen from Figure 9b, for all the mainline outlets except the ninth outlet, the minimum required total head, $H_\ell^{k,r}$, is the same and it is equal to 132.7m and for the ninth mainline outlet it is equal to 136.7m. The total head at the ninth mainline outlet computed in the initial iteration (for H_ℓ^1 = 132.7m) is 132.8m (Figure 9b). Considering an acceptable error margin of 10^{-5}, this solution is

considered infeasible. An iterative computation is initiated to determine the total head at the distal outlet, H_ℓ^1, such that the absolute difference between the required total head for the ninth outlet and the total head computed for the same outlet based on H_ℓ^1 is reduced to a level within the specified error margin. As can be noted from Figure 9b, an H_ℓ^1 value of 136.6m yields an energy line along the main with a total head at the ninth mainline outlet that is sufficiently close to the required total head of 136.7m (Figure 9b). As can be noted from Figure 9b the satisfaction of this requirement implies that at all of the mainline outlets $H_\ell^{k,r} \leq H_\ell^k$.

5. As can be noted from Figure 9b, for most of the mainline outlets the total head, H_ℓ^k, (computed in step 4) above could be significantly larger than their respective $H_\ell^{k,r}$ values (computed in step 3 above). Hence, the corresponding distribution of total head (its components) and discharge along each lateral need to be computed iteratively.

Note that the design computational steps outlined above only ensure that the pressure head at the critical sprinkler in the irrigated field is equal to the minimum specified at the input. It may, however, produce a design scenario with sprinkler pressure heads that are appreciably larger than the optimal (design) sprinkler pressure heads. This may lead to significant spatial variations in pressure heads and discharges over the irrigated field and to low irrigation uniformity. Such a design can be considered feasible (if the sprinkler pressure head range is sufficiently close to the range given in the sprinkler manufacturer's catalogue), but it may well be suboptimal. Nonetheless, acceptable designs can be developed through repeated simulations with different pipe sizes, system layout (i.e., sprinkler and lateral spacing), sprinkler characteristics, and pipe appurtenances.

3.3 Sprinkler system hydraulic simulation mode

With the hydraulic simulation option, the hydraulic, geometric, and topographic characteristics of a field-scale sprinkler system along with the total dynamic head imposed at the mainline inlet, H_s, are specified at the input. The model then computes,

among other outputs, the corresponding field-wide spatial distribution of sprinkler pressure head and discharge over the irrigated field. Because the spatial distribution of sprinkler pressure heads and discharges are good indicators of field-scale irrigation uniformity, the hydraulic simulation functionality of the model described here can be considered as a useful tool in evaluating the potential irrigation uniformity of an existing system. As depicted in Figure 10, the hydraulic simulation computation is conducted in three distinct steps:

1. Conduct system characterization computations: generate Q_ℓ-H_ℓ tables for each of the laterals following the procedure described above in section 3.1 and compute the parameters of the interpolating polynomial following the procedure described in section 2.4 (Figures 6).
2. Compute the distribution of specific energy and its components along the mainline iteratively such that the total head computed at the mainline inlet (as a function of the total head at the distal outlet, $H_s(H_\ell^1)$) is sufficiently close to the total dynamic head specified at the input, H_s. Pertinent numerical procedure implemented in the model described here is presented in section 3.5.
3. Once the distribution of total head, H_ℓ^k, and outlet discharges, Q_ℓ^k, along the mainline are computed (step 2 above), then the longitudinal distribution of total head and discharge along the respective laterals need to be calculated iteratively. Pertinent numerical solution is given in section 3.5.

As described here and in section 3.2, during hydraulic design and simulation computations, the distal sprinkler pressure head along each lateral and the total head at the distal mainline outlet may need to be computed iteratively, such that a design and simulation requirement specified at the input is met. The specific conditions under which iterative solutions are required, formulation of the iterative hydraulic computational problems as one-dimensional optimization problems, and solution algorithm are presented in section 3.5. Before that, however, the field evaluation functionality of the model is presented.

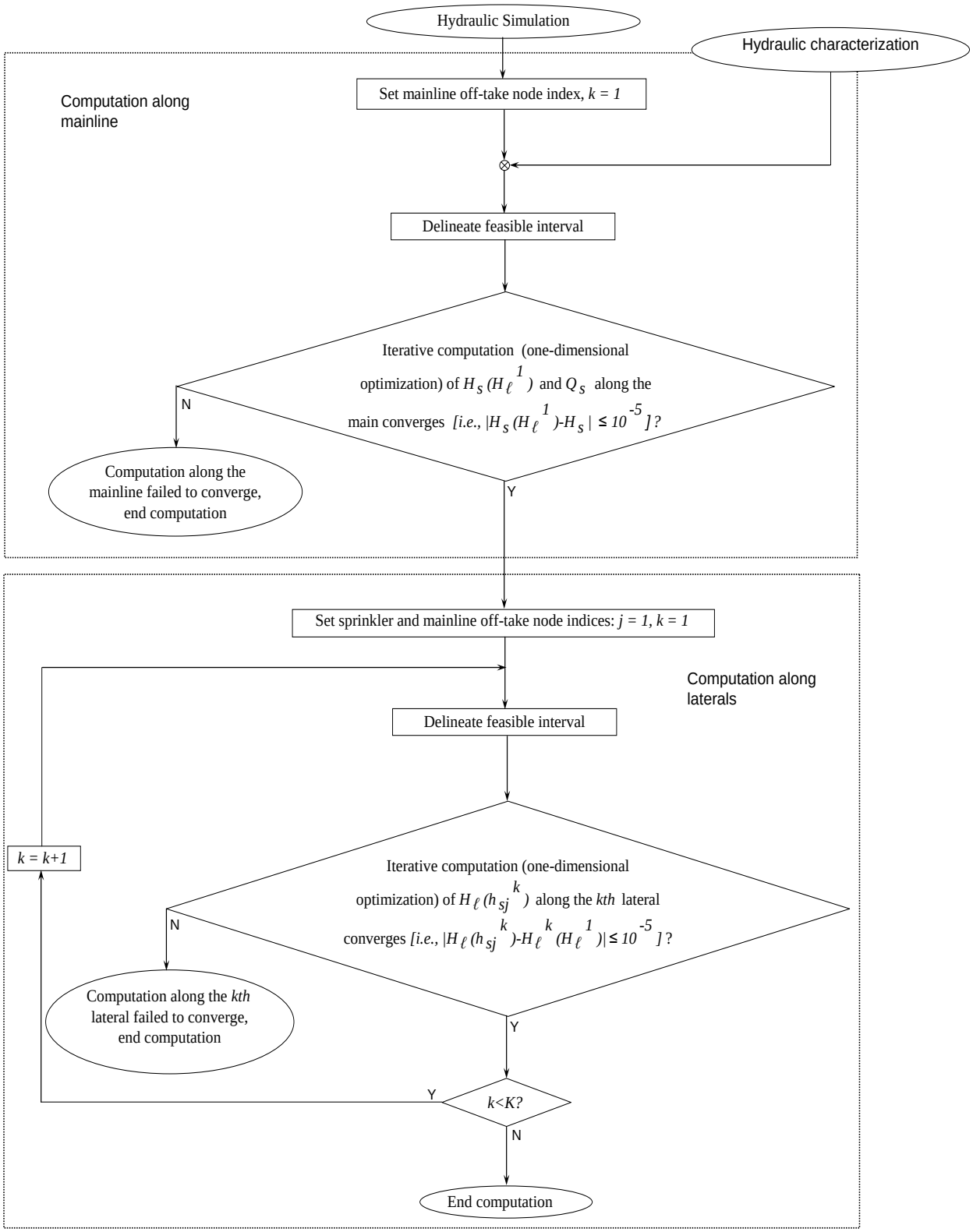

Figure 10 Flow diagram depicting hydraulic simulation computation

3.4 Sprinkler system field evaluation mode

Given a sprinkler irrigated field, the field evaluation mode provides the capability for computing irrigation uniformity at the field-scale and at the scale of a uniformity evaluation-plot. Field-scale irrigation uniformity is a function of several factors that are spatially variable, including: system hydraulics (a function of pipe sizes, hydraulic characteristics, sprinkler design factors, and level of maintenance), field topography, and ambient weather condition (mainly wind speed, but also temperature and relative humidity to a lesser extent). Results of existing studies suggest that accurate field-scale evaluation of sprinkler system irrigation uniformity requires plot-scale uniformity evaluations at more than one locations in the field (e.g., Zerihun et al., 2011). Each irrigation uniformity evaluation-plot can be considered as representative of a certain fraction of the irrigated field, a field-block sufficiently small, over which the system hydraulics and field topography can be realistically assumed spatially invariant. In the model described here, irrigation uniformity in a test-plot is evaluated with two indices: Christiansen's uniformity coefficient, *UCC (*-), which is a good measure of spatially distributed sources of nonuniformity and the low-quarter distribution uniformity, DU_{lq} *(-)*, a more suitable measure of significant localized deviations in the collected precipitation depths from the average. The test-plot scale irrigation uniformity can then be scaled-up to field level through weighed averaging, taking into account the fractional area of each field-block relative to the total field area. In addition to the test-plot scale and field-scale uniformity indices, the model computes the average, minimum, and maximum collected depths for each test-plot and at the scale of an irrigated field.

Overall field-scale irrigation uniformity can be characterized based on data collected in an evaluation-plot, in which case the corresponding field-block is the entire irrigated field. Alternatively, it can be computed based on data collected in more than one test-plots suitably distributed over the irrigated field, each representing a fraction of the irrigate field.

3.5 One-dimensional optimization

3.5.1 Problem formulation

(1) During design computations the minimum sprinkler pressure head along a lateral, $h_s^{k,min}$, can occur upstream of the distal sprinkler (section 3.2). Depending on the pressure head at the distal sprinkler, h_{s1}^{k}, the minimum sprinkler pressure head along the lateral can be smaller than the minimum acceptable sprinkler pressure head specified at the input, h_s^{ma}. In which case, h_{s1}^{k} is computed iteratively such that the absolute difference between $h_s^{k,min}$ and h_s^{ma}, ε_{f1} (Eq. 83), is reduced to within a specified error margin:

$$\varepsilon_{f1} = \left| h_s^{k,\mathbf{min}}\left(h_{s1}^{k}\right) - h_s^{ma} \right| \qquad (83)$$

(2) During design computations, the total head at each of the mainline off-take nodes, H_k (computed as a function of the total head at the distal mainline outlet, H_ℓ^1), should at least be equal to the required total head at the respective off-take nodes. The satisfaction of this constraint makes sure that along each lateral $h_s^{ma} \leq h_s^{k,min}$ (condition 1 above). In the model described here this design requirement is formulated as follows: at the critical mainline outlet (section 3.2), the absolute difference between $H_\ell^k(H_\ell^1)$ and $H_\ell^{k,r}$, ε_{f2}, should be less than a specified error margin:

$$\varepsilon_{f2} = \left| H_\ell^k\left(H_\ell^1\right) - H_\ell^{k,r} \right| \qquad (84)$$

(3) During simulation computations, the total head at the distal mainline outlet, H_ℓ^1, is computed iteratively such that the absolute difference between the computed total dynamic head, $H_s(H_\ell^1)$, and the total dynamic head specified at the input, H_s, (ε_{f3}) is within a specified error margin:

$$\varepsilon_{f3} = \left| H_s\left(H_\ell^1\right) - H_s \right| \qquad (85)$$

As part of this computation, the distribution of total head and discharges (Q_ℓ^k and H_ℓ^k) along the mainline outlets are determined.

(4) During simulation, the pressure head at the distal sprinkler, h_{s1}^k, of each lateral is computed iteratively such that the absolute difference between the total head computed at the hydraulic characterization node of a lateral, $H_\ell^k(h_{s1}^k)$, and the total head at the corresponding mainline outlet computed in step 3 above, H_ℓ^k, (ε_{f4}) is reduced to within a specified error margin:

$$\varepsilon_{f4} = \left| H_\ell^k\left(h_{s1}^k\right) - H_\ell^k \right| \qquad (86)$$

Equations 82-85 summarize the sprinkler hydraulic problems that require iterative solution in order to reduce the absolute difference between computed values of the functions, $\left[h_s^{k,min}\left(h_{s1}^k\right), H_\ell^k\left(H_\ell^1\right), H_s\left(H_\ell^1\right), H_\ell^k\left(h_{s1}^k\right)\right]$, and their required values to within a specified error margin. The required values of the functions are either specified at the input $\left[h_s^{ma}, H_s\right]$ or computed a priori based on a different set of conditions $\left[H_\ell^{k,r}, H_\ell^k\right]$.

The numerical solution of each of the above hydraulic problems involves the minimization of an error function through one-dimensional optimization. In general near the optimal solution the quadratic function is a better behaved function, and is more amenable to numerical computation, than the absolute value function (Eqs. 83-86). Hence, using a quadratic error function, the error minimization problems listed above can be summarized in a more compact and formal optimization format:

$$\begin{aligned} &\textbf{min} \quad \varepsilon_f(x) = \left(f(x) - f_r\right)^2 \\ &x \in [a, d] \end{aligned} \qquad (87)$$

where ε_f = the square of the error functions listed above (Eq. 83-86), f = computed values of the functions, $\left[h_s^{k,min}\left(h_{s1}^k\right), H_\ell^k\left(H_\ell^1\right), H_s\left(H_\ell^1\right), H_\ell^k\left(h_{s1}^k\right)\right]$; f_r = the required values of the functions, which is either specified at the input or computed a priori based on a different set of conditions $\left[h_s^{ma}, H_\ell^{k,r}, H_s, H_\ell^k\right]$; x = the independent variable of the optimization problem, which is h_{s1}^k or H_ℓ^1; [.] = a closed set (the elements of which are real numbers) over which the function, f, is defined; a and d = are the lower and upper limits, respectively, of the closed interval; and $\in$ = an element of the closed interval.

Potential feasible set: For each design and simulation problem described above (Eqs. 83-86), the potential feasible set is defined based on hydraulic considerations. Considering the design and simulation problem posed in Eqs. 83 and 86, the potential feasible set is the range of variation of pressure head for the distal sprinkler of the lateral, i.e., $h_{s1}^{k} \in [h_{s1}^{k,min}, h_{s1}^{k,max}]$; where $h_{s1}^{k,min}$ and $h_{s1}^{k,max}$ = the lower and upper bounds, respectively, of the range of variation of the pressure head at the distal sprinkler of the lateral that obtains its supply from the *kth* mainline off-take node. As described in section 3.1, for each lateral $h_{s1}^{k,min}$ and $h_{s1}^{k,max}$ are either specified at the input, for the distal lateral, or computed as function of them for the laterals upstream. For the hydraulic design and simulation problem posed in Eqs. 83 and 84, the feasible set of H_{ℓ}^{l} is given as, $[H_{\ell}^{l,min}, H_{\ell}^{l,max}]$, where $H_{\ell}^{l,min}$ and $H_{\ell}^{l,max}$ = the lower and upper bounds, respectively, of the range of variation of the total head at the distal mainline outlet. Note that the range $[H_{\ell}^{l,min}, H_{\ell}^{l,max}]$ is determined during the hydraulic characterization computation as a function of the minimum and maximum pressure heads at the distal sprinkler of the distal lateral (section 3.1). Although these are the potential feasible sets for the hydraulic design and simulation problems formulated above (Eqs. 83-86), subsets of them are used in the numerical solution. This will be described in more detail in the description of the numerical algorithm used to solve the hydraulic simulation problems posed above.

Unimodal property of error function (Eq. 87): Given a sprinkler system layout, land slope, pipe diameters, number and type of pipe appurtenances, hydraulic characteristics, and sprinkler characteristics; it can be noted from lateral and mainline hydraulics (sections 2.2 and 2.3*)* that increasing the values of the variables $(h_{s1}^{k}, H_{\ell}^{l})$, will invariably lead to increased function values, $h_{s}^{k,min}(h_{s1}^{k})$, $H_{\ell}^{k}(H_{\ell}^{l})$, $H_{s}(H_{\ell}^{l})$ and $H_{\ell}^{k}(h_{s1}^{k})$ and vice versa. The implication is that each of these functions can be described as strictly increasing functions of their respective variables. A corollary that stems from this property of the functions is that Eqs. 83-86 and their respective quadratic error functions (Eq. 87) are unimodal, provided the design/simulation requirement specified at the input is within the range of variation of the computed values of the functions.

In order to illustrate this point, numerical examples are presented for the $h_{s}^{k,min}(h_{s1}^{k})$ and $H_{s}(H_{\ell}^{l})$ functions (Eqs. 83 and 85), Figures 11a-11f. The input data set

used, in the simulation results summarized in Figures 11a-11f, is the same as that used in the simulation example presented in the companion document for a system with single-line laterals layout configuration(Zerihun and Sanchez, 2012), except that the slope along a lateral is constant and is -0.04% for the upper half of the field and -0.06% for the lower half. Figure 11a shows that the longitudinal profile of the sprinkler pressure head along a lateral is an increasing function of the pressure head at the distal sprinkler of the lateral. For the same lateral, Figure 11b depicts the minimum sprinkler pressure head as a function of the pressure head at the distal sprinkler, which as well is a strictly increasing function. It can then be shown that if the minimum acceptable sprinkler pressure head is set at 30.0m, the corresponding error function (computed with Eq. 87) is unimodal with respect to the pressure head at the distal sprinkler (Figure 11c). Another numerical example summarized in Figure 11d shows that the energy line along the main is an increasing function of the total head at its distal outlet. In Figure 11e the total dynamic head at the inlet to the mainline is shown to be an increasing function of the total head at its distal outlet. Considering a pump supplying the required discharge with a total head of 158.0m, it then follows that the corresponding error function computed with Eq. 87 is unimodal with respect to the total head at the distal mainline outlet. Similar examples can be developed to show the unimodal property of the other design and simulation problems listed above (Eqs. 84 and 86). Since unimodality property implies unique solution (in the current application, $\varepsilon_f = 0$), it is useful in verifying the validity of a numerical solution, described in subsequent section.

3.5.2 Numerical solution

The optimization problem, Eq. 86, can be solved with a number of one-dimensional optimization techniques: methods that require derivatives, polynomial interpolation with interval reduction, or function evaluation and interval reduction based approaches (e.g., Avriel, 1976; Beightler et al., 1979; McCormick, 1983). Because exact evaluation of derivatives is not possible in the current application (Eqs. 82-85), methods that require derivatives are not used here. Although polynomial approximation based techniques can in theory be more efficient, in practice they can have numerical

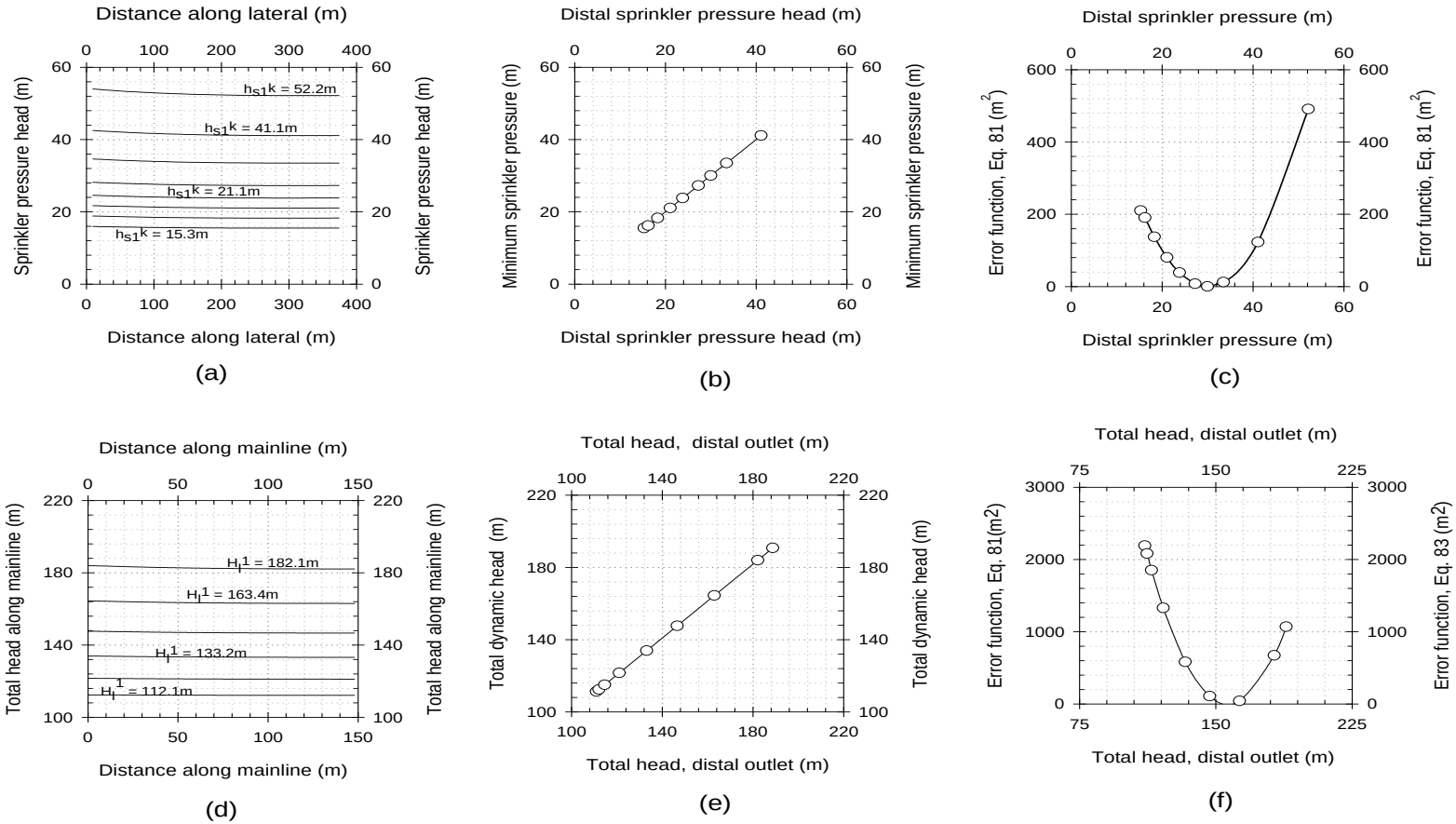

Figure 11: (a) Sprinkler pressure head longitudinal profiles, along the lateral obtaining its supply from the *kth* mainline off-take node, expressed as a function of the distal sprinkler pressure head, h_{s1}^k; (b) Minimum sprinkler pressure head along the lateral, $h_s^{k,min}$, as a function of the distal sprinkler pressure head; (c) Error function for minimum sprinkler pressure head (Eq. 83), $\varepsilon_f(h_{s1}^k) = (h_s^{k,min}(h_{s1}^k) - h_s^{ma})^2$, as a function of the distal sprinkler pressure head; (d) Energy line along the main as a function of total head at the distal outlet, H_ℓ^1; (e) Total dynamic head as a function of the total head at the distal outlet, H_ℓ^1; (f) Error function for total dynamic head (Eq. 85), $\varepsilon_f(H_\ell^1) = (H_s(H_\ell^1) - H_s)^2$, as a function of total head at the distal outlet

instabilities (McCormick, 1983). A robust and simple technique based on function evaluation and solution interval reduction through successive iterations, known as the golden section technique, is implemented in the model described here. This technique is most suitable for minimizing unimodal functions, a property of the functions described above. The technique searches for the optimum solution to the problem posed in Eq. 87, $[x^*, \varepsilon_f(x^*)]$, where x^* is the function minimizer, in two steps: (1) Delineation of the closed interval, $[a,d]$, that contains x^* and (2) computation of the optimal solution $[x^*, \varepsilon_f(x^*)]$. A description of the golden section algorithm as implemented in the model described here is presented subsequently.

At any given iteration (say the *ith* iteration), the golden section algorithm requires the function value be known at the interval bounds, $\varepsilon_f(a^i)$ and $\varepsilon_f(d^i)$, and at two additional points interior to the interval, $\varepsilon_f(b^i)$ and $\varepsilon_f(c^i)$, where $a^i<b^i<c^i<d^i$. During each iteration the function values at the interior points are used to check for solution convergence. If the convergence requirement is met then the solution is obtained. If not, one of two scenarios are used to advance the solution to the next iteration: *(i)* If a comparison of the function values $\varepsilon_f(b^i)$ and $\varepsilon_f(c^i)$ shows that $\varepsilon_f(b^i) \le \varepsilon_f(c^i)$ then the feasible space for the *(k+1)th* iteration, $[a^{i+1},d^{i+1}]$, is reduced such that

$$a^{i+1} = a^i, \quad d^{i+1} = c^i, \quad and \quad c^{i+1} = b^i \qquad (88)$$

and a new interior point, b^{i+1}, within the *(i+1)th* interval is computed with and the function value, $\varepsilon_f(b^{i+1})$, is calculated.

$$b^{i+1} = \frac{3-\sqrt{5}}{2}\left(d^{i+1} - a^{i+1}\right) + a^{i+1} \qquad (89)$$

(ii) If, on the other hand, a comparison of $\varepsilon_f(b^i)$ and $\varepsilon_f(c^i)$ shows that $\varepsilon_f(c^i) < \varepsilon_f(b^i)$, then the feasible space for the *(i+1)th* iteration $[a^{i+1},d^{i+1}]$ is reduced as follows:

$$a^{i+1} = b^i, \quad d^{i+1} = d^i, \quad and \quad b^{i+1} = c^i \qquad (90)$$

and a new point c^{i+1} is computed with

$$c^{i+1} = \frac{\sqrt{5}-1}{2}\left(d^{i+1} - a^{i+1}\right) + a^{i+1} \qquad (91)$$

and the function value $\varepsilon_f(c^{i+1})$ is calculated. In both scenarios, function values at interior points are then used to check for solution convergence. If convergence is not reached, the steps described above are repeated resulting in further reductions in the feasible interval.

An important characteristics feature of the golden section algorithm is that at any given iteration, the placing of the interior points, b^i and c^i, within the closed interval $[a^i,d^i]$ is such that

$$\frac{b^i - a^i}{d^i - a^i} = \sigma_1 = \frac{3-\sqrt{5}}{2} \approx 0.382 \qquad (92)$$

$$\frac{c^i - a^i}{d^i - a^i} = \sigma_2 = \frac{\sqrt{5}-1}{2} \approx 0.618 \qquad (93)$$

If the ratios, σ_1 and σ_2, are true for the *ith* iteration; it can then be shown (based on Eqs. 88-91) that they are also true for all subsequent iterations. If scenario *i* above holds then we have

$$\frac{c^{i+1} - a^{i+1}}{d^{i+1} - a^{i+1}} = \frac{b^i - a^i}{c^i - a^i} = \frac{\sigma_1}{\sigma_2} = 0.618 \qquad (94)$$

on the other hand, if scenario *ii* holds then we have

$$\frac{b^{i+1} - a^{i+1}}{d^{i+1} - a^{i+1}} = \frac{c^i - b^i}{d^i - b^i} = \sigma_1 = 0.382 \qquad (95)$$

Note that the ratio of the interval size at any given iteration, say the *(i+1)th* iteration, to that at the *kth* iteration is a constant, *0.618*, which implies that the rate of convergence for the golden section algorithm is linear. Although it has a slower rate of convergence compared for instance to Newton's method or polynomial interpolation techniques, the main advantage of the golden section technique is that it is a conceptually simple and a more robust algorithm. In addition, although four points are needed to execute a given iteration, at any one iteration only one new function evaluation is required.

Implementation of the golden section algorithm in the model described here is outlined subsequently. First a description of the interval delineation phase is presented, followed by optimal solution phase.

(1) Delineation of the solution interval: The potential feasible sets defined above, based on hydraulic considerations, can in principle be used as the solution space, *[a,d]*, for the optimization problem posed in Eq. 87. However, solution efficiency can be enhanced if an interval delimitation step is used to define a smaller feasible set, *[a,d]*, within $[h_{s1}^{k,min}, h_{s1}^{k,max}]$ or $[H_\ell^{1,min}, H_\ell^{1,max}]$ as the case may be. In the model described here an efficient algorithm based on an approach proposed by McCormick (1983) is used to define the feasible set in Eq. 87.

As described above, in order to execute a golden section iteration, four points need to be defined within the feasible set: the lower and upper bounds of the feasible set, *[a,d]*, and two additional points, *b* and *c*, interior to the interval (such that $a<b<c<d$). Hence, the interval delineation phase is undertaken in at least four steps. The procedure for delineating the feasible interval is:

(i) Set the feasible interval delineation step counting index, $\psi = 1$; and the lower bound of the feasible set, $x^{(\psi=1)}$, to the lower limits of the variable range, x^{min}; where x^{min} = the minimum value of the variable, given as:

(ia) For the design problem given in Eq. 83, set $x^1 = h_{s1}^k = h_s^{ma}$ and proceed to step *(ii)*; or

(ib) For the design problem defined in Eq. 84 set $x^1 = H_\ell^1 = H_\ell^{1,r}$ and proceed to step *(ii)*; or

(ic) For the simulation problem given in Eq. 85, set $x^1 = H_\ell^1 = H_\ell^{1,min}$ and proceed to step *(ii)*; or

(id) For the simulation problem given in Eq. 86, set $x^1 = h_{s1}^k = h_{s1}^{k,min}$ and proceed to step *(ii)*;

(ii) Evaluate the error function, $\varepsilon_f(x^\psi)$ Eq. 87, and proceed to step *(iii)*;

(iii) Set $\psi = \psi+1$ and compute x^ψ, with the following function (McCormick, 1983):

$$x^{\psi} = x^{1} + \delta(\sigma_3)^{\psi} \qquad (96)$$

and proceed to step *(iv)*. where δ is a constant step size, the values of which can be determined based on numerical experimentation. In the model described here values of δ = 0.2 for Eqs. 83 and 86 and δ = *0.1* for Eqs. 84 and 85 and σ_3 is given as:

$$\sigma_3 = \frac{\sigma_2}{\sigma_1} = \frac{\sqrt{5}-1}{3-\sqrt{5}} = \frac{1}{2}(1+\sqrt{5}) \approx 1.618 \qquad (97)$$

It can be shown that the definition of σ_3 in terms of σ_1 and σ_2 allows the interval delineation computation to produce the two interior points along with the interval bounds. In addition, the fact that Eq. 95 is an exponential function implies that it has the mathematical property to be efficiently used over a wide range of feasible interval sizes.

(iv) Feasibility test:

(iva) If $x^{\psi} \leq x^{max}$ (where x^{max} = the upper limit of the feasible interval as determined through hydraulic considerations, section 3.5.1; which could be $h_{s1}^{k,max}$, for Eqs. 83 and 86 or $H_{\ell}^{1,max}$ for Eqs. 84 and 85), then evaluate $\varepsilon_f(x^{\psi})$ and proceed to step *(v);* or

(ivb) If $x^{max} < x^{\psi}$ and design problem (Eq. 83), then evaluate $\varepsilon_f(x^{\psi})$ and proceed to step *(v)* (cautionary note will be attached to output data); or

(ivc) If $x^{max} < x^{\psi}$ and simulation/design problem (Eq. 84, 85, or 86), then x^{ψ} exceeds the upper limit of the feasible space, end computation;

(v) Convergence test:

(va) If $\varepsilon_f(x^{\psi}) < \varepsilon_f(x^{(\psi-1)})$ or $\varepsilon_f(x^{(\psi-1)}) < \varepsilon_f(x^{\psi})$ and $\psi < 4$; then repeat steps *(iii)* and *(iv)*; or

(vb) If $\varepsilon_f(x^{(\psi-1)}) < \varepsilon_f(x^{\psi})$ and $4 \leq \psi$, then the upper limit of the feasible set is computed and is given as $d = x^{\psi}$ and from step *(i)* above the lower limit of the feasible interval is $a = x^{1}$; it can also be shown that when the interval delineation steps are computed with Eq. 96, the interior points are given as $b = x^{(\psi-2)}$ and $c = x^{(\psi-2)}$; proceed to step 2 (computation of optimal solution)*;* or

(vc) If $\psi = 2$ and $\varepsilon_f(x^1) < \varepsilon_f(x^\psi)$, then this could imply that the step size is sufficiently large that the upper bound of the feasible set, d, is computed in a single step or it may mean that the solution lies outside the feasible set. To ascertain which of these scenarios are true proceed to step *(vi)*;

(vi) Set the upper bound of the interval, $d = x^{(\psi=2)}$, and proceed to *(vii)* and initiate a search for a new lower bound and the intermediate points;

(vii) Set $\psi = \psi + 1$ and compute x^ψ in accord with:

$$x^\psi = d - \delta(\sigma_3)^\psi \qquad (98)$$

and proceed to step *(viiia);* note that a smaller step size, δ, is used to compute x^ψ with Eq. 98 than in Eq. 96;

(viii) Feasibility test:

(viiia) If $x^{min} \leq x^\psi$ then evaluate $\varepsilon_f(x^\psi)$ and proceed to step *(ix);* or

(viiib) If $x^\psi < x^{min}$ and design problem (Eq. 83), then evaluate $\varepsilon_f(x^\psi)$ and proceed to step *(ix)* (cautionary note will be attached to output data)*;* or

(viiic) If $x^\psi < x^{min}$ and design/simulation problem (Eq. 84, 85, or 86), then x^ψ is outside the feasible space, end computation;

(ix) Convergence test:

(ixa) If $\varepsilon_f(x^\psi) < \varepsilon_f(x^{(\psi-1)})$ or $\varepsilon_f(x^{(\psi-1)}) < \varepsilon_f(x^\psi)$ and $\psi < 5$; then repeat steps *(vii)* and *(viii)* above; or

(ixb) If $\varepsilon_f(x^{(\psi-1)}) < \varepsilon_f(x^\psi)$ and $5 \leq \psi$, then the lower limit of the feasible set is computed and is given as $a = x^\psi$ and from step *(vi)* above the upper limit of the feasible set is $d = x^{(\psi=2)}$; it can also be shown that when the interval delineation steps are computed with Eq. 98, the interior points are given as $b = x^{(\psi-1)}$ and $c = x^{(\psi-2)}$; and then proceed to step 2 (computation of optimal solution).

(2) Computation of optimal solution

(i) Set iteration index, $i = 1$, and $a^i = a$, $b^i = b$, $c^i = c$, and $d^i = d$ and proceed to step *ii*;

(ii) Convergence test (letting $\varepsilon(b^i) = \left|\sqrt{\varepsilon_f(b^i)}\right|$ and $\varepsilon(c^i) = \left|\sqrt{\varepsilon_f(c^i)}\right|$):

(iia) If $10^{-5} < \varepsilon(b^i)$ and $10^{-5} < \varepsilon(c^i)$ then proceed to step *(iii)*; or

(iib) If $\varepsilon(b^i) \leq 10^{-5}$ and $10^{-5} < \varepsilon(c^i)$ (or $\varepsilon(b^i) \leq 10^{-5}$ and $\varepsilon(c^i) \leq 10^{-5}$, but $\varepsilon(b^i) \leq \varepsilon(c^i)$, then proceed to step *(vi)*; or

(iic) If $\varepsilon(c^i) \le 10^{-5}$ and $10^{-5} < \varepsilon(b^i)$ (or $\varepsilon(b^i) \le 10^{-5}$ and $\varepsilon(c^i) \le 10^{-5}$, but $\varepsilon(c^i) \le \varepsilon(b^i)$), then proceed to step *(vii);*

(iii) Function comparisons for interval reduction:

(iiia) If $\varepsilon_f(c^i) \le \varepsilon_f(b^i)$ then proceed to step *(iv);* or

(iiib) If $\varepsilon_f(b^i) < \varepsilon_f(c^i)$ then proceed to step *(v).*

(iv) Define a new interval as follows:

$$a^{i+1} = b^i,\ d^{i+1} = d^i,\ b^{i+1} = c^i,\ \text{and}\ c^{i+1} = \sigma_2\left(d^{i+1} - a^{i+1}\right) + a^{i+1} \qquad (99)$$

and compute $\varepsilon_f(c^{i+1})$. Set $i = i+1$ and proceed to step *(ii)* above;

(v) Define a new interval as follows:

$$a^{i+1} = a^i,\ d^{i+1} = c^i,\ c^{i+1} = b^i,\ \text{and}\ b^{i+1} = \sigma_1\left(d^{i+1} - a^{i+1}\right) + a^{i+1} \qquad (100)$$

and compute $\varepsilon_f(b^{i+1})$. Set $i = i+1$ and proceed to step *(b)* above;

(vi) The computation has converged the optimal point is $[b^i, \varepsilon_f(b^i)]$;

(vii) The computation has converged and the optimum point is $[c^i, \varepsilon_f(c^i)]$;

In the preceding sections, the computational modes (system hydraulic characterization, design, and simulation) of the hydraulic model (*SprinklerModel*) developed in this study are described. In addition, a one-dimensional optimization algorithm implemented in the model for solving sprinkler systems hydraulic design and simulation problems is presented. The components of the sprinkler model (i.e., the program modules) and their functions as well as the steps for installing and running the model are described in subsequent section.

Chapter 4. Model functionality, installation, and running

4.1 Model components and description

The sprinkler model described here (*SprinklerModel*) is a C++ program developed based on the object oriented programming approach. The model has ten classes (user defined data types and member functions): *CSprinklerModel, CInput, CComputeModesOptimization, CCalculationLateral, CCalculationMainSLL,*

CCalculationMainDLL, CCalculationInterpolation, CCalculationHydraulic, CIrrigationUniformity, and *COutput*. Each of these classes consists of a pair of files: a header file for the declaration of member functions with the extension (*.h*) and an implementation file with extension (*.cpp*). The header files are those in which the member functions and variables of a class are declared and their attributes defined: *CSprinklerModel.h, CInput.h, CComputeModesOptimization.h, CCalculationLateral.h, CCalculationMainSLL.h, CCalculationMainDLL.h, CCalculationInterpolation.h, CCalculationHydraulic.h, CIrrigationUniformity.h,* and *COutput.h*. The implementation files are those in which functions declared in the header files are implemented: *CSprinklerModel.cpp, CInput.cpp, ComputeModesOptimization.cpp, CCalculationLateral.cpp, CCalculationMainSLL.cpp, CCalculationMainDLL.cpp, CCalculationInterpolation.cpp, CCalculationHydraulic.cpp, CIrrigationUniformity.cpp,* and *COutput.cpp*. Figure 12 shows the interrelationship between the different classes that the *SprinklerModel* is composed of. As can be noted from Figure 12, the file *SSDSM.cpp (Sprinkler System Design and Simulation Model)* contains the main function of the program.

The class *CSprinklerModel* has one member function with a public scope called *Run*, which is invoked by a function call from the *SSDSM.cpp* file. This class has four member functions that are private to the class: *SystemCharacterization*, *SystemDesign*, *SystemSimulation*, and *FieldEvaluation*. The class *CSprinklerModel* is one in which variables with global scope are declared and function calls to the member functions of the *CInput, CComputeModesOptimization, CIrrigationUniformity,* and *COutput* classes are made. The *CInput* class has several member functions declared in the header file, *CInput.h*. The functions in the *CInput* class create, the folders in which input and output data files are stored and, read input data from these files during run time (sections 4.2.2 and 4.3). They also copy the input data file templates (*LateralInputDataTableDW.inp, MainInputDataTableDW.inp, LateralInputDataTableHW.inp* and A *SprinklerModel* project consists of all the input and output data files of a given field-scale solid set sprinkler system for which hydraulic characterization, design, and/or simulation computations are to be conducted. The *CComputeModesOptimization* class has several member functions that have both private and public scope. The numerical

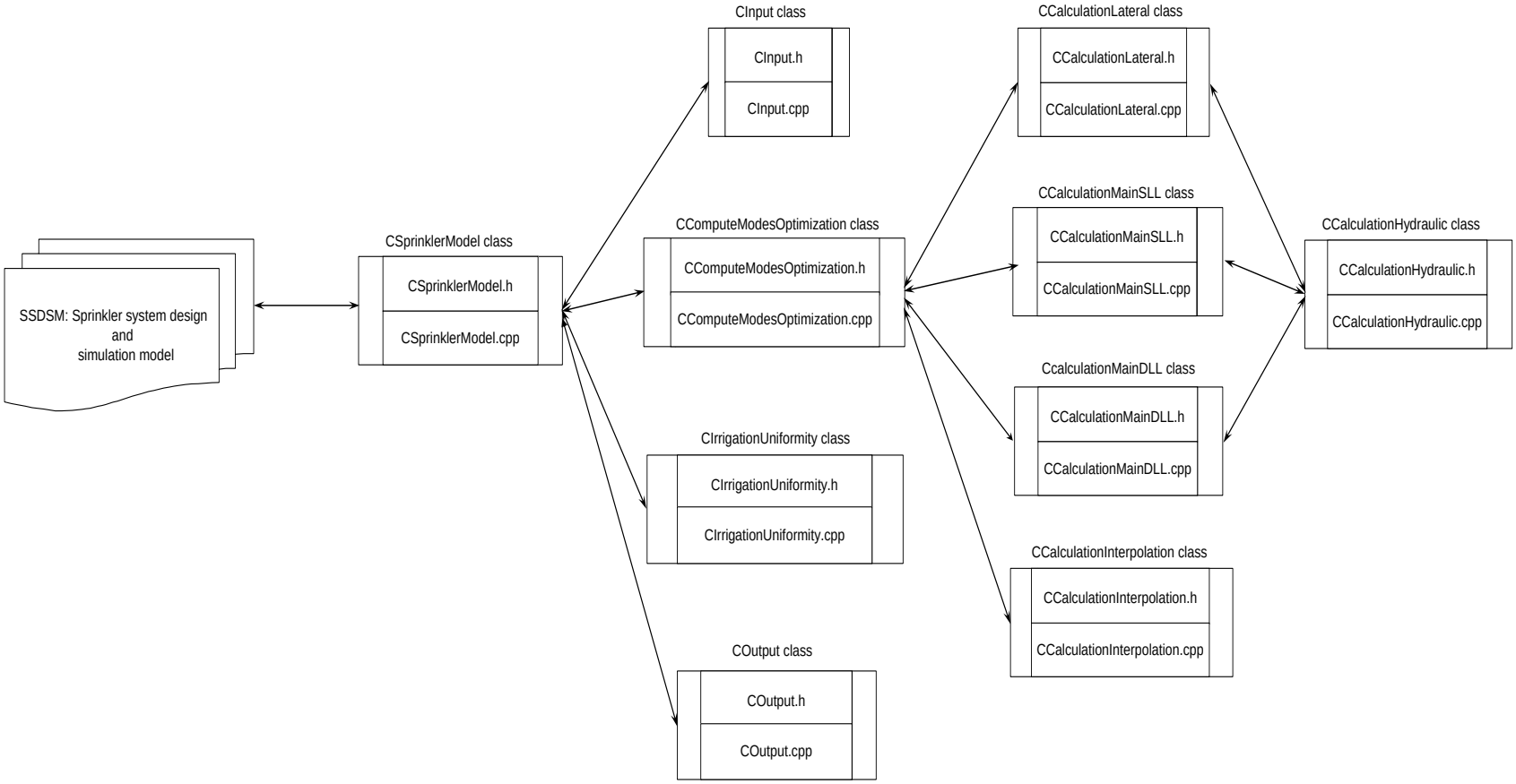

Figure 12. SprinklerModel components

solution of hydraulic design and simulation problems involve one-dimensional optimization, in which the value of the system variables are computed such that the design and simulation requirements specified at the input are satisfied (sections 3.2 and 3.3). The functions for one-dimensional optimization are implemented in this class. In addition, the member functions of those classes where numerical computations take place (*CCalculationLateral*, *CCalculationMainSLL*, *CCalculationMainDLL*, *CCalculationInterpolation*, and *CIrrigationUniformity*) are accessed through member functions of the *CComputeModesOptimization* class (Figure 12).

The *CCalculationLateral* class has member functions, declared in the header file, that have both public scope and are private to the class. The functions that iteratively solve the basic hydraulic equations of laterals (section 2.2), when the model is run under the system design, system simulation, or system characterization options are included in this class.

The *CCalculationMainSLL* class contains the member functions that iteratively solve the hydraulic equations of a sprinkler mainline with single-line laterals: computing the distribution of specific energy and outlet discharges and associated total heads along the main (section 2.3.1).

The *CCalculationMainDLL* has member functions with both public and private scope. These functions are used to compute the longitudinal distribution of specific energy and outlet discharges and associated total heads along a mainline with double-line of laterals (section 2.3.2).

The *CCalculationInterpolation* class has several member functions with both private and public scope. The functions in this class are used to compute the parameter estimates of the cubic spline interpolants that relate total head and discharge for each mainline outlet (section 2.3).

The *CCalculationHydraulic* class has several member functions declared in its header file *CCalculationHydraulic.h*. The member function of the *CCalculationHydraulic* class perform basic hydraulic computations, including the calculation of friction head losses in pipe sections either with the Darcy-Weisbach or Hazen-Williams equation, and the local energy losses associated with various pipe fittings and appurtenances. The functions in this class are accessed through member

functions in the *CCalculationLateral, CCalculationMainSLL,* and *CCalculationMainDLL* classes (Figure 12).

The *CIrrigationUniformity* class has member functions that have both pubic and private scope. These member functions compute evaluation-plot scale and field-scale irrigation uniformity indices. They also compute the maximum, minimum, and average precipitation depths for each uniformity evaluation plot and at the field-scale.

The *COutput* class has several member functions both with public and private scope. These member functions save output data files (section 4.2.3) into appropriate subfolders created during runtime by the program (section 4.3). Functions in this class are accessed through member function in *CSprinklerModel* class (Figure 12).

4.2 Model functionality: computational modes and input/output

4.2.1 Computational modes

The *SprinklerModel* described here has four computational options that are functional: System hydraulic characterization, design, simulation, and field evaluation. Given the hydraulic, geometric, and topographic characteristics of a sprinkler system, the hydraulic characterization computations define the system hydraulic characteristics. Although results of the system hydraulic characterization computations are useful in pump selection or evaluation; its main significance is in generating the necessary data sets for subsequent computations: hydraulic deign and simulation.

With the design computational mode, the design sprinkler pressure head (obtained from manufacturer's catalogue) along with the minimum acceptable sprinkle pressure head are specified at the input. The model then computes the field-wide distribution of sprinkler pressure head and discharges and the corresponding total dynamic head such that the pressure head at the critical sprinkler is sufficiently close to the acceptable minimum. If, however, the system configuration is such that the maximum sprinkler pressure head is an acceptably high, the design can be revised and refined through repeated computations with different lateral/mainline diameters, sprinklers, and spacing combinations.

During simulation computations, the model calculates the spatial distribution of sprinkler discharges and pressure heads over the irrigated field, given the total dynamic head at the system inlet. Because the spatial distribution of sprinkler pressure heads and discharges are good indicators of field-scale irrigation uniformity, the hydraulic simulation functionality of the model described here can be considered as a useful tool in evaluating the potential irrigation uniformity of an existing system. Detailed description of the computational algorithms as related to these computational modes is presented in sections 3.2-3.5.

With the field evaluation mode, the model computes irrigation uniformity indices, as well as maximum, minimum, and average precipitation depths at the scale of a test-plot and an irrigated field based on field measured data.

4.2.2 Input data files

The *SprinklerModel* developed in the current study obtains its input data from space delimited text files. The model has two types of input data files: the project configuration file (*SprinklerModelConfiguration.Inp*) and the files that contain the hydraulic, geometric, and topographic input data and irrigation uniformity field evaluation data. The project configuration file contains input data on the selection of: computational modes, lateral configuration, and friction equation options for the current project and is placed directly under the *Projects* subfolder (section 4.3). Valid numerical inputs for computational mode are *1(*system hydraulic characterization), *2* (system design), *3* (system simulation), and *5*(Field evaluation) computations. Option 4 is skipped in the current version of the model, because it is reserved for the parameter estimation functionality, which is not yet functional; but will be included in subsequent versions. Lateral configuration mode is set to *1* for a sprinkler system with single-line laterals or it is set to *2* for a system with double-line laterals. Friction equation option is set to *1* for Darcy-Weisbach equation and is set to *2* for Hazen-Williams equation.

When the model is run in modes 1, 2, and 3, one of two pairs of files (placed under the current project folder, section 4.2.4) are used for specifying the hydraulic input data for any given project. For projects in which friction head losses are computed with the Darcy-Weisbach equation, the hydraulic input data files are:

LateralInputDataTableDW.Inp (for laterals) and *MainInputDataTableDW.Inp* (for the mainline). For projects in which friction is computed with the Hazen-Williams equation the input data files are: *LateralInputDataTableHW.Inp* (for laterals) and *MainInputDataTableHW.Inp* (for the mainline). These files can be found in the *InputDataTemplate* directory subfolder and also in the *Projects* subfolder (section 4.2.4 and 4.3).

The hydraulic input data types and the volume of the input data file vary depending on the computational modes, the friction formula used, and the lateral configuration option. It also depends on whether the input data file is for the mainline or for a lateral as well as on the specific hydraulic, geometric, and topographic conditions of the sprinkler system being modeled. Each of the hydraulic, geometric, and topographic input data files has two data types. The first set of input data (nontabular data) consists of the number of pipe sections along laterals/main, number of sprinklers/laterals, system hydraulic characterization/ design/ simulation constraints or requirements. For instance, the minimum acceptable and the design sprinkler pressure heads along with the maximum permissible velocity are specified in this section of the lateral input data file, if the system design computational option is selected. On the other hand, if the model is to be run under the system simulation option, then the total dynamic head at the mainline inlet should be specified in this segment of the mainline input data file. The pressure head range for the distal sprinkler need to be specified (in the mainline input data file) for use in the hydraulic characterization computation. If friction is computed with the Darcy-Weisbach equation water temperature should be specified in this section of the input data files.

The second part of a hydraulic input data file has a tabular format, in which each row represents the hydraulic, geometric, and topographic characteristics of the mainline or lateral at a computational node. The tabular format of the hydraulic input data provides maximum flexibility in taking into account spatial variations in these factors along a lateral (between laterals) or along the mainline. The columns represent such data items as: distance of the respective nodes from the inlet of the pipe (mainline or lateral), nodal elevations, pipe (which could be main, lateral, or sprinkler riser) diameters, friction coefficients, sprinkler discharge coefficients for laterals, and local head loss coefficients

for pipe appurtenances. In addition, the tabular section of the mainline hydraulic input data file contains two sets of data columns that define the topographic, geometric, and hydraulic characteristics of each mainline outlet; one for each set of laterals on either side of the mainline (Figure 4). Note that if the sprinkler system has only a single-line of laterals, then the data columns for the second set of mainline outlets are set to zero. Because of space limitations the names of the data columns in both the lateral and the mainline hydraulic input data files are abbreviated, but a definition of the variable name for each data column and allowable data range is provided in the *MetaData.text* file within the *InputDataTemplate* or *Projects* subfolder (section 4.2.4 and 4.3).

When the model is run in the *FieldEvaluation* mode, the input data (collected through field measurements or representing a hypothetical irrigation scenario) is provided though a space delimited text file: *FieldEvaluationInputDataTable.Inp*. This input data file has both tabular and nontabular data. The first data segment in the *FieldEvaluationInputDataTable.Inp* file (a nontabular input) consists of data items that are common to the entire irrigated field, such as area of the irrigated field, number of uniformity evaluation plots, number of rain gage rows and columns in an evaluation-plot, as well as dimensions of an evaluation-plot. This is then followed by data segments for each uniformity evaluation plot in the field. These data sets contain precipitation depths collected within each uniformity evaluation-plot (in a tabular format) and a nontabular data related to ambient weather condition during an irrigation evaluation and associated field-block area. A metadata file (*MetaData.text*) provided in the *InputDataTemplate* or *Projects* subfolder (section 4.2.4 and 4.3) describe the file format and valid ranges for each data type.

4.2.3 Output data files

The model produces various types of output data following system characterization, design, simulation, and field evaluation computations. Model outputs for the mainline and each of the laterals following system characterization, design, and simulation computations are saved in space delimited text files and stored in separate subfolders created by the program during runtime (section 4.3). For each lateral there are three types of output data files (*LateralOutputDataTableDW.Out* or

LateralOutputDataTableHW.Out, ElevationHglEgl.Out, and *HydraulicCharacteristics.Out*). Similarly, there are three types of output data files for the

mainline (*MainOutputDataTableDW.Out* or *MainOutputDataTableHW.Out, ElevationHglEgl.Out,* and *HydraulicCharacteristics.Out*).

For each lateral the *LateralOutputDataTableDW.Out* or *LateralOutputDataTableHW.Out* file contains a summary of the hydraulic input data set as well as such output data items as the longitudinal distribution of sprinkler discharge and pressure head, lateral discharge and pressure head, velocity head, friction head loss, and local head losses. The *MainOutputDataTableDW.Out or MainOutputDataTableHW.Out* file contains a similar set of output data for the mainline. For the mainline and each of the laterals, the data on the longitudinal distribution of the specific energy and its components is stored in the *ElevationHglEgl.Out* file. The file *HydraulicCharacteristics.Out* contains data on the hydraulic characteristics of each lateral and the main (i.e., the Q_ℓ^k-H_ℓ^k table for each lateral and the Q_s-H_s table for the mainline).

Each project (involving hydraulic computational modes) has an output summary subfolder, named *OutputSummary* under the current project folder (section 4.3). Various types of output data, for all the laterals and the main, are aggregated and saved in text files that are stored in the *OutputSummary* subfolder. These files are:

(1) The hydraulic summary file (*HydraulicSummary.Out)* contains a comprehensive summary of the system hydraulic data, which is an aggregation of the contents of the *MainOutputDataTable.Out* file and all of the *LateralOutputDataTable.Out* files;

(2) The *SpecificEnergyDistributionSummary.Out* file contains a summary of the specific energy distribution data along each lateral and the mainline;

(3) The *SystemHydraulicCharacteristics.Out* file contains a summary of the hydraulic characteristics of each of the laterals and the main;

(4) The *SprinklerQdistribution.Out* file contains a summary of the spatial distribution of sprinkler discharges over the irrigated field; and

(5) The *SprinklerHdistribution.Out* file contains a summary of the spatial distribution of sprinkler pressure heads over the irrigated field.

The data sets in the files *SprinklerQdistribution.Out* and *SprinklerHdistribution.Out* are presented in a two-dimensional tabular format with values of variables shown at grid points (sprinkler locations), defined by distances from the system inlet along the mainline and in a direction normal to the mainline. A second version of these output data files (*SprinklerQdistributionContour.Out* and *SprinklerHdistributionContour.Out*), also stored in the *OutputSummary* folder, are formatted in such a way that the data can readily be imported into a contouring software (e.g., *SURFER, Golden Software, Inc.*) and the spatial distribution of the pressure head and discharge over the irrigated field can be shown as contours. The data sets in these files are arranged in three columns, the first two columns contain spatial coordinates of the sprinkle locations referenced from system inlet along the mainline and in a direction normal to the mainline and the third column consists of either the sprinkler discharges or sprinkler pressure heads. The output data file for the *FieldEvaluation* computational mode is *FieldEvaluationOutputDataTable.Out*. It contains a summary of the irrigation uniformity indices, maximum, minimum, and average collected precipitation depths at the field-scale as well as at the scale of uniformity evaluation-plots.

4.2.4 Input/output data files directory structure

The *SprinklerModel* has a specific input/output data files directory structure, which is created by the model when it is run from a folder for the first time. If the model is run from a directory folder for the first time, the subfolder in which the executable file of the *SprinklerModel* (*SprinklerModel.exe*) is placed should also contain a subfolder with the name *InputDataTemplate*. Figures 13a and 13b depicts the directory structure and files under the *InputDataTemplate* folder. Note that this folder itself is not used for

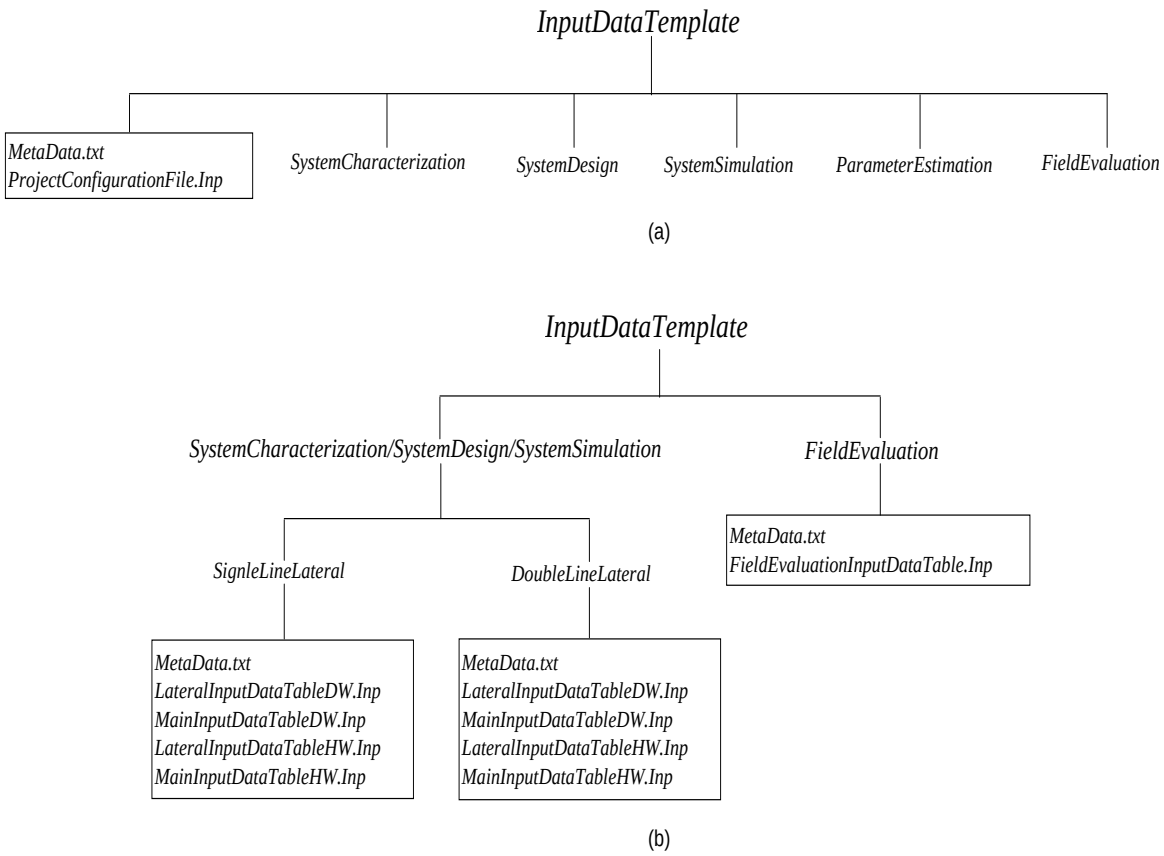

Figure 13 (a) Files and computational mode subfolders under the *InputDataTemplate* directory folder and (b) Subfolders and input data files for projects involving hydraulic computational modes with single-line of laterals (*SingleLineLateral)* or double-line of laterals (*DoubleLineLateral*) and for projects involving field evaluation computation

storing input/output data files of actual projects during program runtime. Instead, when the *SprinklerModel* is run for the first time from a subfolder, it uses the *InputDataTemplate* directory structure as the template based on which it creates an input/output data file directory structure, named as *Projects* (Figure 14a-14c). A description of the procedure whereby the model creates this directory structure will be presented in section 4.3.Prior to that, however, the structure and contents of the *InputDataTemplate* directory folder will be discussed in some detail. The *InputDataTemplate* folder contains two text file (*MetaData.txt* and *SprinklerModelConfiguration.Inp)* and five subfolders (*SystemCharacterization, SystemSimulation, SystemDesign, ParameterEstimation,* and *FieldEvaluation*),

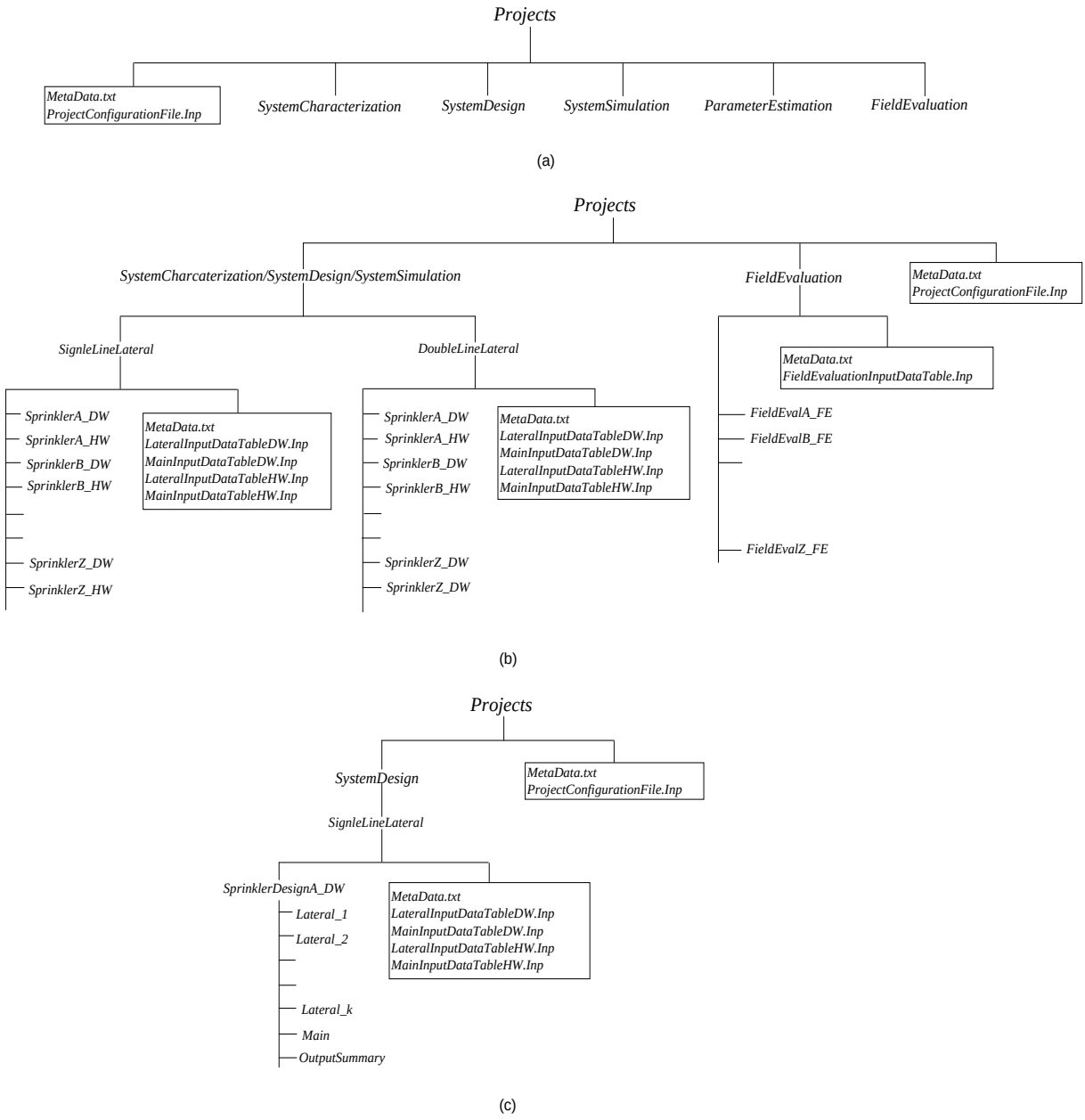

Figure 14 (a) Files and computational mode subfolders under the *Projects* directory folder; (b) Subfolders, input data files, and metadata files for projects involving hydraulic computational modes with single-line laterals *(SingleLineLateral*) or double-line laterals (*DoubleLineLateral*) and for projects involving the field evaluation computational mode; and (c) Subfolders for saving the input/output data files for the mainline and for each lateral and the output summary data files under the current project folder (considering an example in which the computational mode is *SystemDesign*, the lateral configuration option is *SingleLineLaterals*, the friction calculation option is *Darcy-Weisbach* and the project name is *SprinklerDesignA*, hence the current project folder name is *SprinklerDesignA_DW)*

Figures 13a and 13b. The file *MetaData.txt* provides a description of each of the subfolders in the *InputDataTemplate* folder and the contents of the *SprinklerModelConfiguration.Inp* file (section 4.2.2). Each of the subfolders in the *InputDataTemplate* folder represents one of the five computational modes of the sprinkler model (*SprinklerModel*): sprinkler system characterization, design, simulation, parameter estimation, and field evaluation options. In the current version of the program only the sprinkler system characterization, design, simulation, and field evaluation modes are functional. Future versions of the model will include a parameter estimation functionality as well, hence parameter estimation will not be discussed further in this report.

Under each of the *SystemCharacterization*, *SystemDesign*, and *SystemSimulation*, directory folders there are two subfolders, namely: *DoubleLineLaterals* and *SingleLineLaterals* (Figure 13b). Each of these subfolders contains five text files: hydraulic input data files for laterals and the mainline (*LateralInputDataTableDW.Inp, MainInputDataTableDW.Inp, LateralInputDataTableHW.Inp,* and *MainInputDataTableHW.Inp)* and a file describing the contents and data formats, as well as the variable names and ranges of the hydraulic input data files (*MetaData.txt*). A description of the hydraulic input data files is given in section 4.2.2. These files contain default hydraulic input data with which the model can be run. The hydraulic input data files and the project configuration file may, however, need to be modified reflecting the specifics of the project (in terms of hydraulic, geometric, and topographic data and project configuration) for which computations are to be conducted. The *FieldEvaluation* directory folder contains an input data file, *FieldEvaluationInputDataTable.Inp* (section 4.2.2), and a text file (*MetaData.txt*) describing the input data file format and the types and ranges of the data items in the input data file. The following section outlines the step for installing the program, editing input data, and running the program.

4.3 Installation and running of SprinklerModel

The following is a description of the steps to be followed to install and run the program, *SprinklerModel*:

1. *Program installation*: First create a destination directory folder, in the drive where the model is to be placed, and then simply copy the executable file (*SprinklerModel.exe*) along with the *InputDataTemplate* subfolder from the source subfolder into the destination subfolder.

2. *Running the SprinklerModel*: To run the program simply click on the *SprinklerModel.exe* file, the model will then execute the following series of steps:

3. *Check for the Projects subfolder*: when the *SprinklerModel* is run, it first checks if there is a subfolder with the name *Projects* within the program folder (the folder in which *SprinklerModel.exe* is). If there is not one already (if for example the program is run for the first time from the current folder), the program creates the folder *Projects* and subfolders under it with the same structure as the *InputDataTemplate* folder (Figures 13 and 14). The program also copies the input data file templates and the metadata files from the *InputDataTemplate* directory into an appropriate subfolders within the *Projects* folder. If the folder *Projects* already exists in the current folder, the program skips this step.

4. Specify project name: The program then opens a window in which the user is required to specify the name of the current project. Prior to the specification of the project name the project configuration file, *SprinklerModelConfiguration.Inp*, in the *Projects* folder may need to be modified and set to applicable options for the current project (section 4.2.2). In addition, the input data files may need to be modified to represent actual conditions of the field for which computations are to be conducted. The default hydraulic input data files (section 4.2.2) are in the subfolder *SingleLineLateral* or *DoubleLineLateral*, as the case may be, and the input data file for field evaluation computational mode is in the *FieldEvaluation* subfolder (Figure 14b). Hence, before a project name is specified the input data files can be opened in Microsoft Excel program, edited as necessary, and then saved as space delimited text files in the same folder. When data editing is not extensive, basic text editor such as Notepad can also be used. The program provides a second opportunity to edit the input data after the project name is

specified, current project subfolders are created, and input data files are copied into those folders (steps 6 and 7). However, considering a hydraulic computational mode, if all the laterals have the same hydraulic, geometric, and topographic properties, editing the input data at this step involves minimal effort, hence preferable. Following this steps the current project name can be specified, which leads to step 5;

5. *Create subdirectory for the current project*: Based on the project configuration inputs (specified in the *SprinklerModelConfiguration.Inp* file), the program first checks if the specified project already exists in an applicable subfolder (Figures 14a and 14b). If so, it will skip this step but provides the user with the option to edit the input data files; following which the program proceeds to step 9, *Computation*. On the other hand, if the current project is new the program then creates a subdirectory for it directly under an applicable subfolder. For instance, if the directory path to *SprinklerModel.exe* is "*C:\SprinklerModel*", the computational mode is system design, the lateral configuration option is *SingleLineLaterals*, the friction calculation formula used is Darcy-Weisbach, and the name of the project is *SprinklerDesignA* (Figure 14c); then the directory path to the project *SprinklerDesignA* will be: "*C:\ SprinklerModel\Projects\ SystemDesign\ SingleLineLaterals\SprinklerDesignA_DW*". Note that the substring *"_DW"* is appended to the specified project name to indicate that the friction calculation option used in the project is Darcy-Weisbach. On the other hand, if the friction calculation formula was Hazen-Williams, then the substring *"_HW"* would have been appended to the specified project name. The program then proceeds to step 6. On the other hand, if the computational mode selected is field evaluation, the model then creates the current project subfolder directly under the folder *FieldEvaluation*. As can be noted from Figure 14b, the project name specified at the input is automatically appended with the substring *"_FE"* to indicate that the project is field evaluation. The program then copies the input data file (*FieldEvaluationInputDataTable.Inp*) from the *FieldEvaluation* folder into the current project folder. Here the program provides an opportunity to edit the data. Note that unlike the hydraulic computational modes, in the field evaluation mode no subfolder is created under the current project folder. In stead the input and output data are placed

directly under the current projects folder. Hence, steps 6-8 are skipped and model proceeds to computation, step 9.

6. Create subfolder for the mainline (not applicable to the FieldEvaluation mode): The program then creates a subfolder for the mainline (*main*) under the current project folder, *SprinklerDesignA_DW* (step 5 above). It also copies the mainline hydraulic input data file from the source folder (*SingleLineLateral*, Figure 14c) into the folder *main* within the current project folder. Note that depending on the friction calculation option specified in the project configuration file, *SprinklerModelConfiguration.Inp,* the mainline hydraulic input data file is either *MainInputDataTableDW.Inp* or *MainInputDataTableHW.Inp* (section 4.2.2).

7. Create subfolder for each lateral (not applicable to the FieldEvaluation mode): The program obtains the number of laterals in the system from the mainline hydraulic input data file (*MainInputDataTableDW.Inp* or *MainInputDataTableHW.Inp*) and then creates the subfolders for each lateral under the current project folder (e.g., *SprinklerDesignA_DW*). As can be seen from Figure 14c, the subfolders for the laterals are named by appending an underscore and a numeral to the term "*Lateral*" (e.g., *Lateral_1*, *Lateral_2*, …*Lateral_k*). The numerals identify the laterals in the sprinkler system. Note that in the program, the laterals are numbered sequentially starting from the upstream end lateral and ending at the downstream end lateral. The program also copies the lateral hydraulic input data files (*LateralInputDataTableDW.Inp* or *LateralInputDataTableHW.Inp*) from an applicable source subfolder (e.g., *SingleLineLateral*) into the subfolders for the respective laterals (Figure 14c). Following this steps the program provides the user with an opportunity to edit the hydraulic, geometric, and topographic input data for the mainline as well as the laterals. If the input data is variable from one lateral to another, then this is the step where lateral hydraulic input data file for the pertinent laterals should be edited. The model allows variable inputs for slopes, pipe diameters, friction coefficients, the number and type of pipe appurtenances, and sprinkler characteristics along a lateral or from one lateral to another.

In addition, the length of laterals can be varied following irregularities in the field boundary, if any.

8. Create OuputSummary subfolder (not applicable to the FieldEvaluation mode): Under the current project folder (e.g., *SprinklerDesignA_DW*), the program creates another subfolder for output summary files, with the name *OutputSummary* (Figure 14c). In *OutputSummary* subfolder, a number of output data files containing a summary of the output data sets are saved following computations (section 4.2.3).

9. Computation: The program then proceeds with numerical computations, which could be done in one of four modes: hydraulic characterization, design, simulation, and field evaluation (sections 3.1-3.4).

10. Output: Following successful numerical computations, output data files (described in section 4.2.3) are saved in the relevant subfolders. For hydraulic computations, the output data files for the mainline (*ElevationHglEgl.Out* and *HydraulicCharacteristics.Out,* along with *MainOutputDataTableDW.Out* or *MainOutputDataTableHW.Out*) are saved in the subfolder *Main* (Figure 14c). The output data files of each lateral *(ElevationHglEgl.Out, HydraulicCharacteristics.Out,* and *LateralOutputDataTableDW.Out* or *LateralOutputDataTableHW.Out*) are saved in the subfolders for the respective laterals. A number of files that contain summaries of various hydraulic output data (section 4.2.3) are saved in the *OutputSummary* subfolder. For field evaluation computations the output data file (*FieldEvaluationOutputDataTable.Out*) is saved under the current project folder, which comes directly under the *FieldEvaluation* directory folder (Figure 14b).

4.4 Model input and runtime error detection functionality

The *SprinklerModel* model developed in this study has functionalities for detecting various kinds of data input and runtime errors. Data input errors that can be detected by the model are invalid numeric format, data item that is out of range, and inconsistencies in input data items. The model generates an error message describing the nature of the error and the location of the data item in the input data file, suggesting that

the data needs to be edited. During runtime intermediate model outputs could be infeasible or violate a physical constraint, in which case the model prints an error message on the screen describing the nature of the error and suggested solutions (often required adjustments in input data) to obtain results.

Chapter 5. Model limitations

Given the layout of a field-scale solid set sprinkler system, the diameters of the laterals and the mainline, nodal elevations, the friction factor, the locations, and types of pipe fittings/appurtenances along with their associated local head loss coefficients, the model in it is current state of development can compute the spatial distribution of sprinkler discharges and pressure heads over an irregularly shaped field assuming a well maintained system with negligible leakage losses. Based on these data the uniformity of sprinkler discharges as affected by system hydraulics can be computed. Although the model provides a significant level of flexibility in terms of allowing spatially variable lateral slope, pipe diameter, sprinkler head-discharge characteristics, hydraulic resistance characteristic of pipe sections, and that it takes into account local head losses along the lateral and the mainline; there are some significant limitations that need to be overcome through further development before the model can be ready for use in field-scale solid set sprinkler irrigation system design, management, and evaluation. The following are the main limitations of the model: (1) model cannot evaluate field-scale irrigation performance, (2) limited flexibility in terms of the location of the sprinkler system inlet along the mainline, (3) model lacks a user friendly interface, and (4) limited field evaluation of the hydraulic model.

(1) Limitations related to irrigation performance computation: the sprinkler hydraulic model described here needs to be further developed in order to have the capability to compute field-scale sprinkler irrigation system performance: uniformity, adequacy, and efficiency. In order for the hydraulic model to be able to quantify field-scale irrigation performance it needs to be augmented with two additional modeling functionalities:

(1a) Modeling precipitation distribution pattern around a sprinkler taking into account wind drift and spray evaporation losses: a physically based modeling functionality that is capable of simulating the distribution pattern of precipitation around a sprinkler taking into account sprinkler design factors, nozzle pressure head, and wind speed and direction (e.g., Playan et al., 2009) should be developed and coupled with the hydraulic model. Currently the authors are working on the development of a physics based droplet dynamics model capable of simulating the pattern of precipitation about a sprinkler with support from the USBR. Given the field layout, the output of such a model can be used to determine the number of overlapping sprinklers contributing to any given point in the irrigated field and the depth contributed by each sprinkler to that point (e.g., Martin et al., 2007). The total application depth can then be computed as the sum total of the contribution of each sprinkler reaching that point. Empirical approaches can be used to estimate wind drift and spray evaporation losses (Playan et al., 2009).

(1b) Soil water flow functionality: a well designed and maintained system should generally apply irrigation water at a rate lower than the steady state intake rate of the soil to prevent surface runoff. In any case, considering the complexity of the interaction of spatially varying precipitation rates, soil intake characteristics, and the overland flow hydraulics; there is no simple and reliable way of determining the amount of field-scale surface runoff from a sprinkler irrigated field. Hence, it is a design imperative to limit sprinkler application rates to a level lower than the soil steady state intake rate. Infiltration of irrigation applied water into the soil and its subsequent flow and redistribution through the soil profile can be modeled with a one-dimensional soil water flow model (e.g., HYDRUS-1D, Simunek et al., 2009). Coupling a subsurface flow model with the sprinkler hydraulic model provides a capability for matching sprinkler application rates with soil intake characteristics during system design. It also provides the functionality for computing the disposition of irrigation applied soil water with respect to crop availability at any given time subsequent to an irrigation event, based on which irrigation performance can be computed.

(2) Limited flexibilty in terms the location of the sprinkler system inlet along the mainline: Currently the model is designed to simulate the hydraulics of a solid set sprinkler network in which the mainline inlet is located at the edge of the irrigated field. Slight modification of current model can increase model flexibility in this regard.

(3) Lack of a well developed user interface: Currently the hydraulic model uses space delimited text files prepared with such programs as *MS Excel, Notepad* (or other applications with the same functionality) for data input. Output data is also saved by the program in space delimited text files and can be accessed only using application software listed above. However, a user friendly interface for editing inputs and presentation of output can be developed and integrated with the simulation engine, resulting in a standalone program that can be run in machines without the above listed applications.

(4) Limited evaluation of the hydraulic model: Evaluation of the sprinkler hydraulic model based on limited field data shows that the model is accurate. However, the model requires more extensive testing with field data in order to establish its limit of applicability and identify possible improvements.

References

Avriel, M. (1976). *Nonlinear programming: Analysis and methods*. Prentice-Hall, Inc., Englewood Cliffs, NJ.

Beightler, C.S., Phillips, D.T., and Wilde, D.J. (1979). *Foundations of optimization*. Prentice-Hall, Inc., Englewood Cliffs, NJ.

Burden, L.R., Fairies, J.D., and Reynolds, A.C. (1981). *Numerical analysis*. Prindle, Weber, & Schmidt, Boston, MA.

Granger, R.A. (1995). *Fluid Mechanics*. Dover Publications, Inc. New York, N.Y.

Harris, J.W., and Stocker, H. (1998). *Handbook of mathematics and computational science*. Sprinnger-Verlag. NY.

Larock, B. E., Jeppson, R.W., and Watters, G. Z. (2000). *Hydraulics of pipeline systems*. CRC Press, Washington, D.C.

Martin, D.L., Kincaid, D.C., and Lyle, W.M. (2007). *Chapter 16. Design and Operation of sprinkler systems.* In Design and operation of farm irrigation systems (eds. Hoffmann, G.J., Evans, R.G., Jensen, M.E., Martin, D.L., Elliott, R.L). 2nd ed, ASABE, St. Joseph, MI, pp.557-631.

Mathews, J.M.and Fink, K.D. (2004). *Numercial methods using Matlab*. Prentice Hall, Inc., Upper Saddle River, N.J.

McCormick, G.P. (1983). *Nonlinear programming: Theory, algorithms, and applications*. John Wiley & Sons, Inc., N.Y.

Miller, D.S. (2009). *Internal flow systems*. Miller Innovations, Bedford, UK.

Playan, E., Burguete, J., Zapata, N., Salvador, R., Buatista-Capetillo, C., Cavero, J., Martinez-Cob, A., Faci, J., and Dechmi, F. (2009). Mathematical problems and solutions in sprinkler irrigation. *Monografias de la Real Academia de Ciencias de Zaragoza*, 31:153-174.

Press, W.H., Teukolsky, S.A, Vetterling, W.T., and Flannery, B.P (1997). *Numercial Recipes in C, the art of scientific computing*. Cambridge University Press, New York, NY.

Simunek, J., van Genuchten, M. Th. and Šejna, M. (2009) The HYDRUS-1D Software Package for Simulating the One-Dimensional Movement of Water, Heat, and Multiple Solutes in Variably-Saturated Media. Version 4.08. *Dept. of Environmental Sciences. University of California Riverside*, Riverside, CA.

Zerihun, D. and Sanchez, C.A. (2011). SprinklerModel: a field-scale solid set sprinkler irrigation system hydraulic model, *program documentation*. Report submitted to Arizona Specialty Crops Council.

Zerihun, D., Sanchez, C.A., and K. Nolte. (2011). Evaluation of sprinkler irrigation system for season long vegetable production in the Yuma Valley Irrigation District. Report submitted to Arizona Specialty Crops Council.

Zerihun, D. and Sanchez, C.A. (2012). Field and Modeling study of sprinkler irrigation for season long vegetable production in the Yuma Valley Irrigation District. Report submitted to the USBR.